INL/EXT-21-64221

AGR 5/6/7 Irradiation Test Final As-Run Report

September 2021

Binh T. Pham
Joe J. Palmer
Douglas W. Marshall
James W. Sterbentz
Grant L. Hawkes
Dawn M. Scates

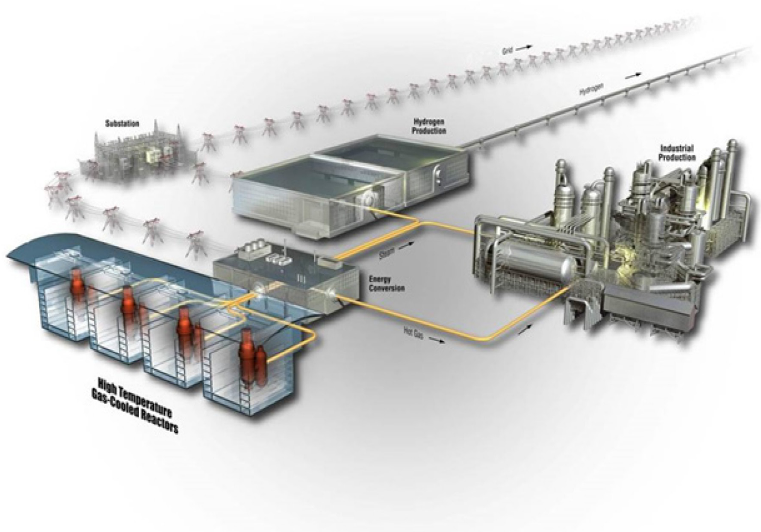

Idaho National Laboratory

INL is a U.S. Department of Energy National Laboratory operated by Battelle Energy Alliance, LLC

INL/EXT-21-64221

AGR 5/6/7 Irradiation Test Final As-Run Report

Binh T. Pham
Joe J. Palmer
Douglas W. Marshall
James W. Sterbentz
Grant L. Hawkes
Dawn M. Scates

September 2021

Idaho National Laboratory
Advanced Reactor Technologies
Idaho Falls, Idaho 83415

http://www.ART.INL.gov

Prepared for the
U.S. Department of Energy
Office of Nuclear Energy
Under DOE Idaho Operations Office
Contract DE-AC07-05ID14517

Page intentionally left blank

INL ART Program

AGR-5/6/7 Irradiation Test Final As-Run Report

INL/EXT-21-64221

September 2021

Technical Reviewer: (Confirmation of mathematical accuracy, and correctness of data and appropriateness of assumptions.)

Mitchell Plummer

Mitchell A. Plummer
NDMAS Technical Lead

9/3/2021
Date

Approved by:

Paul Demkowicz

Paul A. Demkowicz
AGR Program Technical Director

9/7/2021
Date

Travis Mitchell

Travis R. Mitchell
INL ART Program Manager

9/3/2021
Date

Michelle Sharp

Michelle T. Sharp
INL Quality Assurance

9/3/2021
Date

ACKNOWLEDGEMENTS

This work is supported by the Department of Energy Advanced Reactor Technologies Program at Idaho National Laboratory under the U.S. Department of Energy Contract DE-AC07-05ID14517.

SUMMARY

This document presents the as-run analysis of the Advanced Gas Reactor (AGR)-5/6/7 irradiation experiment. AGR-5/6/7 is the last of a series of experiments conducted in the Advanced Test Reactor (ATR) at Idaho National Laboratory in support of the development and qualification of tri-structural isotropic low-enriched fuel for use in high-temperature gas-cooled reactors. The test train contained five separate capsules that were independently controlled and monitored. Each capsule contained multiple 24.91-mm-long and 12.25-mm-dimeter compacts filled with low-enriched uranium carbide/oxide tri-structural isotropic fuel particles. The objectives of the AGR-5/6/7 experiment were to:

- Irradiate reference-design fuel particles to support fuel qualification.
- Establish operating margins for the fuel, beyond normal operating conditions.
- Provide irradiated-fuel performance data and irradiated-fuel samples for post-irradiation examination and safety testing.

The primary objective of the AGR-5/6 test (Capsules 1, 2, 4, and 5) was to verify the successful performance of the reference-design fuel under normal operating conditions. The AGR-7 test (Capsule 3) was designed to explore fuel performance at higher temperatures. Its primary objective was to demonstrate the capability of the fuel to withstand conditions beyond normal operating conditions, in support of plant design and licensing. AGR-5/6/7 will also provide irradiated-fuel performance data based on the fission gas release from particles during irradiation.

To achieve the test objectives, the AGR-5/6/7 experiment was irradiated in the northeast flux trap of the ATR with a planned duration of 500 effective full-power days. The northeast flux trap was selected because its larger diameter provided greater flexibility for test-train design compared to the Large B positions used for the AGR-1 and AGR-2 irradiations, significantly enhancing test capabilities for the combined irradiation campaigns. Due to delays in the ATR schedule, the AGR-5/6/7 irradiation was significantly shorter than the originally planned 13-cycle schedule. Irradiation began on February 16, 2018 and ended on July 22, 2020, spanning nine ATR cycles (162B–168A) over two and a half years. Thus, the AGR-5/6/7 fuel compacts were irradiated for a total of approximately 360.9 effective full-power days.

Final burnup values, on a per-compact basis, ranged from 5.66 to 15.26% fissions per initial heavy metal atom, while fast fluence values ranged from 1.62 to 5.55×10^{25} n/m^2 (E >0.18 MeV). Time-averaged volume-averaged fuel temperatures on a capsule basis at the end of irradiation ranged from 756°C in Capsule 5 to 1313°C in Capsule 3 excluding days with significantly lower temperature during the two short powered axial locator mechanism cycles, 163A and 167A. By the end of irradiation, 48 out of 54 installed thermocouples had failed (the bottom three capsules lost all thermocouples).

During the first five cycles (162B – 165A), the fission-gas isotope release-rate-to-birthrate (R/B) ratios were stable in the 10^{-8}–10^{-6} range, and no in-pile particle failures were observed based on the gross gamma counts. During this time, the high exposed kernel fraction and high fuel particle temperatures in Capsule 1 led to a maximum R/B value of around 2×10^{-6} for Kr-85m. The fission gas release in all capsules started to increase from the second half of Cycle 166A, when a large number of in-pile particle failures occurred in Capsule 1 and a gas line problem in this capsule caused fission gas leakage at various degrees into the other four capsules. This gas line problem also prevented a fission gas release measurement for Capsule 1 during the last three cycles due to gas flow isolation.

By the end of irradiation, it is estimated that approximately 15 particles failed in Capsule 3, which was considered possible because the experiment was designed to operate beyond the high-temperature gas-cooled reactor normal operating temperature range. A few hundred in-pile particle failures were estimated for Capsule 1 by the end of Cycle 166A, but the total number of failures is unknown due to the lack of fission gas release data in the later cycles. Additionally, four potential in-pile failures were identified for Capsule 2 during the last cycle, Cycle 168A. In contrast, no in-pile failures were identified in the top two capsules (4 and 5) based on the absence of the typical spikes in gross gamma counts and low failure estimates using the AGR-3/4 R/B per exposed kernel model.

CONTENTS

FIGURES

TABLES

ACRONYMS

AGR	Advanced Gas Reactor
ART	Advanced Reactor Technologies
ATR	Advanced Test Reactor
DU	dispersed uranium
DUF	DU fraction
ECAR	engineering calculation and analysis report
EFPD	effective full-power day
EK	exposed kernel
EKF	exposed kernel fraction
FIMA	fissions per initial heavy metal atom
FG	fission gas
FPMS	fission-product monitoring system
GG	gross gamma
HPGe	high-purity germanium
HTGR	high-temperature gas-cooled reactor
HTIR	high-temperature irradiation resistant
INL	Idaho National Laboratory
IPyC	inner pyrolytic carbon
LE	low-enriched
LL	lower limits
NE	northeast
MCNP	Monte Carlo N-Particle (code)
NDMAS	Nuclear Data Management and Analysis System
NEFT	northeast flux trap
OPyC	outer pyrolytic carbon
ORIGEN	Oak Ridge Isotope Generation
PALM	powered axial locator mechanism
PIE	post-irradiation examination
R/B	release-rate-to-birthrate
TC	thermocouple
TRISO	tristructural isotropic
UCO	uranium carbide/oxide
UL	upper limits

AGR 5/6/7 Irradiation Test Final As-Run Report

1. INTRODUCTION

AGR-5/6/7 is the last of a series of Advanced Gas Reactor (AGR) experiments sponsored by Advanced Reactor Technologies (ART) and conducted in the Advanced Test Reactor (ATR) at Idaho National Laboratory (INL) in support of the development and qualification of tri-structural isotropic (TRISO) low-enriched (LE) fuel for use in a high-temperature gas-cooled reactor (HTGR). The configuration and irradiation conditions of the AGR experiments were based on prismatic HTGR technology, a technology involving the use of a helium coolant, a low-power-density ceramic core capable of withstanding very high temperatures, and a coated-particle fuel (Mitchell, 2020). AGR-5/6/7 combined the fifth, sixth, and seventh in this series of planned experiments to test TRISO-coated LE uranium oxycarbide (UCO) fuel.

This combined experiment was intended to verify the performance of the reference-design fuel for HTGR normal operating conditions and to explore fuel performance at temperatures substantially beyond those typical of normal operation to establish the temperature margin for acceptable performance. Knowledge from this experiment can be used to support plant design and licensing.

To achieve the test objectives, the AGR-5/6/7 experiment was irradiated in the northeast (NE) flux trap of the ATR with a planned duration of 500 effective full-power days (EFPDs). The NE flux trap was selected because its larger diameter provided greater flexibility for the test-train design and significantly enhancing test capabilities for the combined irradiation campaigns. Due to delays in the ATR schedule, the AGR-5/6/7 irradiation was significantly shorter than the originally planned 13-cycle schedule. Irradiation began on February 16, 2018 and ended on July 22, 2020, spanning nine ATR cycles over two and a half years. Thus, the AGR-5/6/7 fuel compacts were irradiated for a total of approximately 360.9 EFPDs, resulting in final burnup values, on a per-compact basis, ranging from 5.66% to 15.26% fissions per initial heavy metal atom (FIMA), and fast fluence values ranging from 1.62×10^{25} n/m^2 to 5.55×10^{25} n/m^2 (E >0.18 MeV).

The AGR-5/6/7 experiment was largely successful in keeping the fuel temperature in the five capsules within a wide range of temperature distributions that are typical of HTGRs under normal operating conditions and beyond. For AGR-5/6 capsules (Capsules 1, 2, 4, and 5), the actual fuel proportions are close to the 30% specification for the two middle temperature ranges (between 900 °C and 1250 °C); lower than the 10% specification for the highest temperature range (≥ 1250 °C); and higher than the 30% specification for the lowest temperature range (< 900 °C). For AGR-7 Capsule 3, the time average peak fuel temperature was 1432°C (close to the specification of 1500 ± 50 °C) when data from the two low-power powered axial locator mechanism (PALM) cycles are excluded from time averaging.

By the end of irradiation, numerous particle failures were observed in Capsule 3, as might be expected due to the high temperatures to which it was subjected. Additionally, a significant number of in-pile particle failures were apparent in Capsule 1, starting in Cycle 166A, and a small number of potential failures were indicated in Capsule 2 during the last cycle, Cycle 168A. No in-pile failures were apparent in the top two capsules (4 and 5), based on the absence of the typical spikes in gross gamma counts and on the failure estimates using the AGR-3/4 release-rate-to-birthrate (R/B) per exposed kernel (EK) model.

This document presents the collected AGR-5/6/7 irradiation data and analysis results of the as-run fuel irradiation conditions, including a summary of the experimental approach, as-run reactor physics and thermal analyses, fission-product R/B ratio calculations and measurements, issues encountered during the test, and a summary of data qualification work. All AGR-5/6/7 work and analyses were performed in accordance with quality standards described by the INL ART Quality Assurance Program Plan (Sharp, 2020).

At the time this report, the AGR-5/6/7 test train had been unloaded from the reactor and some initial post-irradiation observations have been made, but post-irradiation examination (PIE) is not complete, and those results will be documented in separate reports.

1.1 Test Objectives

The objectives of the AGR-5/6/7 experiment (Collin, 2018) were to:

1. Irradiate reference-design fuel containing LE UCO TRISO fuel particles to support fuel qualification.
2. Establish operating margins for the fuel beyond normal operating conditions.
3. Provide irradiated-fuel performance data and irradiated-fuel samples for PIE and safety testing.

The primary objective of the AGR-5/6 test was to verify the successful performance of the reference-design fuel by demonstrating compliance with statistical performance requirements under normal-operating conditions. The AGR-7 test was designed to explore fuel performance at higher fuel temperatures. Its primary objective was to demonstrate the capability of the fuel to withstand conditions beyond normal operating conditions.

AGR-5/6/7 provided irradiated-fuel performance data on the release of fission-gas from failed particles during irradiation. The in-pile gas release, PIE, and safety testing data on the fission-gas and metal release from the fuel will be used in the development of improved fuel performance and fission-product transport models.

1.2 Advanced Gas Reactor-5/6/7 Experimental Approach

To achieve the test objectives outlined above, a multi-capsule, instrumented lead test train was designed that allowed each capsule to be independently controlled for temperature and monitored for fission product gas release. This provided flexibility in the testing and gathering of meaningful data under multiple test conditions during a single irradiation experiment. The AGR-5/6/7 test train was designed to meet the following test capsule requirements (SPC-1749):

- *The AGR-5/6/7 test train shall be a multi-capsule, instrumented-lead design.*
- *The test train shall contain up to 12 independent capsules. AGR-5/6 capsules shall be separate from AGR-7 capsule(s).*
- *Each capsule shall be independently controlled for temperature and independently monitored for fission product gas release.*
- *Each capsule shall have at least five thermocouples initially installed.*
- *Other than graphite holders (including grafoil spacers) and sweep gas, no capsule components (such as thermocouples, advanced thermal monitors, gas lines, neutron monitors or pressure barriers) shall come in contact with the irradiation test fuel compacts.*
- *Test fuel compacts shall not make radial contact with each other but can make axial contact with each other.*

The five AGR-5/6/7 capsules were irradiated in the NE flux trap (NEFT) position of the ATR at INL. A core cross-section indicating this location is displayed in Figure 1. The NEFT provides greater flexibility for the test train design compared to the Large B positions used for the AGR-1 and AGR-2 irradiations, significantly enhancing test capabilities for the combined irradiation campaigns "AGR-5/6/7 Irradiation Experiment Test Plan" (Collin, 2018). Advantages of the NEFT position include that it:

- Provides ample space to accommodate enough fuel for qualification and margin test needs
- Reduces the required irradiation time by taking advantage of the higher flux levels relative to other ATR irradiation locations

- Allows the use of neutron filters to maintain a more consistent compact power as the fuel burns out
- Allows power-level control (corner lobes are controlled independently).

In addition, the rate of burnup and fast fluence accumulation, or acceleration, in this position is less than three times that expected in a HTGR. Past U.S. and German experiences indicate that by keeping the acceleration factor under three, an irradiation test is more prototypical of an actual reactor irradiation (Petti, 2002).

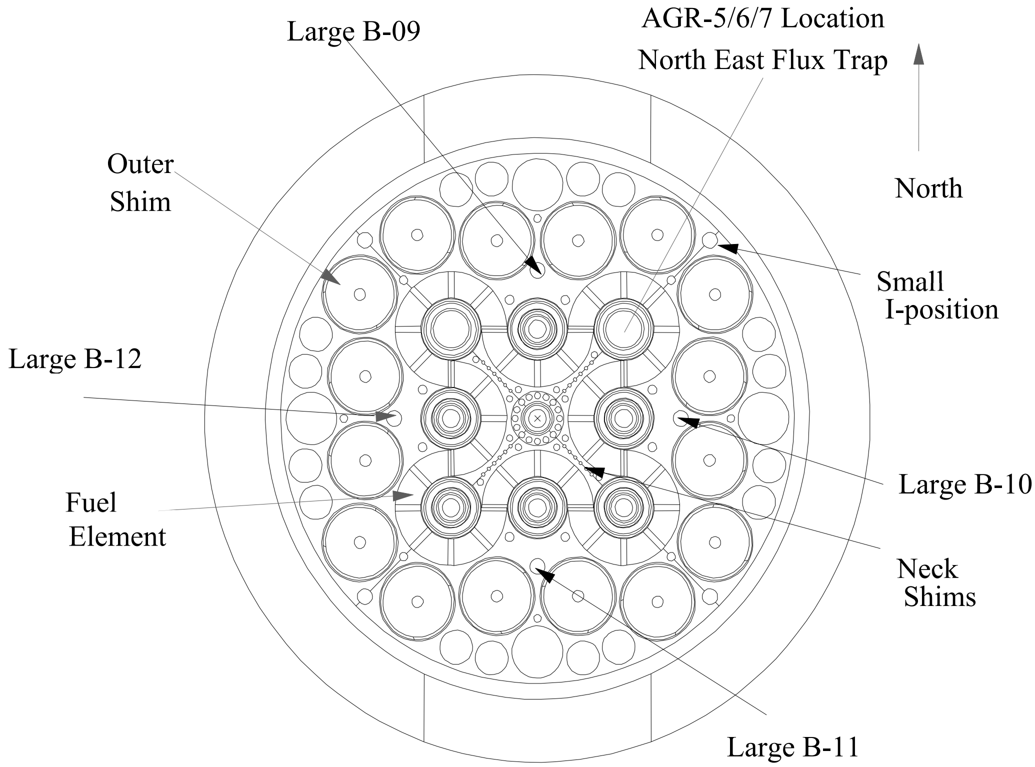

Figure 1. AGR-5/6/7 NEFT location in ATR core cross section.

1.2.1 Test Fuel

Fuel for AGR-5/6/7 consists of reference design LE UCO TRISO-coated particles that are slightly less than 1 mm in diameter. Each particle has a central kernel containing the fuel material, a porous carbon buffer layer, an inner pyrolytic carbon (IPyC) layer, a SiC barrier coating, and an outer pyrolytic carbon (OPyC) layer. AGR-5/6 and AGR-7 used the same reference design fuel. This fuel design is illustrated in Figure 2 (Collin, 2018). The test train was designed to meet the following test fuel requirements (SPC-1749):

- *Each AGR-5/6 capsule shall contain the same reference-design UCO fuel particles.*
- *The goal for the total number of AGR-5/6 fuel particles should be ≥ 500,000.*
- *Each AGR-7 capsule shall contain only one fuel type or variant. This fuel type may be the same as the reference-design fuel to be used in AGR-5/6.*
- *The goal for the total number of AGR-7 fuel particles should be ≥ 50,000 per capsule.*

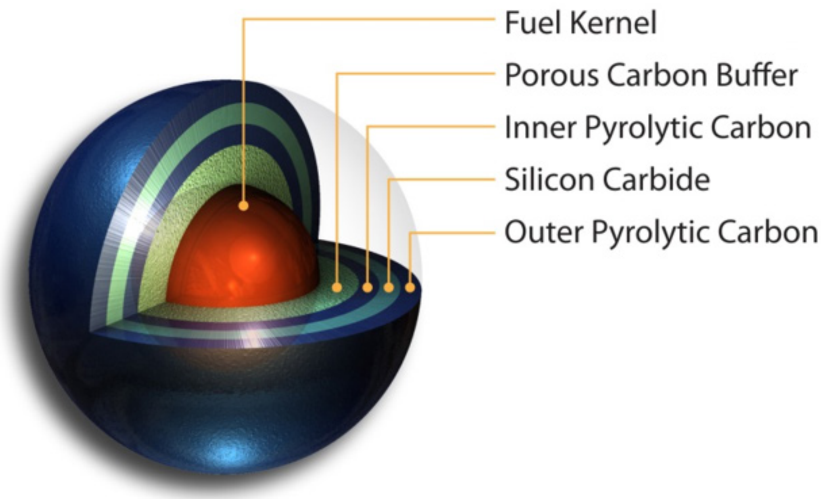

Figure 2. Graphic of a typical TRISO-coated fuel particle.

Kernel batches for AGR-5/6/7 consist of LE UCO fuel fabricated by BWX Technologies in accordance with the AGR-5/6/7 Fuel Specification (Marshall, 2017). These were combined into a single composite kernel lot, J52R-16-69317. These UCO kernels were then coated, in batches, and those batches were combined into a single particle composite lot, J52R-16-98005. After overcoating with a thick layer of resinated-graphite matrix precursor powder, AGR-5/6/7 fuel TRISO particles were formed into right cylindrical compacts. The compact matrix material is composed of natural and synthetic graphite powders and a thermosetting phenolic resin. The overcoat is intended to reduce particle-to-particle contact and to achieve the desired packing fractions and distribution of fuel particles.

AGR-5/6/7 compacts are nominally 25.0 mm in length and 12.3 mm in diameter. The AGR-5/6/7 fuel compacts were fabricated with two different nominal particle loadings (packing fractions of 25% and 40%). 194 compacts out of a total of 432 compacts sent to INL were irradiated in the five AGR-5/6/7 capsules. These compacts were taken from four batches: J52R-16-14154A and J52R-16-14155A, with a 40% packing fraction, and J52R-16-14156A and J52R-16-14157A, with a 25% packing fraction (Table 1). The packing fraction is defined as the total volume of particles divided by the total volume of the compact.

Details of the fabrication process and characterization data for the AGR-5/6/7 fuel were reported in the AGR-5/6/7 Fuel Fabrication Report (Marshall, 2019) and selected properties of fuel kernels, fuel particles, and fuel compacts are presented in Appendix A.

Table 1. AGR-5/6/7 compact batches.

Batch	Nominal Packing Fraction	Compact Serial Number Range	Capsule	Number of Compacts
J52R-16-14154A	40%	0001–0108	1	55
J52R-16-14155A	40%	0109–0216	1 5	35 24
J52R-16-14156A	25%	0217–0324	2 3	32 24
J52R-16-14157A	25%	0325–0432	4	24

1.2.2 Test Train Capsules

The experimental test train consisted of five independently controlled and monitored capsules stacked on top of each other, as shown in Figure 3. Capsules 1, 2, 4, and 5 comprise the AGR-5/6 experiment while Capsule 3 is the AGR-7 experiment.

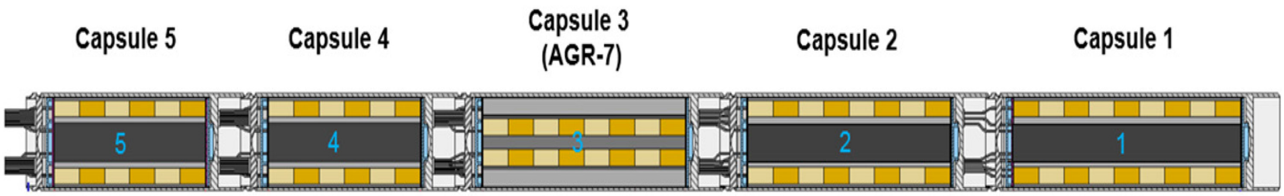

Figure 3. Schematic view of the AGR-5/6/7 test train, rotated 90° from actual orientation (Note: Capsule 5 is at the top of the test train).

The five separate capsules used the full 1.2 m active core height in ATR to maximize the amount of irradiated fuel and span the broad range of fuel burnup and temperature combinations expected in a modular HTGR. To achieve test goals and still be able to control the capsule temperatures, compacts with two different packing fractions of particles were included in the test train; Capsules 1 and 5 contained compacts with a 40% nominal packing fraction, and Capsules 2, 3, and 4 contained compacts with a 25% nominal packing fraction. Capsule 1 contained the greatest number of compacts (90). Capsules 3, 4, and 5 each contained 24 compacts; and Capsule 2 contained 32 compacts (Table 2). The total numbers of fuel particles for both AGR-5/6 and AGR-7 satisfied the requirements stated in Section 1.2.1.

Table 2. AGR-5/6/7 capsules.

Capsule	Numbers of			Average Packing Fraction (%) [a]	Approximate Number of Particles [b]
	Levels	Stacks	Compacts		
5	6	4	24	38.4	3393 [c]
4	6	4	24	24.9	2197 [c]
3	8	3	24	25.5	2265 [c]
2	8	4	32	25.5	2265 [c]
1	9	10	90 [d]	38.4	3434 / 3393 [c]
AGR-5/6 AGR-7 Total	—	—	170 24 194	—	515,700 54,360 570,000

(a) Average packing fraction for each compact lot.
(b) Number of particles obtained by dividing uranium mass content of a compact by uranium mass content of a particle.
(c) Number of particles per compact.
(d) For Capsule 1: 55 compacts from J52R-16-14154A batch and 35 compacts from J52R-16-14155A batch.

To satisfy fuel irradiation requirements, the fuel stacks were contained in a graphite holder, separated from the capsule shell by a gas gap (Figure 4). AGR-7 Capsule 3 had two gas gaps because fuel stacks were contained in the inner graphite holder, which was separated from the outer graphite holder by an inner gas gap. The temperature-control gas gaps had axially varying widths within each capsule and varied by capsule to compensate for the axial variation in heating. The temperature of the graphite holder was monitored by TCs to ensure that the fuel was operating at the target irradiation temperatures. Each capsule contained an individual gas line to provide the helium-neon gas mixture flow in the control gas gap needed to adjust the temperature in the capsule based on feedback from the control TC readings. The capsules were welded together to form the core section of the test train. The plenum regions between capsules were lengthened over previous AGR designs to accommodate the bending of larger and stiffer

TCs. The core section was welded to a lead-out tube that housed and protected the gas lines and TC leads. The leadout was routed from the NEFT position straight up from the ATR core to the experiment penetration in the reactor vessel top head. Above the vessel top head, the gas lines and TC leads were connected to their facility counterparts in the temperature-monitoring, control, and data-collection systems.

To shape the temporal and spatial fuel power distribution, two techniques were used to adjust the neutron flux incident on the test train: placing a neutron filter around the capsules and raising the NE lobe power throughout irradiation as the test fuel was depleted. Two different filters (shrouds) were used during irradiation (Figure 5): a standard medium filter (partial tube of hafnium foil sandwiched between stainless-steel tubes on the left) and a light filter (stainless-steel tube on the right). The hafnium foil was centered axially about the ATR core midplane and extends 50.8 cm above and below the core midplane for a total axial length of 101.6 cm. The axial extent of the hafnium did not fully cover the top of Capsule 5 or the bottom of Capsule 1 to increase the compact power densities and burnup in these regions. As a result, the compact power densities remained relatively constant and uniform despite the NE-lobe power variations incurred during irradiation.

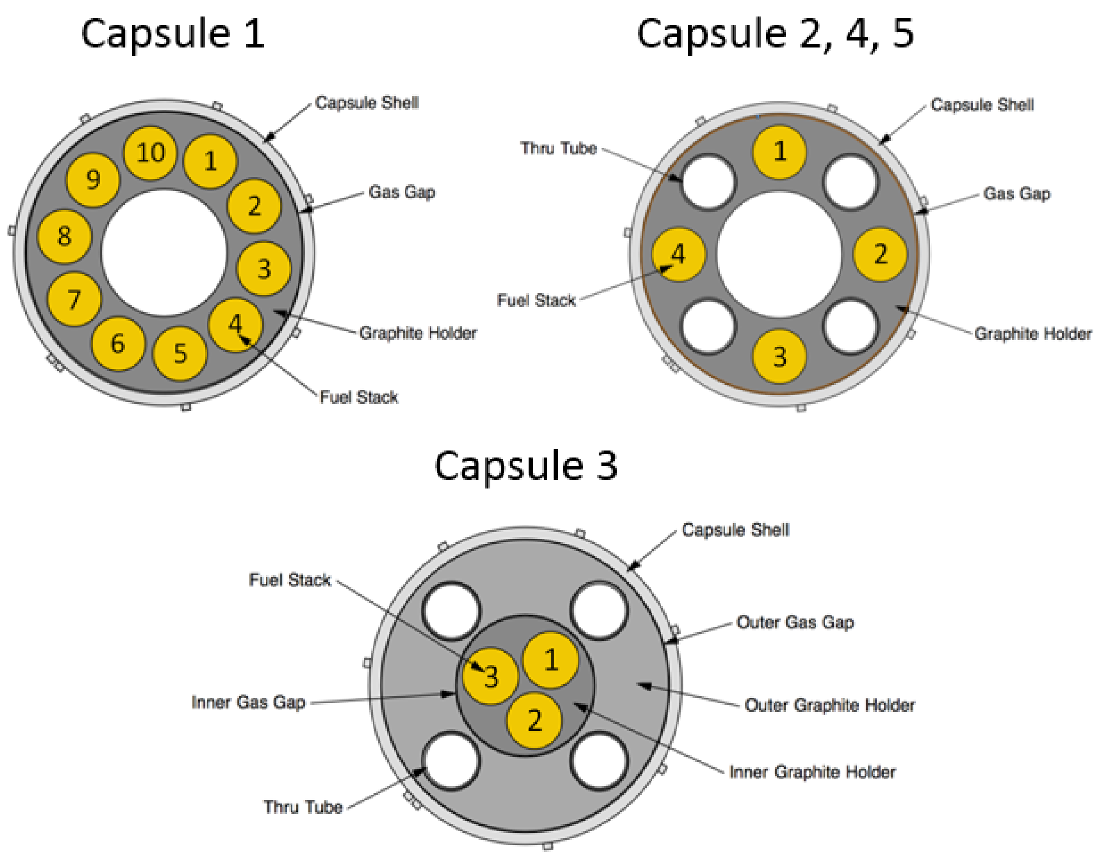

Figure 4. Cross sections of the AGR-5/6/7 capsules showing the compact stacks (Top: Capsule 1 [left] and Capsules 2, 4, and 5 [right]; Bottom: Capsule 3).

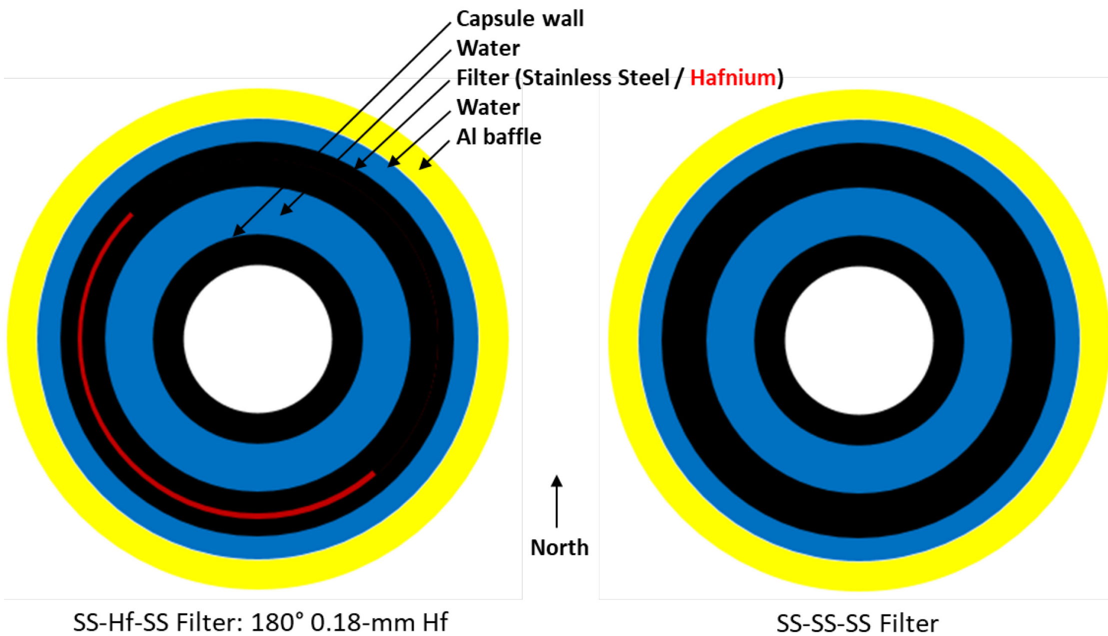

Figure 5. The AGR-5/6/7 neutron filters.

1.2.3 Thermocouples

Thermocouples (TCs) were essential for independent temperature control in the capsules. Per the test train requirements, the number of TCs installed in the AGR-5/6/7 capsules was substantially increased, relative to previous experiments, based on the high failure rate previously experienced. Seventeen TCs were installed in the highest-temperature capsules (Capsules 1 and 3) to maximize the likelihood that at least one TC would survive the entire irradiation campaign. Capsules 4 and 5 had the lowest number of TCs (six), which was more than the required five. The four types of TCs used in the capsules are

- Type N (Ni/Cr/Si/Mg wire), with an Inconel 600 (Ni/Cr/Fe/Mn alloy) sheath, MgO insulation, and Nb sleeve (standard baseline).
- Type N, with a Cambridge low-drift pure Ni sheath, MgO insulation, and Nb sleeve in the AGR-5/6 capsules and with a ZrO_2 sleeve in AGR-7 Capsule 3.
- Type N, with a Inconel 600 sheath, Spinel ($MgAl_2O_4$) insulation, and Nb sleeve.
- High-temperature irradiation resistant (HTIR), with a Nb sheath, Al_2O_3 insulation, and Mo sleeve (HTIR, Mo/Nb wire).

The selection of these TCs relied on the established performance of commercial TCs, furnace testing in support of the AGR-5/6/7 test, and feedback from prior AGR experiments. Among commercial TCs, standard base metal TCs (Types K and N) decalibrate (drift) at high temperatures due to metallurgical changes (>600°C for Type K and >1000°C for Type N). Based on commercial data and AGR-1 experience, Type N TCs (both standard and Spinel insulated) were deemed appropriate and selected for the low-temperature capsules (Capsules 2, 4, and 5 as shown in Table 3). For the high-temperature capsules (Capsules 1 and 3), the Cambridge Type N TCs were used in locations expected to experience temperatures between 1000°C and 1200°C, and HTIR TCs were used in locations expected to experience temperatures above 1200°C (Table 3). A summary of TC type and placement within the test train is provided in the AGR-5/6/7 irradiation experiment test plan (Collin, 2018).

Table 3. AGR-5/6/7 TCs by capsule.

Capsule	Installed TCs	TC Type (# TCs)	TC Temperature Range (°C)
1 (bottom)	17	Spinel (1) HTIR (9) Cambridge (7)	780–1400
2	8	Type N (8)	740–900
3	17	Spinel (4) HTIR (6) Cambridge (7)	680–1500
4	6	Type N (6)	780–940
5 (top)	6	Type N (6)	700–820

1.2.4 Sweep Gas System

Independent gas lines routed a mixture of inert helium and neon gases through each of the five capsules to provide temperature control and to sweep released fission-product gases to the fission-product monitoring system (FPMS). Figure 6 shows a simplified flow path for the AGR-5/6/7 sweep gas from the mass-flow controller to the FPMS. Sweep-gas flow, originating from gas-supply bottles, was routed to the mass-flow controller cabinet, where the helium and neon gases (low-neutron-activation inert gases) were blended for each capsule. The blending of sweep gases was accomplished by a computerized mass-flow controller before the gas enters the test train, based on feedback from the control TC. The sweep gas was then routed to the capsule inlet isolation panel, which could be used to isolate the inlet gas flow to each capsule independently during reactor outages or in the event of a failure. Upon exiting the capsule and test train, the gas flowed through the outlet isolation panel to another panel containing a particulate filter, moisture detector, and three-way valve. The valve routed the gas either to the designated fission-product monitor or to the standby, backup fission-product monitor. After passing through the FPMS, the gas lines were combined into a common exhaust header that routes the gas through a silver-zeolite filter. The exhaust gas was finally routed to the ATR stack.

Helium and neon sweep gases had the following requirements (SPC-1749):

- *Purities of ≥99.99% by volume for each gas to limit the amount of contamination to the test articles and to limit the background activity*
- *New gas-bottle verification: thermal conductivity and moisture measurements are performed for both the helium- and neon-gas lines*
- *Moisture content of <5 ppm H_2O within the sweep gas to reduce possible reactions with the graphite contained in the test capsule*
- *Gas flow of ≤50 sccm at a pressure of about 7–21 kPa-gauge (or 1–3 psig).*

To prevent capsule to capsule gas leakage, the original plan called for a nominal helium or/and neon flow of 1–5 sccm per capsule at about 6.9 kPa-gauge (or 1 psig) above the capsule pressure to be provided via a mass-flow controller into the leadout cavity, for a total flow of 5–20 sccm, which then flowed into the common plenums between capsules. Through tubes were only present in Capsules 2–5; Capsule 1, being the bottom capsule, does not require through tubes.

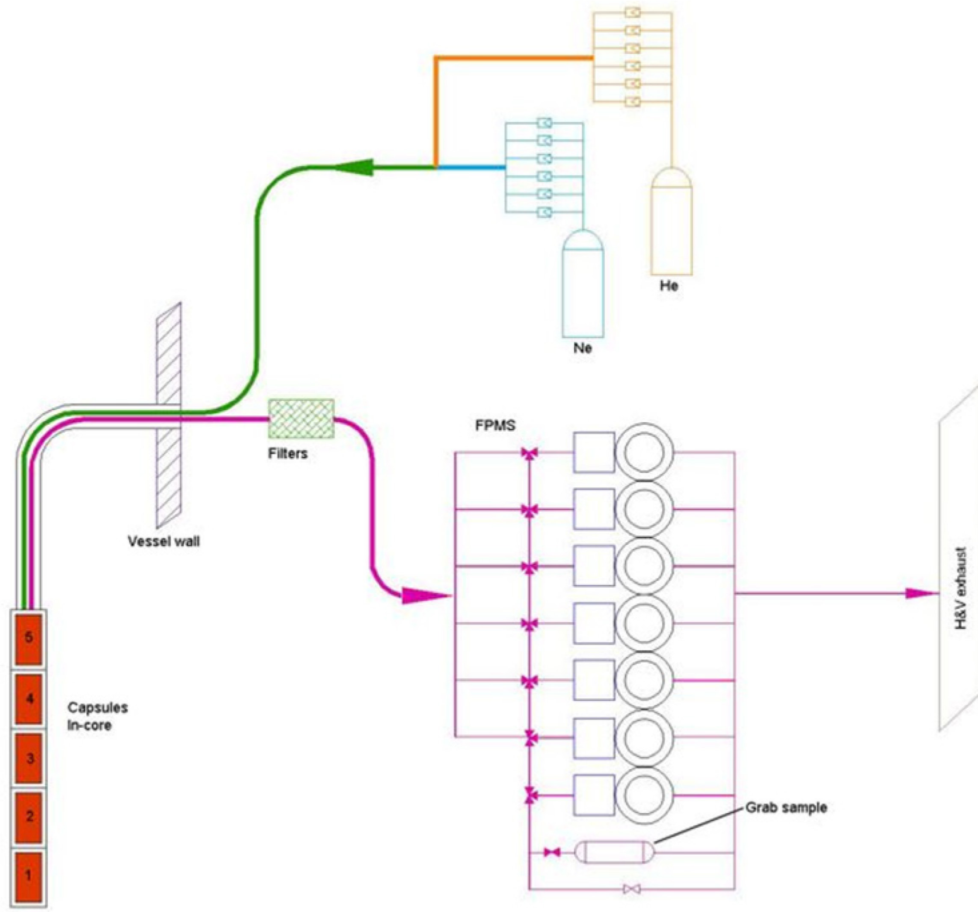

Figure 6. Simplified flow path for AGR-5/6/7 sweep gas.

1.2.5 Fission Product Monitoring System

Each AGR-5/6/7 capsule was continuously monitored for fission gas (FG) release by the FPMS, which consisted of seven sets of gross-radiation monitor and spectrometer detector pairs. One detector set was designated for each of the five capsules, while the two remaining detector sets served as spares. A detector set is illustrated in Figure 7. Under normal operation, computerized data acquisition, analysis, and storage occurred continuously without operator intervention.

Sweep gas carried released FG from the capsules to the detector system under normal conditions with an expected transit time of around 150 seconds. The sweep gas passed in front of the gross-radiation monitor, which used a thallium-doped sodium iodide (NaI[Tl]) detector to detect each fuel-particle failure up to the first 250 failures.

Flow continued to the spectrometer system, which used a high-purity germanium (HPGe) detector. The spectrometer detector systems measured the concentrations of various krypton and xenon isotopes in the sweep gas from each capsule. During normal operation, 8-hour counting intervals were used to measure the concentrations of Kr-85m, Kr-87, Kr-88, Kr-89, Kr-90, Xe-131m, Xe-133, Xe-135, Xe-135m, Xe-137, Xe-138, and Xe-139. These nuclides were selected because they are chemically inert fission-product gases with relatively short half-lives, allowing each isotope to reach equilibrium concentration in the fuel during each reactor cycle. The measured concentrations were converted to per-capsule release rates for each isotope, which were automatically stored and backed up.

During reactor outages, the capsules were swept with pure helium; the effluent was analyzed for FG. Of particular interest are the FG concentrations of Xe-133, Xe-135, and Xe-135m, which were measured and recorded for at least 2 days following each reactor shutdown. These xenon concentrations were used to calculate concentrations of their parent iodine isotopes, which are an indication of fuel performance.

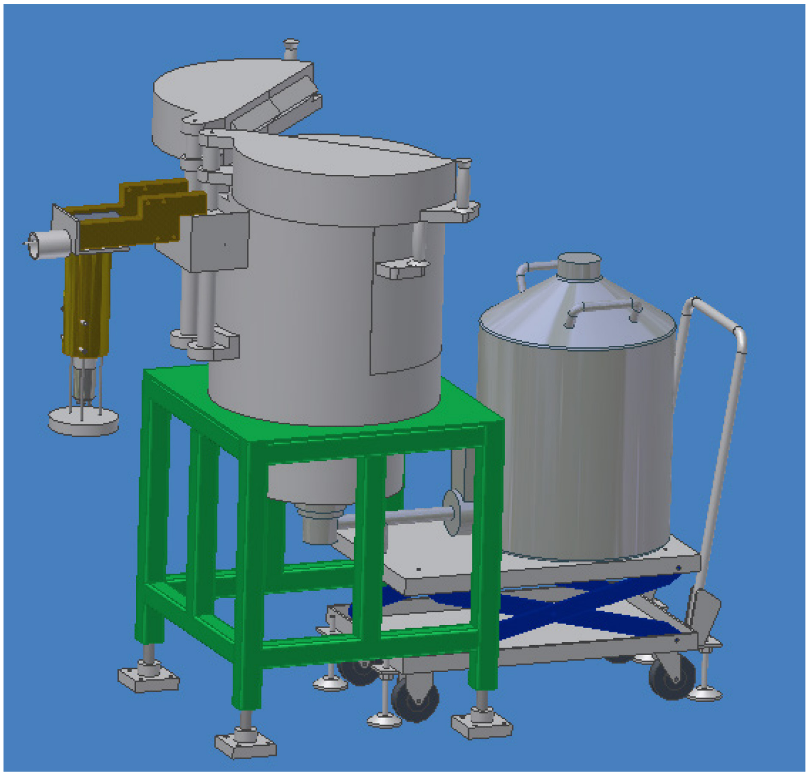

Figure 7. Gross-radiation monitor and spectrometer detector for one AGR-5/6/7 sweep gas line.

1.3 Advanced Gas Reactor-5/6/7 Irradiation

The AGR-5/6/7 experiment irradiation started on February 16, 2018 (ATR Cycle 162B), and ended on July 22, 2020 (ATR Cycle 168A), resulting in nine cycles spanning over two-and-half years. This brought the total irradiation duration to approximately 360.9 EFPDs. Measurements from instruments in ATR and the AGR-5/6/7 test train were essential for control of the specified experimental irradiation and provided necessary data inputs to simulation codes. The ATR- and capsule-measured data were transferred to the INL's Nuclear Data Management and Analysis System (NDMAS) database and automatically processed every hour during the entire irradiation period.

Among the nine ATR cycles during the AGR-5/6/7 irradiation: six were regular cycles (162B, 164A, 164B, 166A, 166B, and 168A); one was a short high-power PALM cycle (165A); and two were intermittent (mostly low-power and about one day high power) short PALM cycles (163A and 167A). The overview summary of these cycles is presented in Table 4, including cycle type, neutron filter, number of timesteps used in physics and thermal models, lobe burnup, EFPDs, and average NE lobe power (Sterbentz, 2020). The lobe burnup in MWd is the product of daily average NE lobe power and number of power days per cycle. Among the 408 timesteps used in the physics and thermal models, there are 10 timesteps representing scram periods within power cycles and 40 partial days at lower power (power-up or power-down). An EFPD is an irradiation day scaled by the target reactor power. Hence, approximately a week of irradiation during the two intermittent PALM cycles (163A and 167A) resulted in less than three EFPDs.

Table 4. ATR cycles during the AGR-5/6/7 irradiation.

Cycle #	Cycle Name	Cycle Type	Neutron Filter[(a)]	No. of Timesteps for Physics & Thermal Analysis [(a)]	Lobe Burnup [MWd] [(a)]	No. of EFPDs [(b)]	Average NE Lobe Power [MW] [(a,f)]
1	162B	Regular	Medium	42	564.6	38.51 [(c)]	14.54
2	163A	PALM	Medium	10	61.2	2.99 [(d)]	7.21
3	164A	Regular	Medium	61	890.3	54.91	16.01
4	164B	Regular	Medium	69	1,046.0	64.06 [(e)]	16.27
5	165A	PALM	Medium	17	259.1	13.37	18.75
6	166A	Regular	Light	66	1,052.9	62.50	16.87
7	166B	Regular	Light	63	1,033.7	61.23	16.89
8	167A	PALM	Light	12	47.6	2.33[(d)]	4.86
9	168A	Regular	Light	68	1,212.8	61.02	19.81
			Total	**408**	**6,168.2**	**360.90**	

(a) Taken from the engineering calculation and analysis report (ECAR) 5321 (Sterbentz 2020).
(b) EFPDs per reactor cycle was taken from the Table “Summary of ATR Power History by Cycle” provided by the ATR.
(c) The 162B cycle ran 14 days at 14 MW and 25 days at 15 MW.
(d) The 163A and 167A PALM cycles ran most days at 5 MW and about a day at 20 MW.
(e) The 164B cycle ran 27 days at 17 MW and 37 days at 16 MW.
(f) The average NE lobe power is based on the average power of whole days (i.e., 24 hours) during the cycle, when the reactor ran at full power.

ATR data that describe the core neutronics and thermal-hydraulic environment are used to inform the physics and thermal analyses, as well as support temperature control. The ATR data used as input for the physics analyses include total core power, individual lobe powers, shim cylinder (hafnium absorber) positions, neck shim positions, and regulatory rod positions. NDMAS receives the ATR operating data in 5-minute increments and daily averages are presented in Figure 8.

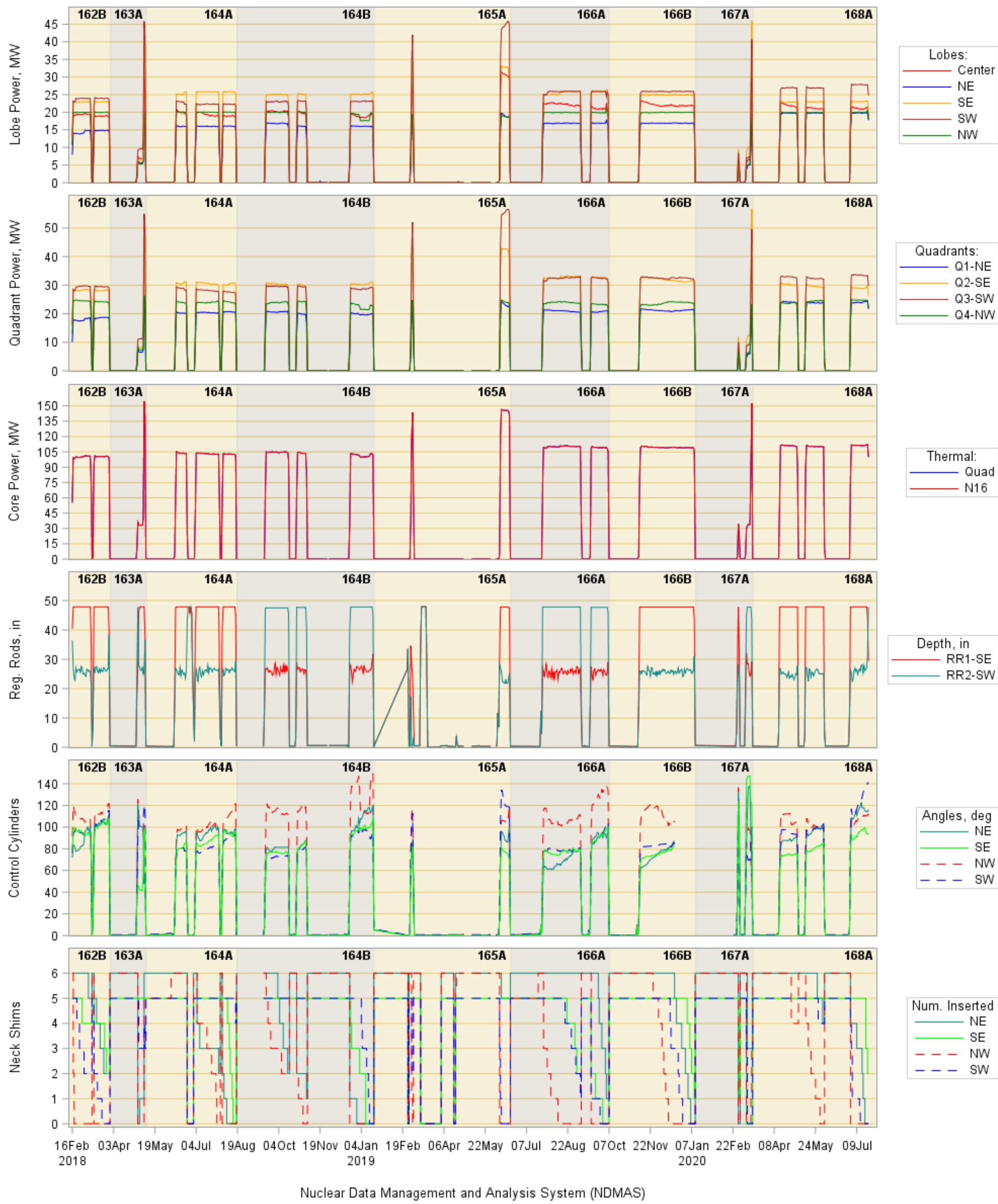

Figure 8. ATR daily operating parameters during AGR-5/6/7 irradiation.

1.4 Data Management and Qualification

The preservation and management of the AGR experimental data are critical contributions to the experiment's ability to meet its objectives. INL's ART program established the NDMAS to ensure that the AGR data are qualified for use and stored in a readily accessible electronic form that can be analyzed to extract useful results. The system is described in the NDMAS Plan (Lybeck, 2016). The qualification status of the instrumentation data—which consisted of 1-minute measurements of TC temperature, sweep gas flow rate, gas pressure, and moisture content—are documented in the AGR-5/6/7 data qualification report (Pham, 2021).

During the entire course of the irradiation period, three streams of data were continually generated:

- Irradiation data, which include thermocouple readings, sweep-gas flow rates, pressure, and moisture-monitor readings
- FPMS data, which include gross gamma (GG) counts
- ATR operating-condition data, which include lobe powers, outer shim control cylinder positions, neck shim positions, and control-rod positions.

AGR-5/6/7 data also comprise the following calculated quantities resulting from release-rate calculations, neutronics modeling, and thermal modeling performed after the end of each ATR cycle:

- Fission product release-rate data, which include release rates and R/B ratios per capsule for 12 krypton and xenon isotopes: Kr-85m, Kr-87, Kr-88, Kr-89, Kr-90, Xe-131m, Xe-133, Xe-135, Xe-135m, Xe-137, Xe-138, and Xe-139.
- Neutronics data, which include the fission and gamma power density and fast neutron fluence for fuel compacts and graphite holders; burnup for fuel compacts; fission/gamma power density for non-fuel components; inventory of 1,007 isotopes decayed at three times after the end-of-irradiation (i.e., +1day, +1year, and +2years) for fuel compacts; and I-135 inventory at the end of each of nine AGR-5/6/7 reactor cycles.
- Thermal data, which include temperatures for fuel compacts and TC locations.

NDMAS provides a single controlled repository for all AGR-5/6/7 data and makes the data available to users on an easily accessible website. During the experiment, the website showed the irradiation progress with plots that were updated approximately hourly, to allow researchers to quickly identify and correct any issues. The Highcharts JavaScript library is used to generate compact interactive plots that are useful for monitoring as-run experimental conditions. Many of the plots in this document are examples of the displays available on the website.

Another important function of NDMAS is the facilitation of data qualification and storage of the associated documentation. Specific data qualification activities within NDMAS depend on the data qualification category for each data entity as assigned by the data generator. Activities include: (1) capture testing to confirm data stored within NDMAS are identical to the raw data supplied, (2) accuracy testing to confirm data are an accurate representation of the system or object being measured, and (3) documentation that data were collected under a Nuclear Quality Assurance NQA-1 or equivalent quality assurance program. Within the INL ART program, the NQA-1 requirements are implemented through the INL ART Quality Assurance Program Plan (Sharp, 2020). "*Capture Passed*" data are data whose capture has been verified by showing that the data pushed to the database match the raw data provided by the generator. Codes used for capturing data are recorded using a change request process that documents all steps taken (i.e., various reviews, testing, and archive) to ensure that data are stored correctly in appropriate tables that allow complete data retrieval with all associated attributes, including data state and qualification status. The most important testing task is to make sure data loaded into the system are verified against raw data through manual inspection. An example of the data table structure for irradiation monitoring data is presented in the AGR-5/6/7 Data Qualification Report for ATR Cycles 162B–168A (Pham, 2021).

The qualification status and basis for qualification of the AGR-5/6/7 data streams are summarized below:

1. Fuel fabrication data – All data have been processed into the NDMAS database and qualified. Details of the fabrication process and data were reported in INL/EXT-19-53720 (Marshall, 2019) and selected properties of fuel kernels, fuel particles, and fuel compacts used in AGR-5/6/7 capsules are presented in Appendix A.
2. Fuel irradiation data – NDMAS processed a total of 94,989,908 records for TC temperature and gas flow data from irradiation monitoring of the nine AGR 5/6/7 reactor cycles. Of those records, 41,565,069 records (43.7% of the total) met the requirements for *Qualified* records, 53,424,839 (56.2%) were *Failed*, and 74,641 (0.1%) were classified as *Trend* as documented in the report INL/EXT-21-62180 (Pham, 2021).
3. ATR operating conditions data – Data for all nine AGR-5/6/7 reactor cycles have been stored and capture tested. These data, which come from outside the INL ART program, are assumed to be qualified by ATR quality control procedures.
4. FPMS data – NDMAS processed a total of 110,388 release rate records and 110,388 R/B records for 12 reported radionuclides for nine AGR-5/6/7 reactor cycles. Each release rate or R/B record is accompanied by an estimated uncertainty using knowledge about the FPMS measurement. The qualification status of these data was based on the ECAR-5352 (Scates, 2021) that has been recorded in NDMAS.
5. Neutronics and thermal modeling data – All data have been stored in NDMAS and marked as *Capture-Passed* and *Qualified.* The qualification status of the neutronics data and thermal data were determined by ECAR-5321 (Sterbentz, 2020) and by ECAR-5633 (Hawkes, 2021), respectively.

1.5 Documentation Requirements

This as-run data report shall contain at least the following calculated values with their associated uncertainties (SPC-1749):

- *Time-average peak fuel temperature for each capsule*
- *Time-average, volume average fuel temperature for each capsule*
- *Histories of minimum, average and peak fuel temperatures for each compact*
- *Average fast neutron fluence (E>0.18 MeV) for each compact*
- *Average burnup for each compact*
- *R/B values for at least Kr-85m, Kr-87, Kr-88, Xe-131m, Xe-133, and Xe-135 for each capsule*
- *Estimated number of particle failures within each capsule.*

2. PHYSICS ANALYSIS

Most of the physical parameters describing the irradiation conditions of the AGR test fuel were calculated using neutronics analysis models. The neutronics depletion code calculated fission-power density, fast neutron fluence, and burnup for fuel compacts, and FG isotope birthrates from each capsule. After the completion of each cycle, an as-run neutronics analysis was performed using actual ATR operating parameters. The heating rate and fast fluence from neutronics analysis, combined with the neon fraction in the gas flow to each capsule, were used in the thermal model to calculate daily fuel-compact temperatures. During this time, the R/B ratios were also calculated using FG isotope birth rates and release rate for each capsule. The neutronics analysis methodology and software modules used to perform the AGR-5/6/7 as-run depletion calculation were documented in ECAR-5321 (Sterbentz 2020).

For AGR-5/6/7 compacts, the specified maximum compact average burnup of 18% FIMA was established so that the test approaches, or exceeds, what may be considered full burnup in a HTGR for 15.5 wt% enriched fuel. The specified minimum compact average burnups of 6% FIMA was established so that a level of significant irradiation is achieved in all compacts. The specified maximum AGR-5/6/7 fast neutron fluence of $\geq 5.0 \times 10^{25}$ n/m^2, E >0.18 MeV, bounds expected HTGR service conditions. The minimum fast neutron fluence of $>1.5 \times 10^{25}$ n/m^2, E >0.18 MeV, was established so that the fuel pyrocarbon experiences the transition from creep-dominated strain to swelling-dominated strain (at 1250°C) for high-temperature compacts. Finally, the instantaneous peak power per particle requirement of ≤400 mW/particle limits the peak kernel temperature and the temperature gradient across the particle, which reduces fission product diffusion and potential fission product/silicon carbide interactions.

2.1 Neutronics Analysis Methodology

Neutronics analysis of the AGR-5/6/7 test train was performed using an Monte Carlo N-Particle (MCNP) - Oak Ridge Isotope Generation (ORIGEN) Coupled Utility Program (JMOCUP) developed at INL by James Sterbentz that combines the continuous-energy MCNP transport code (LANL 2004) and the depletion code ORIGEN (Croff 1983). The MCNP5 Code, Version 1.60, is a general purpose, continuous energy, generalized geometry, and coupled neutron photon electron Monte Carlo transport computer code. The ORIGEN (Oak Ridge Isotope Generation) code, Version 2.2, is used to calculate the time-dependent, coupled behavior of radioactive and stable isotope buildup, depletion, and decay under constant power or flux conditions. The similarity in test-train design between AGR-3/4 and AGR-5/6/7, in conjunction with the similarity in reactivity worth of the two test-train configurations and the low worth of the fuel compacts, allowed the same JMOCUP depletion methodology and software modules to be used in both the AGR-3/4 neutronics calculation (Sterbentz 2015) and the AGR-5/6/7 neutronics calculation (Sterbentz 2020).

2.1.1 Model Description

The JMOCUP depletion calculation coordinated three depletions: (1) the ATR driver core, (2) the AGR-5/6/7 TRISO compacts, and (3) the AGR-5/6/7 hafnium capsule shroud (i.e., the thermal neutron filter). The ATR driver core consists of 840 depletion cells in the MCNP model, or three radial and seven axial cells per each of the 40 driver elements in the serpentine ATR core. The 194 AGR-5/6/7 fuel compacts were homogenized, and each was split into four axial segments for a total of 776 compact depletion cells (4 × 194). The hafnium shroud had 40 depletion cells, two azimuthal by 20 axial segments. Therefore, there were 1,656 depletion cells in the MCNP full-core ATR model. JMOCUP depleted each cell at each time step. The ATR driver-fuel depletion cells each contain nine actinide isotopes and 24 fission-product isotopes, the concentrations of which, along with their fission and radiative-capture cross-sections, are tracked and updated at each time step. Similarly, the compacts have 21 tracked actinides and 71 tracked fission products. In the hafnium-shroud cells, the six naturally occurring hafnium isotopes are tracked. The MCNP code calculates cell flux and specified nuclear reaction rates for every isotope in each depletion cell at every time step. Using these data, updated isotopic concentrations and one-group cross sections are fed to the ORIGEN input files along with the cell-average neutron flux for the next ORIGEN depletion calculation.

The neutron transport problem in the JMOCUP method is solved using the KCODE option in the MCNP code. For the KCODE option to be effective, the ATR driver fuel must be simultaneously depleted along with the AGR-5/6/7 experiment depletions. Modeling the depletion of the entire ATR core provides realistic neutron and gamma sources for analyzing the AGR-5/6/7 experiment's radiation environment. The effects of important operational details (such as the positions of the outer shim control cylinders and neck shims) can be considered on a daily average basis using this methodology. The ATR operating parameters used in the depletion model include total core power, lobe powers, rotational movement of the outer shim control cylinders, and withdrawal of neck shim rods. The AGR-5/6/7 compacts are solid cylinders composed of TRISO particles and a graphite binder matrix with selected fabrication data presented in PLN-5245 (Collin, 2018). The TRISO-particle compacts are homogenized in the MCNP full-core models.

The JMOCUP software modules successfully underwent a rigorous verification for the three earlier AGR experiments (AGR-1, -2, and -3/4). The verification of JMOCUP focused on three areas: the verification of transformation of the as-run ATR data into JMOCUP formatted data, the verification of the JMOCUP module functionality and execution performance, and the assessment of performance and accuracy of the JMOCUP depletion results based on data trending and comparisons between measured and calculated key physics parameters such as the calculated compact burnup at the end of irradiation and measured compact burnup during PIE. For as-run AGR-5/6/7 JMOCUP depletion calculations, the JMOCUP software underwent only limited verification since the same software modules were used. The AGR-5/6/7 as-run physics depletion calculation was executed properly, and calculated parameters were in-line with expectations as reported in ECAR-5321 (Sterbentz 2020).

2.1.2 Technical Input Parameters

Material, dimensional, and operational data needed for the MCNP models, ORIGEN2 models, and the JMOCUP software modules included the following:

1. *As-run ATR driver core loading data*: The U^{235} mass loadings, type of fuel element, and core location for each of the 40 ATR driver elements.

2. *As-run ATR measured data*: The ATR total core power, five lobe powers, outer shim control cylinder rotation positions, and neck shim insertion or withdrawal status for the 24 neck shim rods in the aluminum housing in the center of the ATR core.

3. *AGR-5/6/7 test train data*: The components, dimensions, and material data taken from the INL drawings describing the capsules.

4. *TRISO particle and compact data*: The material and dimensional data for the TRISO-particle fuel and compacts, which were used to derive the homogenized compact number densities of U^{234}, U^{235}, U^{236}, U^{238}, C, O, and Si. As-manufactured characterization data for the AGR-5/6/7 fuel are presented in Appendix A.

5. *Data libraries*: The standard MCNP cross section data was libraries ENDF 7 [ATR driver fuel used 293 K (20°C) temperature cross section libraries (.70c) and the compacts used 1200 K (927°C) libraries (.73c)]. The ORIGEN2 base library was the PWRU.LIB that comes with the Radiation Safety Information Computational Center standard issue of the ORIGEN code.

2.1.3 Calculation Uncertainties

There are uncertainties associated with the calculated JMOCUP depletion results. The calculated uncertainty sources are uncertainties of model inputs such as the ATR as-run data, ENDF cross-section data, and MCNP statistical errors. There are also unquantifiable propagation errors associated with Monte Carlo depletion calculations, although it has been shown that these errors tend to be well-behaved and average out over the depletion calculation. The high-resolution JMOCUP calculation (using daily time steps) was expected to average out better than similar Monte Carlo calculations with longer time steps.

The estimated uncertainties associated with the JMOCUP input parameters are listed in Table 5. The ATR total core power and lobe powers had the largest uncertainties based on two different references. These ATR powers were used in the JMOCUP calculation to normalize the neutron fluxes, reaction rates, and fission power densities. However, the excellent agreement between calculated and measured compact burnup in %FIMA and fast fluence for all fuel compacts from previously completed AGR-1, AGR-2, and AGR-3/4 experiments would indicate that the referenced uncertainty estimates for the ATR lobe powers and total core power are overestimated in magnitude. Estimated uncertainties of the measured ATR lobe powers and total core power are much less than the quoted ±4%.

The as-run AGR-5/6/7 depletion calculation behaved in a manner similar to the previous three JMOCUP depletion calculations for AGR-1, AGR-2, and AGR-3/4. Therefore, the excellent agreement between measured and calculated compact burnups and fast fluence for these earlier experiments also indicates low uncertainties of the JMOCUP calculated results. In addition, the heat rates calculated by JMOCUP were used as the main input to the thermal models that produced very good agreement between measured and calculated TC data. This led to high confidence in the neutronics calculated results. Finally, for the six regular AGR-5/6/7 cycles, the k-effectives tended to hover around 1.0 (i.e., 0.985–1.015), which indicated that the as-run AGR-5/6/7 JMOCUP depletion calculation was executed properly and in an expected manner (Sterbentz 2020).

Table 5. Variables and associated uncertainty estimates (Sterbentz 2015).

Entity/Item	Variable	Units	Uncertainty Estimate
ATR	Total core power	MW	±4.1% to ±8.0%
ATR	Lobe power	MW	±4.1% to ±8.0%
ATR	OSCC position	degrees	<1.0%
ATR	OSCC hafnium isotope number densities	a/b/cm	<1.0%
ATR	Beryllium reflector poison	-	<1.0%
ATR	Flux trap reactivity	-	Unknown
Fuel Compacts	BOL number densities	a/b/cm	±0.5%
JMOCUP-MCNP	k-effective	-	±0.5%
JMOCUP-MCNP	Flux (statistical error)	$1/cm^2/sn$	±0.8%
JMOCUP-MCNP	Reaction rates (statistical error)	$1/cm^2/sn$	±2.0%
JMOCUP-MCNP	Fission powers (statistical error)	MeV/gm/sn	±1.5%
JMOCUP-MCNP	ENDF nuclear data	-	0-10%
JMOCUP Calc	Lobe power normalization	MW	+1-3%
JMOCUP Calc	nu	n/fiss	±0.1%
JMOCUP Calc	Q	MeV/fiss	±1.0%
JMOCUP-ORIGEN	Cross section	barns	±2.0%
JMOCUP-ORIGEN	Numerical error	-	±0.5%

2.2 As-Run Neutronics Analysis Results

The as-run AGR-5/6/7 neutronics calculated data was archived on NDMAS and on the Falcon supercomputer system. The neutronics analysis provides daily values of fission power density (W/cm^3) and fast neutron fluence (n/m2, E > 0.18 MeV) for the 194 AGR-5/6/7 compacts and non-fuel components, and burnup in %FIMA for all compacts. Fast neutron fluence is defined as those neutrons with energies greater than 0.18 MeV. For each of 408 timesteps over the nine irradiation cycles, neutronics data include:

- For fuel compacts: 776 values of fission power density and fast neutron fluence (four axial segments per compact); and 194 values of burnup (one per compact).
- For nonfuel components: 907 values of neutron and gamma heat rates for graphite holders, capsule shell, neutron filters (shrouds), capsule lids, spacers, thru tubes, TCs, and gas lines; 45 values of fast neutron fluence for graphite holders in five capsules.
- Compact birthrates for 12 krypton and xenon radioactive isotopes (atoms/sec).
- Compact I-135 concentrations at the end of each ATR power cycle.
- Compact actinide and fission-product concentrations at the end of irradiation for three different decay times (end of irradiation +1day, +1year, and +2years).

2.2.1 Compact Heat Rate

Compact fission power varied by timestep and cycle, but typically ranged between approximately 200—480 watts/compact during the regular ATR power cycles (Sterbentz 2020). The distribution along the vertical axis of the ATR core of the daily calculated heat rates (watts/axial segment) for the five capsules are plotted as function of cycle (Figure 9). Only representative compact/stacks in each capsule and one full power day were selected. These plots show the vertical variation of compact fission power along the reactor core and over irradiation time. For the six regular cycles, the general trend for the fission powers was a slow decrease in power with each successive cycle (specifically, the lowest heat rates occurred during the last cycle, Cycle 168A), despite the progressive increase in NE lobe power with each cycle. This is because the burnup of the U^{235} in the compacts was in greater extent than increase in the ATR NE lobe power. During the last day of the first PALM cycle, Cycle 163A, most compact fission powers were notably higher than the upper limit of regular cycles because of fresh fuel and much higher NE lobe power (20 MW); during the last PALM cycle, Cycle 167A, most compact fission powers were much lower than the lower limit because of depleted fuel and lower NE lobe power (5 MW) (Figure 9).

The daily calculated compact power densities (W/cm^3) plotted versus irradiation time by capsule in Figure 10, also depict the same trend as in Figure 9. For each compact, daily minimum, average, and maximum values are calculated based on the provided values from the four axial segments per compact. For each capsule, these daily values are calculated from per-compact values. The power density in the three middle capsules (Capsules 2, 3, and 4) decreased more rapidly as each cycle progressed than in the two peripheral capsules (Capsules 1 and 5) due to exposure to higher fast fluence, as shown in Figure 10. For each timestep, the heat rate varied most for compacts in Capsules 1 and 5 because of the reducing fast fluence profile near the top and bottom of the reactor core. Capsule 3 compacts had almost the same heat rate by the end of irradiation because they were depleted and exposed to the similar neutron flux near the core center.

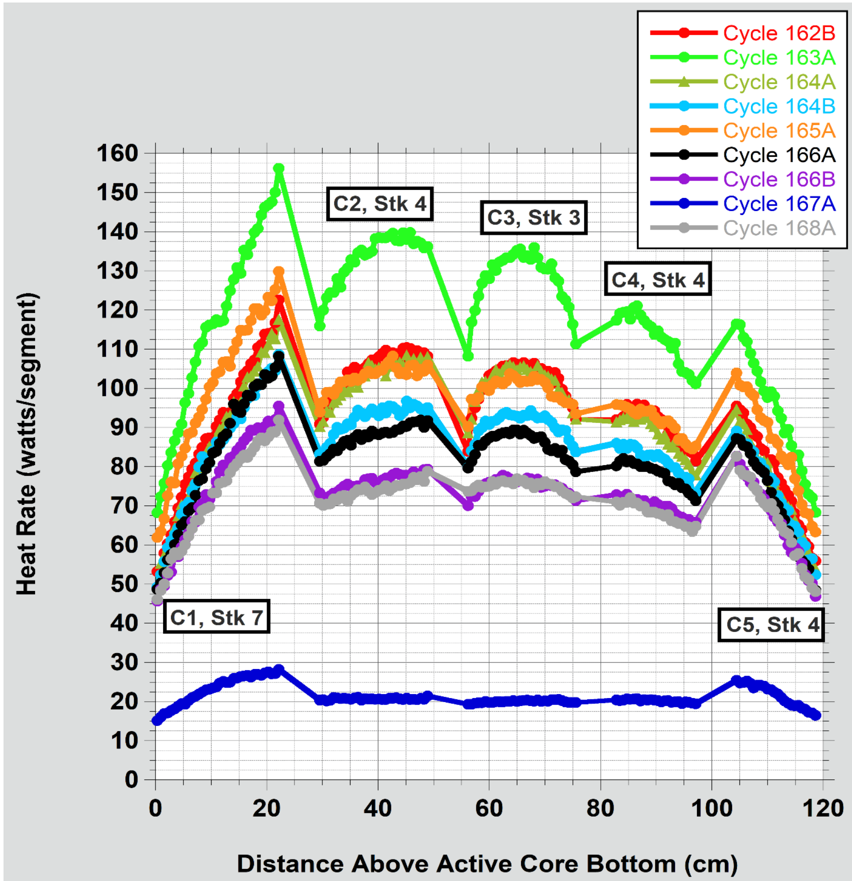

Figure 9. Calculated AGR-5/6/7 compact heat rates (watts/axial segment) as a function of cycle.

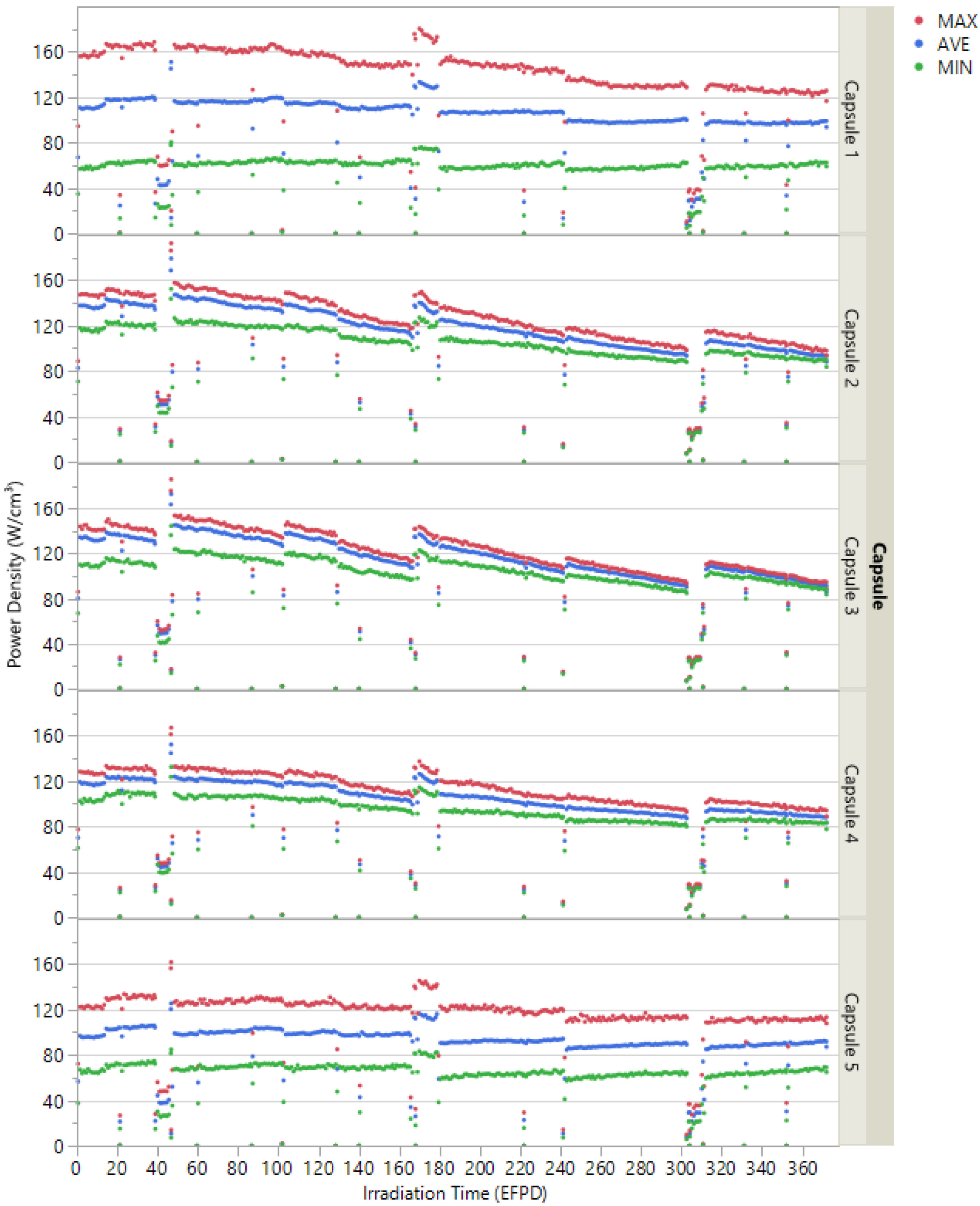

Figure 10. Calculated daily minimum, maximum, and volume-averaged compact power density as a function of EFPD by capsule.

The daily power per particle in milliwatts per particle, which is subject to fuel specification, can be converted from the provided compact fission power, compact volume, and number of particles per compact. Table 6 gives particle power ranges (minimum to maximum) for all the compacts in each of the five capsules for all nine ATR power cycles at the middle of the cycle on a single irradiation day in which the core was at full power. The daily capsule-peak instantaneous powers per particle (mW/particle) calculated from all fuel segments in a capsule are plotted in Figure 11.

Table 6. Particle power ranges (mW/particle) as a function of capsule and cycle (Sterbentz, 2020).

Cycle	Capsule 1	Capsule 2	Capsule 3	Capsule 4	Capsule 5
162B	59—137	164—193	160—186	150—172	65—110
163A (PALM)	75—178	202—247	201—238	180—216	77—135
164A	58—133	162—188	163—186	142—167	63—107
164B	57—124	145—167	147—164	133—154	62—102
165A (PALM)	69—148	165—187	162—182	150—174	73—119
166A	55—124	136—160	141—156	123—147	57—101
166B	54—108	121—138	125—136	113—131	57—94
167A (PALM)	18—33	34—38	33—36	34—38	19—30
168A	55—136	122—136	127—134	115—128	59—93

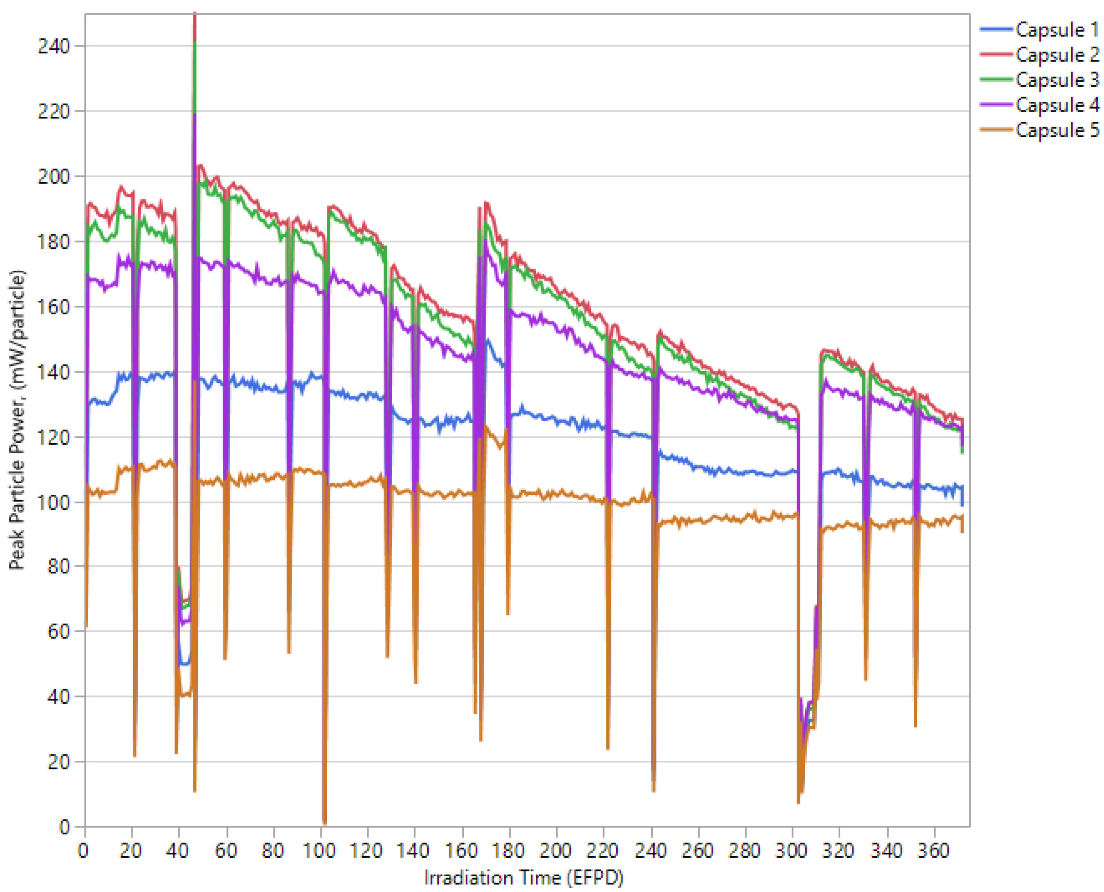

Figure 11. Calculated daily capsule-peak particle power.

2.2.2 Compact Burnup and Fast Fluence

As irradiation progressed, compact burnup and accumulated fast fluence increased to their peaks at the end of irradiation or Cycle 168A (Figure 12). The burnup and fast fluence are highest near the ATR active core midplane, where the reactor neutron flux is the highest (Figure 12). Fluence and burnup increased the least during short PALM cycles, especially the two intermittent PALM cycles, Cycles 163A and 167A, when only about 3 EFPDs accumulated (Table 4) over approximately a week of irradiation. This is because the ATR NE lobe power was only ~5MW instead of the normal 17-20 MW range for most of fuel power period, except for the last day. During these two low-power cycles, the AGR-5/6/7 fuel compacts accumulated a very insignificant burnup from 0.15 (Capsules 1 and 5) to 0.30% FIMA (Capsules 2, 3, and 4) per capsule on average.

The end-of-irradiation compact burnups ranged from 5.66 to 15.26% FIMA (Table 7). The highest compact burnups occurred in Capsule 2 (located just below the ATR active core midplane) and the lowest compact burnups occurred in Capsule 1 (located on the bottom of the test train). Specifically, Compacts (2-7-4) and (2-8-4) in Capsule 2 had the highest burnups at 15.26% FIMA and Compact (1-1-2) in Capsule 1 had the lowest burnup at 5.66% FIMA.

The end-of-irradiation compact fast fluence ranged from approximately 1.62 to 5.55 ($\times 10^{25}$ n/m^2, E >0.18 MeV) (Table 7). The highest compact fast fluence occurred in the middle Capsule 3 and the lowest occurred in the bottom Capsule 1. Specifically, Compacts (3-3-2) and (3-3-3) in Capsule 3 both had the highest fluence of 5.55×10^{25} n/m^2, and Compacts (1-1-1) and (1-1-2) in Capsule 1 had the lowest fluence of 1.62×10^{25} n/m^2. Even though Capsules 2 and 3 were both located near the ATR core midplane, Capsule 3 had the highest fast fluence and Capsule 2 had the highest burnup as shown in Figure 12. This is because Capsule 3 compacts had slightly reduced fission rates caused by stack shielding or thermal neutron shielding surrounding Capsule 3. The AGR-5/6/7 maximum compact fast fluence (5.55×10^{25} n/m^2) was in the same order of maximum compact fluences in the AGR-1 (4.30×10^{25} n/m^2), AGR-2 (3.53×10^{25} n/m^2), and AGR-3/4 (5.32×10^{25} n/m^2) experiments.

The fuel compact burnups (capsule-average, -maximum, and -minimum based on all fuel segments in a capsule) as a function of irradiation time are presented in Figure 13 for each capsule, and fast neutron fluences in the same manner are given in Figure 14. As expected, Capsules 2 and 3, located near the ATR active core midplane and exposed to the highest thermal-neutron levels, have the highest burnup and the least variation across compacts. Capsule 4 was exposed to slightly lower thermal-neutron levels, which led to less burnup and fluence. The bottom Capsule 1 and top Capsule 5 received the least fast fluence and accumulated the least burnup, but their burnup and fast fluence varied widely across compacts, which is consistent with the typical ATR core axial neutron profile.

The compact-average burnup and fast neutron fluence accumulated at the end of irradiation (Cycle 168A), for each of the 194 compacts are presented in Appendix B.

Table 7. Minimum, average, and peak burnup and fast fluence on compact average at the end of irradiation.

Capsule	Compact Burnup (% FIMA)			Compact Fast Neutron Fluence (10^{25} n/m^2, E >0.18 MeV)		
	Specification at the end of irradiation: Minimum > 6% for all compacts Maximum > 18% for at least one compact			Specification at the end of irradiation: Minimum >1.5 for all compacts Maximum ≤7.5 for all compacts and ≥5.0 for at least one compact.		
	Minimum Compact	Capsule Average	Peak Compact	Minimum Compact	Capsule Average	Peak Compact
5	6.75	8.20	9.40	1.67	2.57	3.40
4	12.35	13.39	14.09	4.00	4.55	5.03
3	13.58	14.45	14.95	5.18	5.43	5.55
2	13.51	14.66	15.26	4.56	5.07	5.44
1	5.66	9.12	11.68	1.62	3.18	4.40

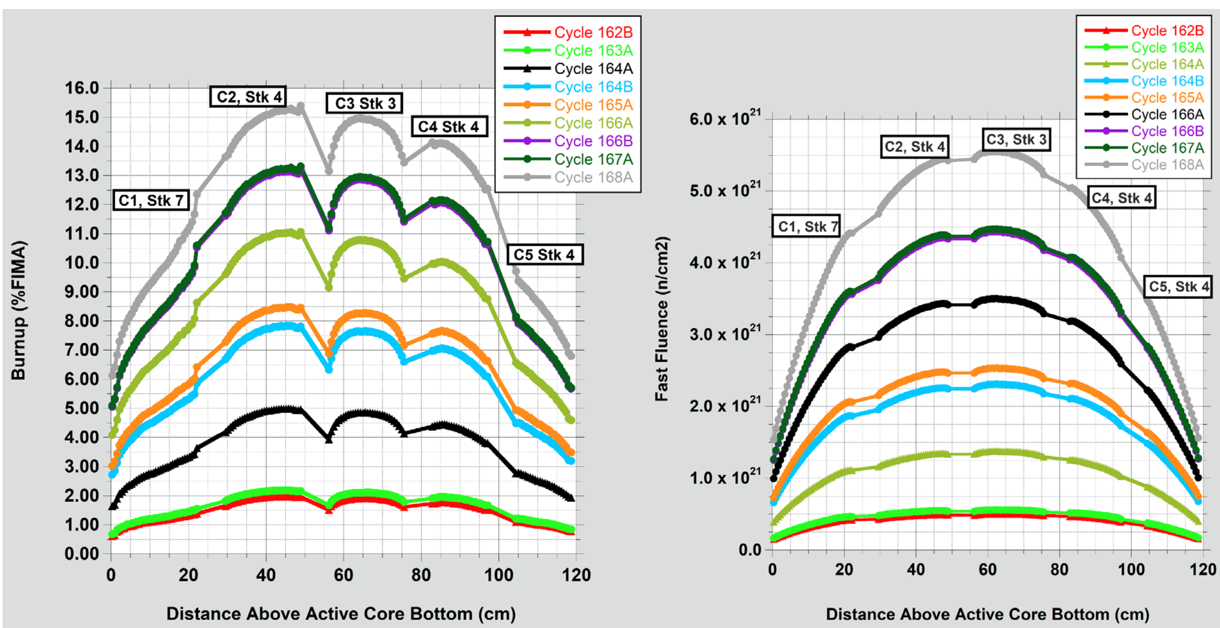

Figure 12. AGR-5/6/7 burn up and fast neutron fluence of ¼-compact segments as a function of capsule and cycle.

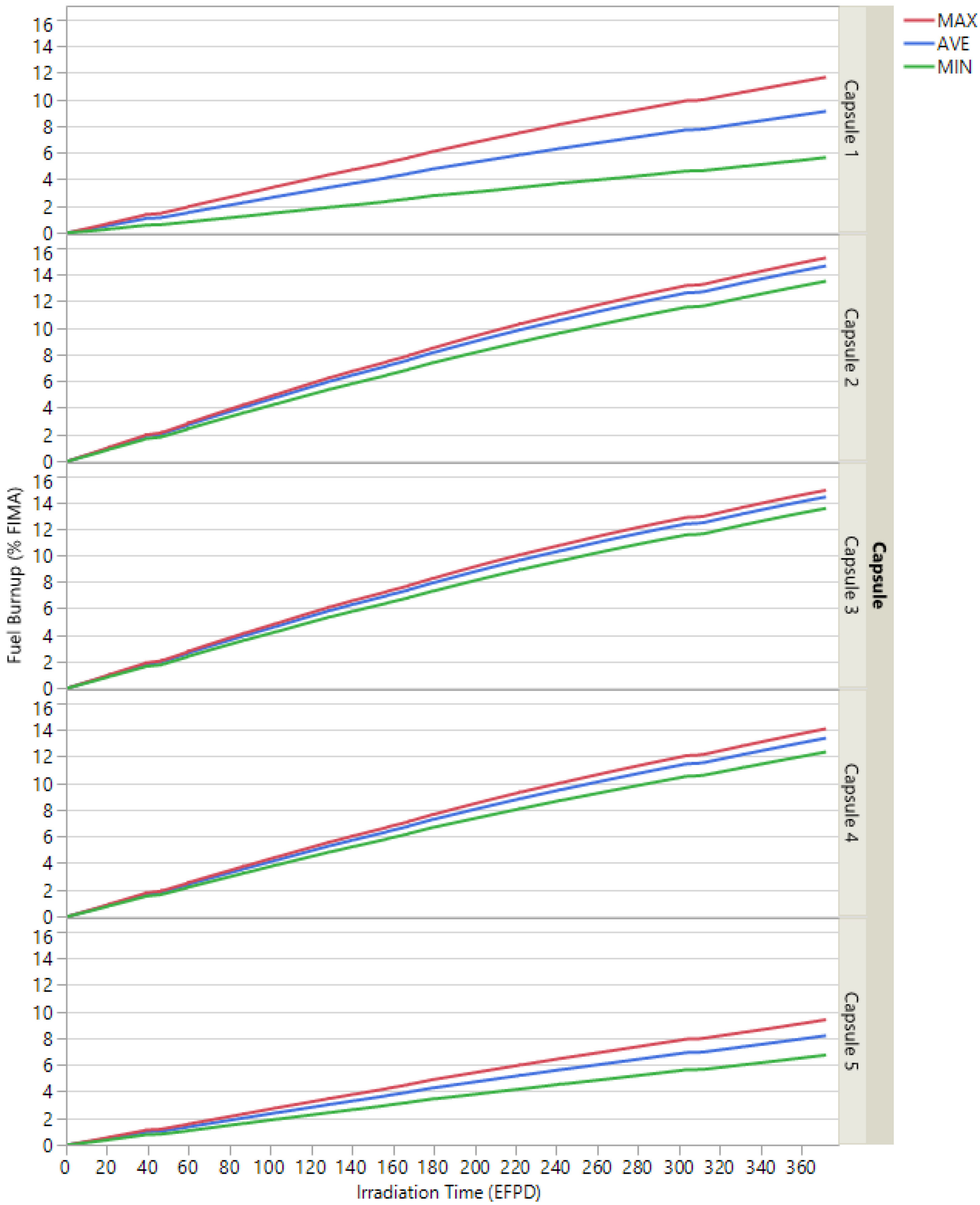

Figure 13. Burnup versus irradiation time in EFPD.

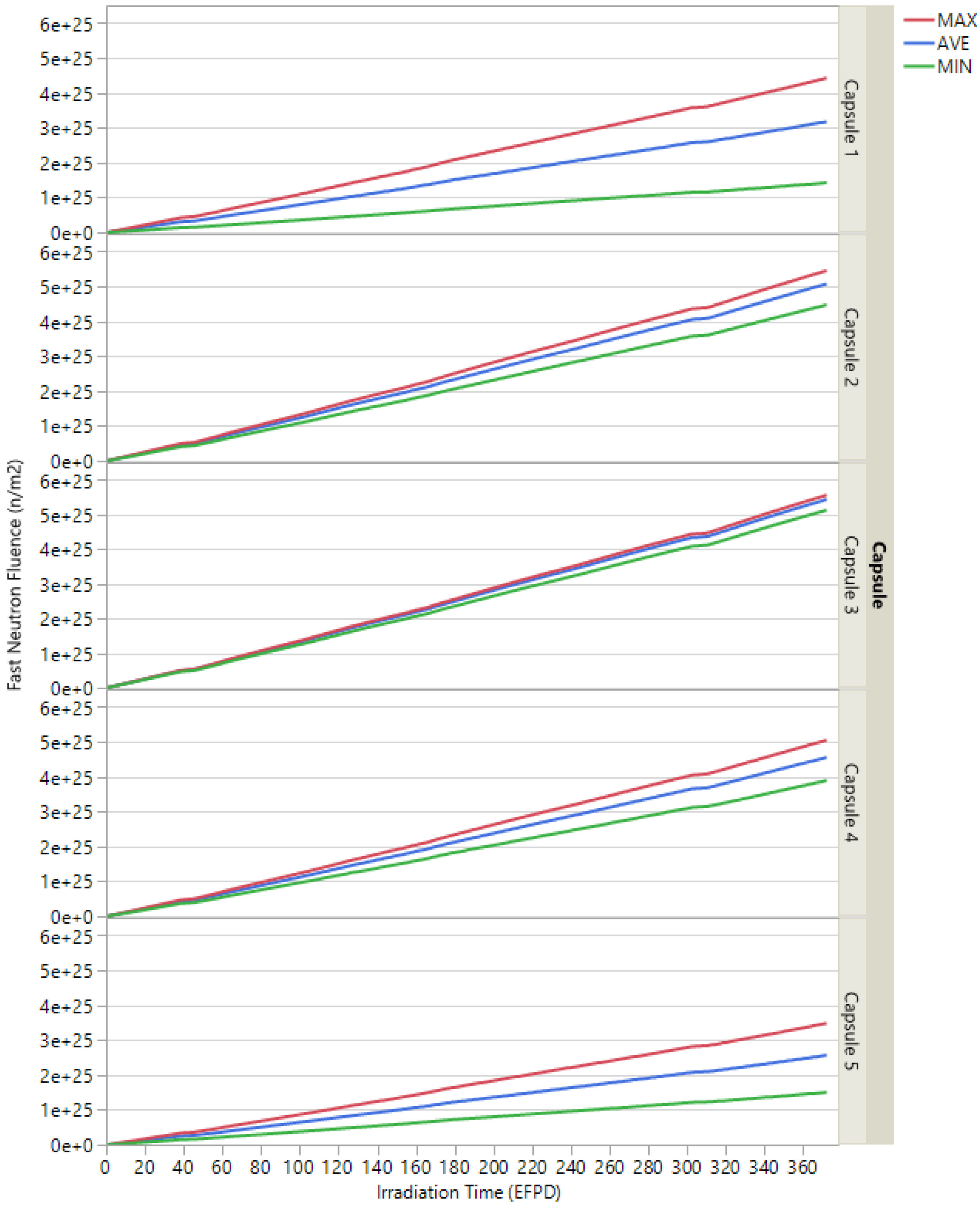

Figure 14. Fast neutron fluence (E >0.18 MeV) versus irradiation time in EFPD.

2.2.3 Compact Nuclide Inventories

Nuclide inventories for the AGR-5/6/7 compacts at the end of irradiation (end of Cycle 168A) are 1,007 isotopic concentrations (moles per compact) for each of 194 compacts, which resulted in 195,358 nuclide concentrations (194 × 1007). Then, these isotopic concentrations were decayed by three decay times of 1 day, 1 year, and 2 years after the end of irradiation. The end-of-irradiation datetime, as stored in the NDMAS database, is July 22, 2020 at 1:10 am MST. As an example, the calculated beginning-of-irradiation and end-of-irradiation actinide concentrations for Compact 2-7-4 in Capsule 2 (the highest burnup compact) are given in Table 8. At the end of irradiation, approximately 85.6% of U^{235} in Compact 2-7-4 had depleted. For all 194 AGR-5/6/7 compacts, the U^{235} mass decreased from 34.917 g at the beginning-of-irradiation to 11.849 g at the end of irradiation, which contributed to 66% of U^{235} depletion.

Table 8. Actinide isotopic concentrations at the beginning and end of irradiation for Compact 2-7-4.

Isotope	Beginning-of-Irradiation (moles)	End-of-Irradiation (moles)
U-234	6.438E−06	3.705E−06
U-235	5.903E−04	8.495E−05
U-236	2.180E−06	7.791E−05
U-238	3.181E−03	2.945E−03
Pu-239	0.000E+00	4.272E−05
Pu-240	0.000E+00	1.615E−05
Pu-241	0.000E+00	1.331E−05
Pu-242	0.000E+00	7.695E−06

The I-135 concentration was calculated for each compact at every time step for each of the nine AGR-5/6/7 ATR power cycles. However, of particular interest to researchers was the equilibrium concentration of I-135 at the end of each cycle (typically, the maximum I-135 concentration) just prior to reactor shutdown (no decay). Therefore, the end of Cycle I-135 concentrations for all compacts and all nine AGR-5/6/7 cycles were stored in NDMAS. I-135 equilibrium concentrations at end of Cycle 168A were in the range of 2.21E−08 to 3.85E−08 (moles/compact).

2.2.4 As-Run Neutronics Results Versus Requirements

Neutronics irradiation test condition requirements are the same for both AGR-5/6 and AGR-7. These requirements of compact irradiation conditions as enumerated in the AGR-5/6/7 Irradiation Test Specification (SPC-1749) are listed below with comments on the performance of the experiment with respect to each:

- *The minimum fuel compact average burnup shall be >6% FIMA for all compacts* – 191 out of 194 compacts meet this requirement; only three compacts in Capsule 1 had an average burnup between 5.66 and 6% FIMA (Compacts 1-1-1, 1-1-2, and 1-1-3).

- *The maximum fuel compact average burnup goal should be >18 % FIMA for at least one compact* – no compact met this requirement due to the reduced irradiation period of 306.9 EFPDs instead of the planned 500 EFPDs. The maximum fuel compact average burnup for the entire test train was 15.26% (Compact 2-8-4 in Capsule 2).

- *The maximum average fast neutron fluence for each fuel compact shall be ≤ 7.5×10^{25} n/m^2, E>0.18 MeV and ≥ 5.0×10^{25} n/m^2, E>0.18 MeV for at least one compact* – all compacts met requirement; no compact fluence exceeded the upper limit requirement and 48 of 194 compacts had compact average fluence > 5.0×10^{25} n/m^2, E >0.18 MeV (24 in Capsule 3, 22 in Capsule 2 and two in Capsule 4). The remaining 146 compacts had average fluence between 1.62 and 4.96×10^{25} n/m^2, E>0.18 MeV.

- *The minimum average fast neutron fluence for each fuel compact shall be >1.5×10^{25} n/m^2, E>0.18 MeV* – all compacts met requirement; the minimum compact-average fast neutron fluence is 1.62×10^{25} n/m^2, E >0.18 MeV for Compacts 1-1-1 and 1-1-2 in Capsule 1.

- *The instantaneous peak power per particle shall be < 400 mW/particle* – all particles met requirement; the highest instantaneous peak power per particle on a compact average basic is 247 mW/particle, which occurred for Compact 2-6-3 in Capsule 2 during the last day of the PALM Cycle 163A.

Even though the AGR-5/6/7 irradiation period was shortened by as much as four cycles relative to the plan, the peak burnup reached 85% of the goal and fast neutron fluences still meet their specification. This is due to measures taken during irradiation to increase fuel exposure to fast neutrons such as increasing NE lobe power above what was originally planned during some cycles and using only two lighter filters (Figure 5) instead of the three planned filters (Collin 2018).

3. THERMAL ANALYSIS

The goal for AGR-5/6 was to adequately bound the irradiation conditions expected in a HTGR. Specifically, time-average fuel temperatures from less than 900°C to over 1250°C will conservatively span a range expected in a prismatic reactor. On the other hand, the primary goal of AGR-7 was to explore the temperature margin for UCO fuel performance. A dominant fuel performance parameter is time at temperature, so the AGR-7 fuel was to be tested at a higher peak temperature of 1500°C. An instantaneous peak temperature specification of ≤1800°C for both AGR-5/6 and AGR-4 provided an operational limit to minimize the overheating of the test fuel.

3.1 Thermal Analysis Methodology

The Abaqus finite-element stress and heat transfer code (Abaqus 2014) was used to perform the daily as-run thermal analysis for the AGR-5/6/7 capsules (Hawkes et al. 2019). These calculations were performed using compact and capsule components' heat-generation rates and fast neutron fluence provided by the neutronics analysis (see Section 2.1) and with additional operational input for daily helium/neon gas-mixture compositions and flow rates. The entire AGR-5/6/7 test train was discretized by a finite-element mesh formed from approximately 1,200,000 hexahedral finite-element bricks (Figure 15). Each compact was discretized with ~3,500 of such brick elements. Abaqus Version 6.14-2 was used to create the mesh, apply boundary conditions, solve the system equations, and post-process the results.

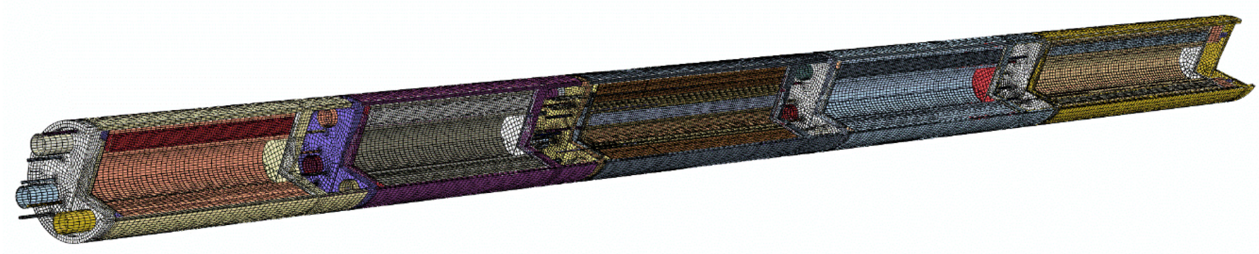

Figure 15. Cutaway view of finite-element mesh of entire capsule train.

The capsules are designed to transfer heat in the radial direction as zirconia insulators and gaps are placed on top and bottom of the capsule to insulate it in the axial direction. The top of capsule 1 is an exception as a ring spring on the bottom pushes up on the graphite holder and fuel so the capsule has good contact with the top. This was done because a lot of heat generation at the top of the fuel and it can conduct out through the top stainless-steel cap and into the coolant water. The top and bottom caps of all the capsules are tapered to remove material and hence gamma heat. There are very small gas gaps between the TC and its sheath and between the sheath and the graphite holder. The stainless-steel thru tubes and thru tube protective sleeves (molybdenum) along with TCs and gas lines protrude out the top of the top cap. Gamma heat produced from the gas lines and TCs in the thru tubes is modeled as a surface heat flux on the inside of the thru tubes.

3.1.1 Thermal Model Input Considerations

Heat rates: The heat rates are taken from results of the AGR-5/6/7 JMOCUP depletion code (Sterbentz, 2020) for the fuel compacts (fission) and graphite holders (gamma). Gamma heat rates are also implemented for the water, stainless-steel capsule walls, thru tubes, TCs, and other small components on the top and bottom of each capsule. Figure 16 shows volumetric heat generation rates of all compacts imported from the physics calculations (top at left) for Day 20 during Cycle 162B. The highest heat rates are at the top of capsule 1, as there is a lot of fissionable material closer to the core center.

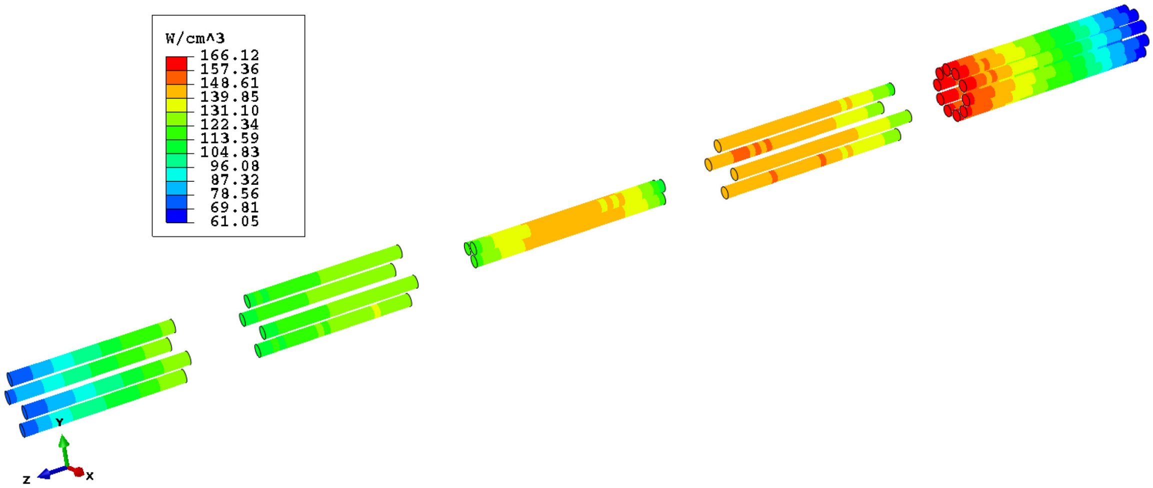

Figure 16. Compact heat generation rates imported from physics calculations.

Fuel compact: Thermal conductivity was taken from historical correlations that account for heat treatment temperature, irradiation temperature, fast neutron fluence, and the TRISO-particle packing fraction (Gontard and Nabielek, 1990). To adjust for matrix density differences, the compact matrix thermal conductivity was scaled according to the ratio of the AGR-5/6/7 compact matrix density (1.75 g/cm^3 for Capsules 2–4 and 1.73 g/cm^3 for Capsules 1 and 5) to the compact matrix density used to develop the correlations (1.75 g/cm^3). The result was then combined with particle thermal conductivity obtained from Folsom et al. (2015), following an approach described by Gonzo (2002) to obtain an effective thermal conductivity for the compact at a given TRISO-particle volume packing fraction.

Figure 17 shows the resulting three-dimensional plot of the fuel compact effective thermal conductivity varying with fast neutron fluence (E >0.18 MeV) and temperature.

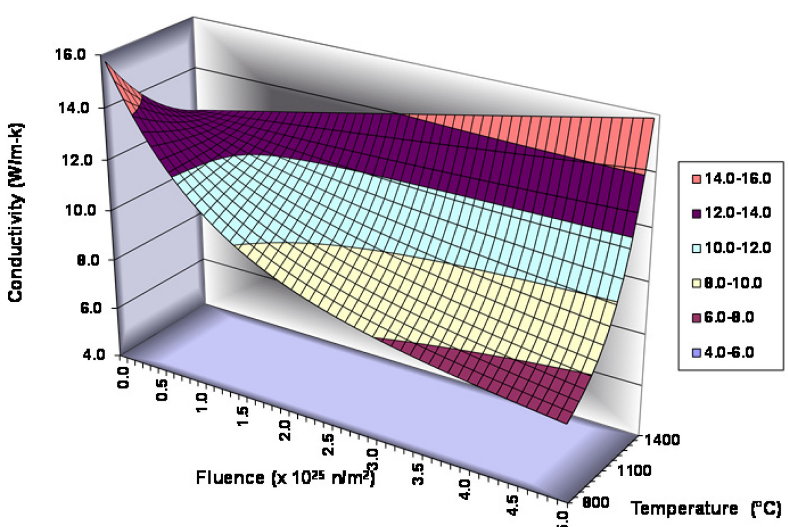

Figure 17. Three-dimensional plot of fuel compact thermal conductivity as a function of fast neutron fluence and temperature.

Graphite holder: The AGR-5/6/7 graphite holders are made of IG-430 nuclear-grade graphite. Material properties for unirradiated graphite IG-430 were determined as follows: specific heat values as a function of temperature were taken from the American Society for Testing and Materials (2014); density and expansion coefficients (measured at 20°C) were taken from Windes et al. (2017) and Swank et al. (2012); and thermal diffusivities for the temperature range 20–1000°C (left plot in Figure 18) were taken from Windes et al. (2013). Unirradiated thermal conductivity as a function of temperature is calculated as the product of the diffusivity, specific heat, and density.

The effect of irradiation on graphite thermal properties was accounted for by incorporating multipliers for thermal conductivity and thermal expansion, expressed as a function of temperature and fast neutron fluence (right plots in Figure 18 and Figure 19, respectively). These multipliers were taken from the Japanese multiplier data (Shibata et al. 2010) and used to adjust the density and thermal conductivity of the graphite holders under actual irradiation conditions. The resulting thermal conductivity of the IG-430 graphite as function of temperature and fast neutron fluence is plotted on the left of Figure 19.

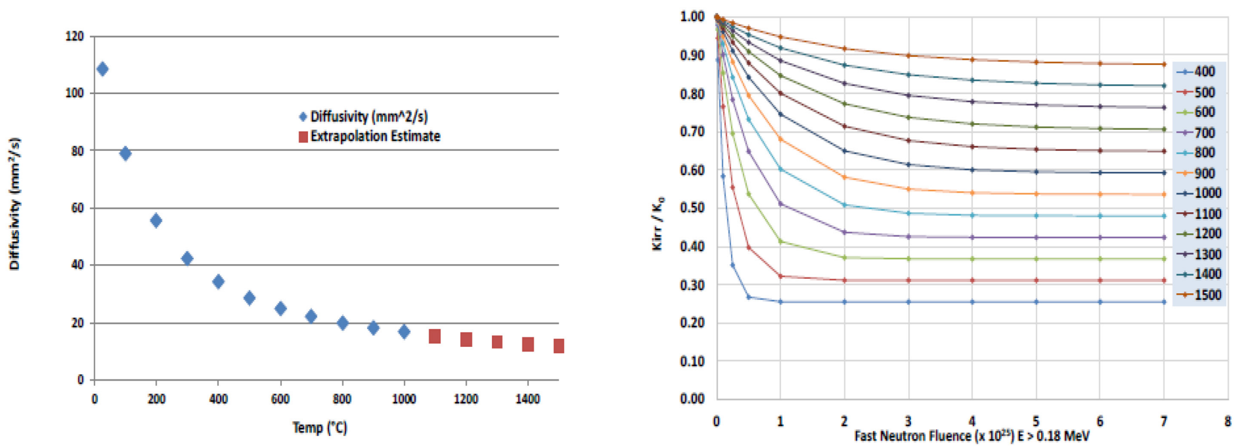

Figure 18. Unirradiated IG-430 thermal diffusivity (left) and conductivity multiplier (k_{irr}/k_0) varying with temperature and fast neutron fluence.

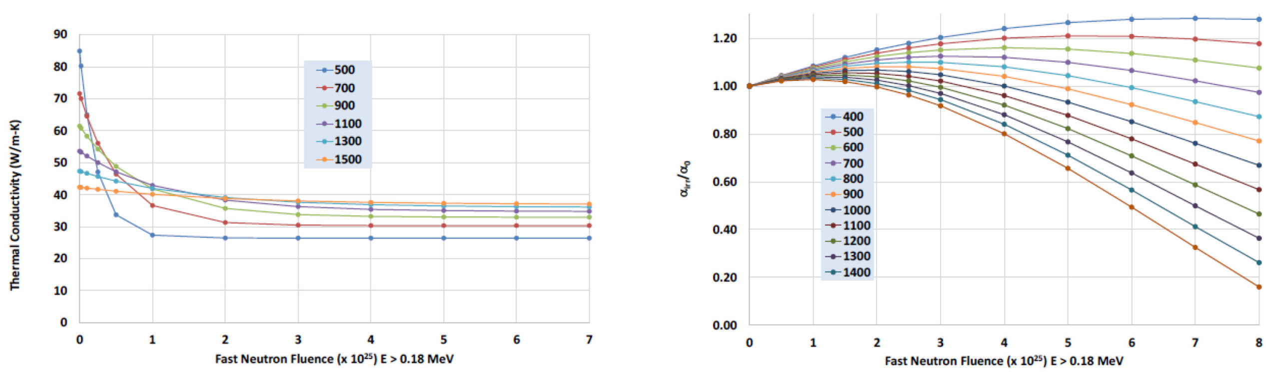

Figure 19. Thermal conductivity of IG-430 (left) and coefficient of thermal expansion multiplier (right) as function of temperature and fast neutron fluence.

Like the previous AGR models, the offset of the graphite holder was also considered in the AGR-5/6/7 thermal models. Graphite-holder offset could possibly be caused by wearing down of the nubs—due to vibration in the reactor and a slight bit of clearance between the outside of the nubs and the capsule wall—that held the holder away from the capsule wall. The impact of the holder offset can be seen in Figure 20, where the image on the right shows increased temperatures on the southwest side, as the holder is offset in the southwest direction, making a bigger gap on the southwest side. This holder offset helped in reducing residuals (measured minus calculated) for many TC locations throughout the holder(s) in each capsule. The fuel temperatures reported in Section 3.2 below were calculated by the thermal models with the same graphite-holder offset for all capsules. The TC residuals could be reduced by as much as 15 °C on average by optimizing the offset for each individual capsule as demonstrated in the conference paper (Hawkes 2020). Thus, a more thorough study attempting to minimize the residuals by adjusting the offset for each capsule could be performed in the future.

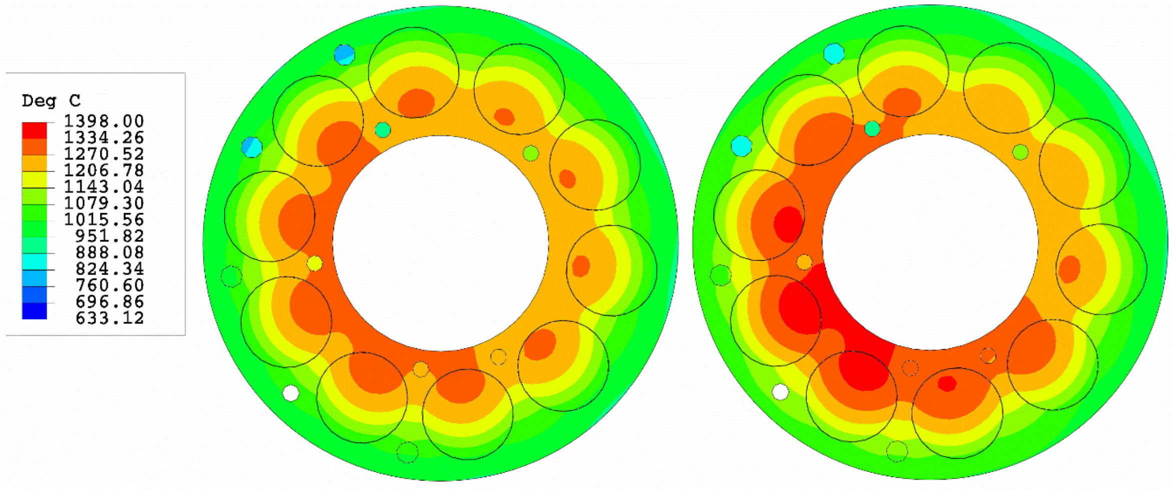

Figure 20. Straight on top-down view temperature contours of the Capsule 1 graphite holder and fuel compacts at axial midplane. Left is capsule centered; right is capsule offset 0.0254 mm in the southwest direction.

Gas Gaps: Heat produced mainly in the fuel compacts and graphite holders was transferred through the gas gaps surrounding the compacts and graphite holders via a gap-conductance model using the gap width and conductivity of the sweep gas. The heat transfer across every gap was considered by both radiation (15–20% of the heat transfer depending on the temperature of the compacts) and conduction (80–85%). Because the thermal capacitance of the sweep gas is very low, advection was not considered in the sweep gas, and it was modeled as stationary. The convective heat transfer from the sweep gas would be <0.01% of the heat transfer across the gap because of the low density, low flow rate, and low thermal capacitance.

All gas gaps were modeled as changing linearly with time in response to the graphite dimensional change with fast neutron fluence (left plots in Figure 21). The rate of diameter changes for the graphite IG-430 specimens due to fast neutron fluence was taken from (Windes 2012). The gas gap change in thermal models was modeled by having the gas-gap conductivity of each capsule change with fast neutron fluence. The thermal conductivity of the sweep gas (right plots in Figure 21) was determined using a set of correlations from Brown University for mixtures of noble gases (Kestin et al. 1984).

The gap conductance was used to calculate heat transfer across the gap between the outside of the graphite holders and the stainless-steel capsule wall. The following equations show the details of the gap conductance across this gap:

$$gap = \{r_0[\alpha(T_i - T_0) + 1]\}_{ss} - \left\{r_0\left[1 + \alpha(F,T)(T_i - T_0) + \frac{\Delta r \cdot F}{r}\right]\right\}_{holder}$$

$$gap\ conductance = \frac{k_{gas}(T)}{gap}$$

where i=instantaneous, 0= original at room temperature, Δr/r is the slope (left plots in Figure 21), $k_{gas}(T)$ is the gas mixture thermal conductivity (right plots in Figure 21), and $\alpha(F, T)$ is the coefficient of thermal expansion, which is the product of the unirradiated coefficient of thermal expansion and the irradiated multiplier presented on the right side of Figure 19.

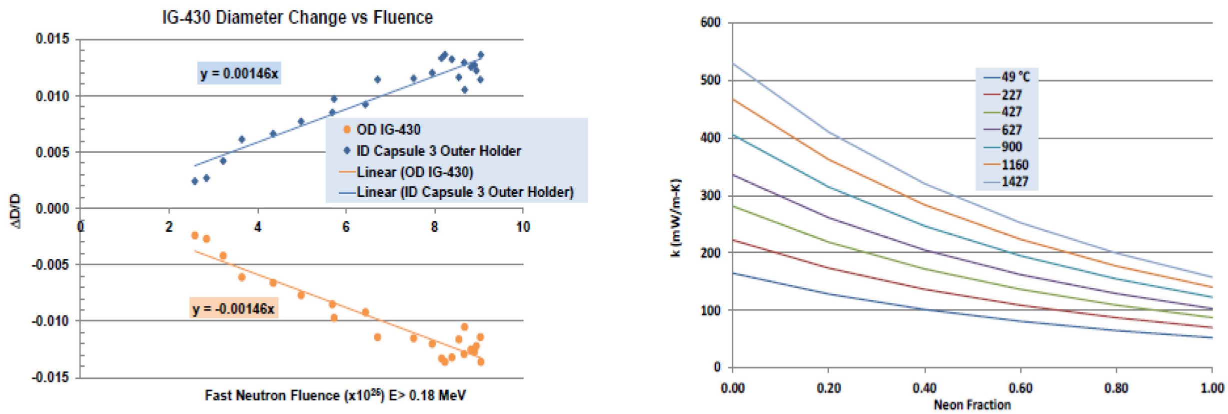

Figure 21. Inner (ID) and outer (OD) diameter change of IG-430 holder as function of fast neutron fluence (left) and of thermal conductivity of the helium-neon gas mixture as a function of the neon fraction and temperature (right).

3.1.2 Thermal model outputs

The thermal model provides daily temperature distributions for all components of the AGR-5/6/7 capsules, including fuel compacts and TC locations. Figure 22 shows a typical temperature distribution for the entire AGR-5/6/7 test train, and Figure 23 shows a temperature contour plot cutaway view of the graphite holder and fuel compacts for Capsule 3. As expected, Capsule 3 is the hottest capsule, followed by Capsule 1. Capsule 5 is the coldest of the capsules.

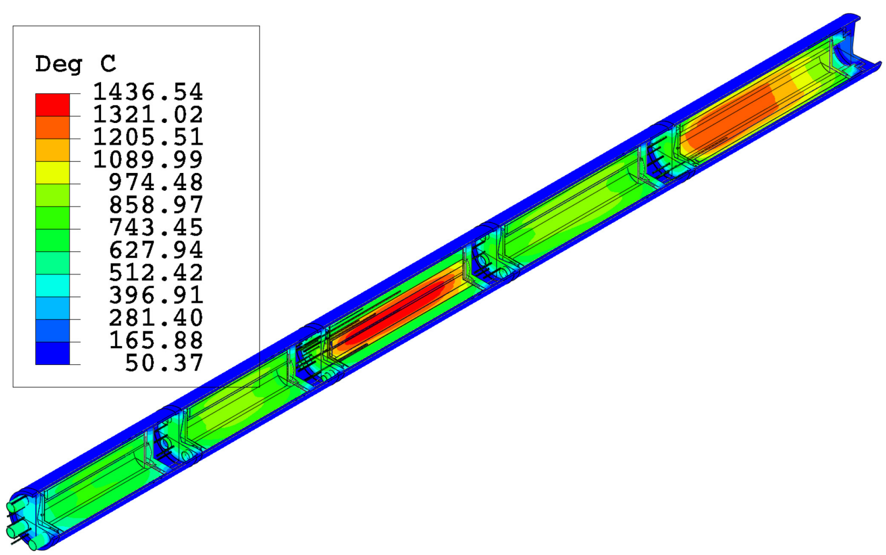

Figure 22. Cutaway view of temperature distribution of entire test train.

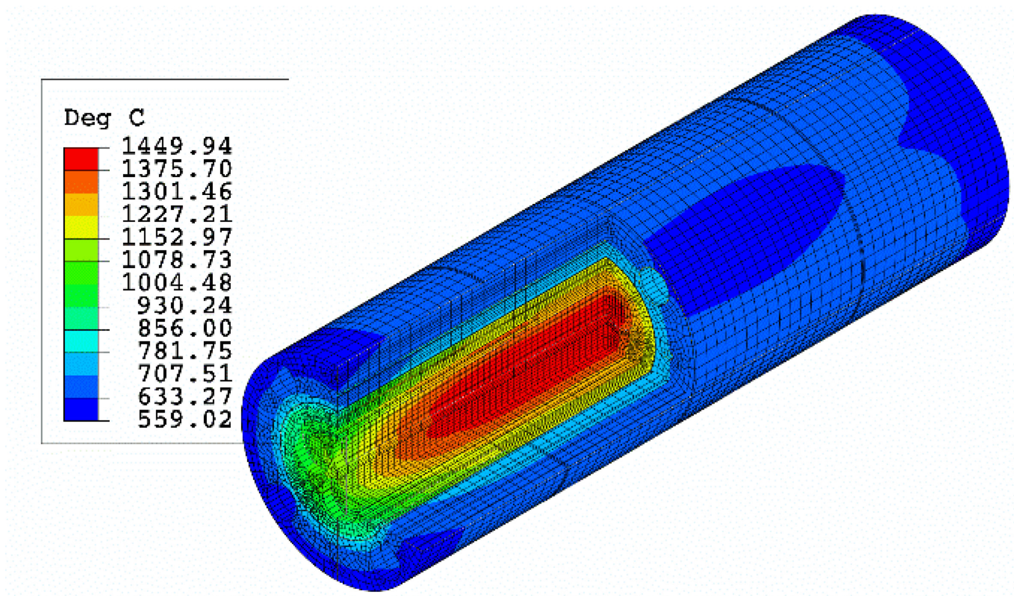

Figure 23. Temperature contours plot cutaway view of Capsule 3 graphite holder and fuel compacts.

3.1.3 Thermal Model Performance

The AGR-5/6/7 thermal models predict temperatures for all TCs in addition to temperatures for each finite element of all compacts. TC readings during the first cycle (Cycle 162B) were used to calibrate the AGR-5/6/7 thermal model, adjusting input parameters within their expected ranges to achieve the best match between measured and predicted TCs. Figure 24 shows a history plot of the TC residual temperatures (measured minus calculated) for all full power days for all cycles. A modest match between calculated and measured TCs during the first cycle was achieved. The continuing good match between measured and calculated TCs for Cycles 163A–168A indicates that thermal models simulate the thermal conditions well.

Capsule 5 shows excellent agreement between the measured and calculated TC temperatures and Capsule 4 shows good agreement, with mostly negative TC residuals indicating the model slightly overpredicts capsule temperature. Capsule 2 TC residuals varied within a wider range (between -60°C and 60°C) and Capsule 1 has an even larger variation in predictions compared to actual TCs. However, the TC residuals in Capsules 1 and 2 lie on both sides of the horizontal line at zero, indicating that the current thermal model provides a reasonable fit to data. Capsule 3 had a good agreement during the first four cycles, but TC residuals were much larger during the last three cycles, which might indicate an unexpected change in the Capsule 3 gas gap that impacted temperature at TC locations but was not captured by the thermal model. The TC residual plots over time ended when the TCs failed.

Verification that the calculation executed properly was done by both technical checkers and a post-processing of calculated data, which are documented in ECAR-5633 (Hawkes 2021). The uncertainty quantification for the AGR-5/6/7 calculated temperatures will be addressed in a separate document.

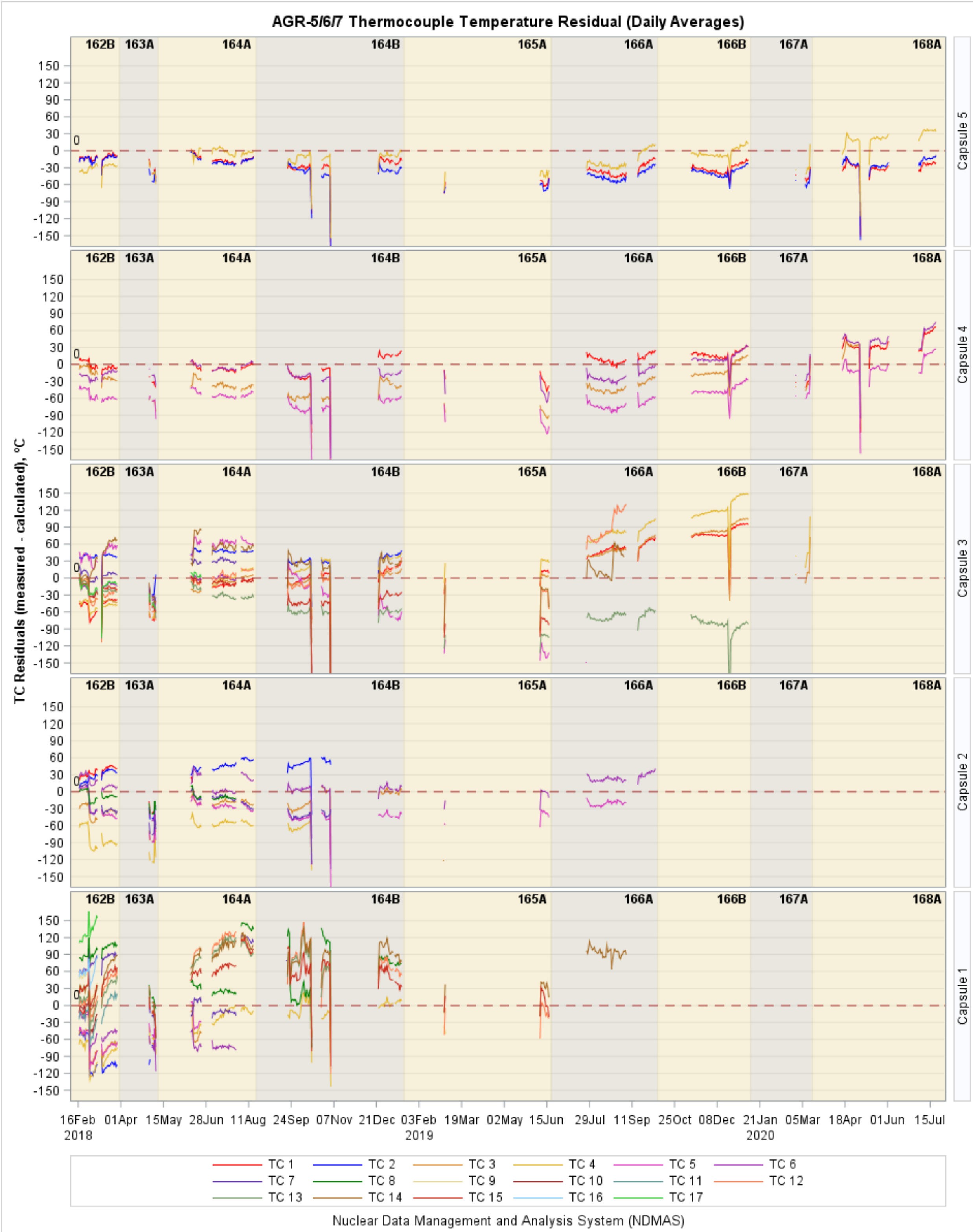

Figure 24. Difference between measured and calculated temperature for TCs in AGR-5/6/7 capsules.

3.2 As-Run Daily Fuel Temperatures

The AGR-5/6/7 thermal model provides detailed temperatures calculated for each finite-element volume of the entire test train. The detailed temperatures of 194 fuel compacts are used to calculate daily instantaneous and time-averaged values for minimum, volume-averaged, and maximum (or peak) fuel temperatures per compact and per capsule for each time step (or each day).

Figure 25 shows the calculated daily fuel temperatures (capsule minimum, capsule maximum, and capsule-average) for each of the five capsules of the AGR-5/6/7 test train versus irradiation time in EFPD. Figure 26 show the corresponding time-average minimum, time-average maximum, and time-average volume-average fuel temperatures versus time for the five capsules. During the last ATR cycle (Cycle 168A), the gas flow for Capsule 1 was isolated after purging the capsule with pure neon flow before powering up for this cycle (Pham 2021). However, some of gas from the leadout could enter Capsule 1 through a break in the capsule gas line, which could increase the Capsule 1 neon fraction from zero to the leadout neon fraction. This leak rate is unknown, and therefore the Capsule 1 neon fraction was not known with certainty during Cycle 168A, which led to a high uncertainty in Capsule 1 calculated temperatures. Therefore, Capsule 1 temperatures can only be bounded from the minimum value at zero neon fraction (darker-color dots in Figure 25) and the maximum value at the leadout neon fraction (light-color dots in Figure 25). The instantaneous temperature differences between these two cases during Cycle 168A are approximately 200°C.

The instantaneous fuel temperatures remained relatively constant in all capsules for most cycles, except for the two low-power PALM cycles, Cycles 163A and 167A. This is because fuel compact heat rates were considerably lower during these PALM cycles (Figure 10). Therefore, the time-average temperature calculations were performed for two scenarios: include all nine cycles and exclude the two low-power PALM cycles (Cycles 163A and 167A). The daily plots of time-average fuel temperatures are presented in Figure 26 for both scenarios. The time-average values of the volume-average and peak compact temperature at the end of irradiation for both scenarios are presented in Table 9 for each capsule and each experiment. The exclusion of two low-power PALM cycles increases the end-of-irradiation time-average temperatures between 20 and 30 °C. The instantaneous peak temperature from all volumes and all timesteps for each capsule and experiment are also included in Table 9.

Table 9. Peak and time-average temperature (°C) per capsule and experiment. The two time-average values given in some cells correspond to values with and without the inclusion of data from low-power PALM Cycles 163A and 167A.

Capsule and Experiment	Instantaneous Peak Temperature	Time-average Minimum Temperature	Time-average Average Temperature	Time-average Peak Temperature
All Capsule 5 compacts	983	458 / 467	741 / 756	847 / 864
All Capsule 4 compacts	1091	546 / 558	839 / 857	950 / 970
All Capsule 2 compacts	1039	536 / 546	817 / 833	929 / 948
All Capsule 1 compacts (0 Cap 1 Ne)	1386	579 / 588	984 / 1001	1210 / 1231
All AGR-5/6 compacts (0 Cap 1 Ne)	**1386**	**458 / 467**	**898 / 914**	**1210 / 1231**
All AGR-7 Capsule 3 compacts	**1536**	**969 / 989**	**1289 / 1313**	**1405 / 1432**
All Capsule 1 compacts (LO Ne)	*1386*	*614 / 624*	*1022 / 1041*	*1244 / 1267*
All AGR-5/6 compacts (LO Ne)	*1386*	*458 / 467*	*918 / 936*	*1244 / 1267*

The minimum, volume-averaged and peak values of time-averaged temperatures at the end of irradiation for all 194 compacts are presented in Appendix B for both scenarios (with and without Cycles 163A and 167A).

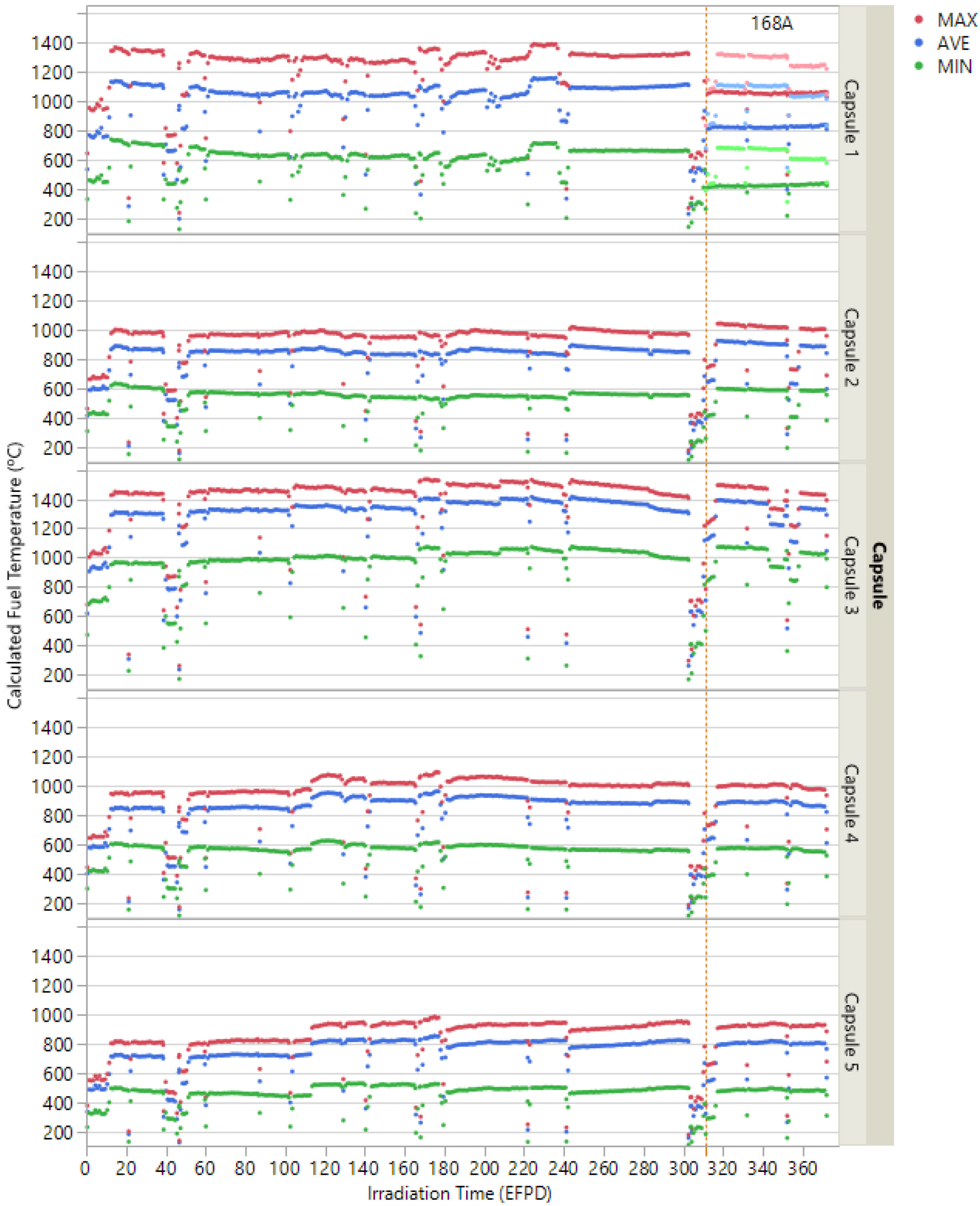

Figure 25. Calculated daily minimum, maximum, and volume-averaged fuel temperatures (light color dots for Capsule 1 are for the assumed leadout neon fraction instead of zero).

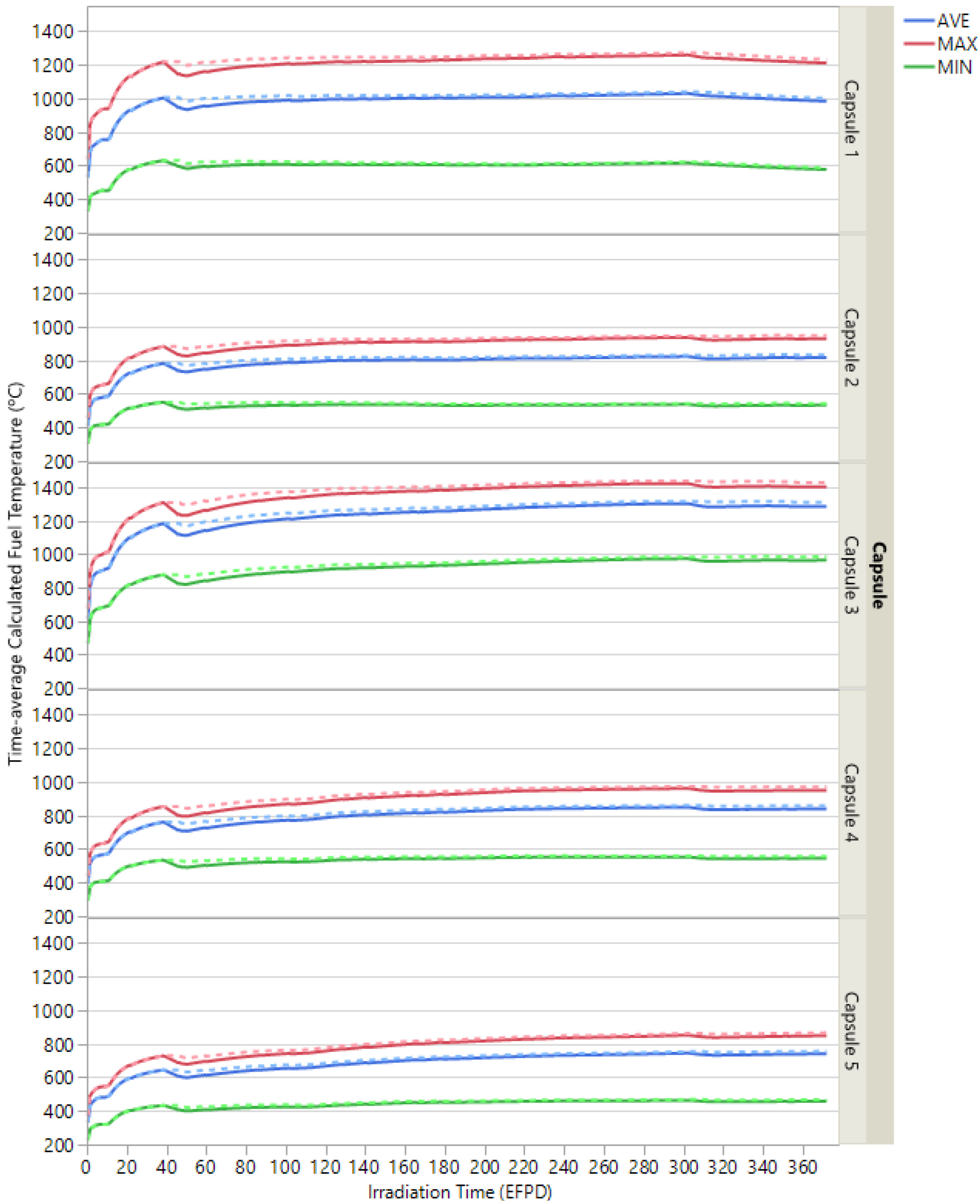

Figure 26. Calculated time-averaged minimum, time-averaged maximum, and time-averaged volume-averaged fuel temperatures: solid lines were calculated using all days, and the dashed lines were calculated by excluding the two low-power PALM Cycles 163A and 167A. We assumed that the neon fraction was zero in Capsule 1 during Cycle 168A.

3.3 Fuel Temperature Distributions

Requirements for the AGR-5/6 fuel temperatures (Capsules 1, 2, 4, and 5) included the time-average temperature distribution goals. Thus, the detailed calculated temperatures for all fuel finite-element volumes are used to determine fractions of particles that were exposed to each temperature range to compare against these requirements.

Instantaneous fuel temperature distributions

Capsule 1 contained the largest number of compacts (90 out of 170 compacts) that were exposed to the widest range of temperatures, between 400°C and 1400°C. The remaining three capsules in the AGR-5/6 portion of the experiment (Capsules 2, 4, and 5) contained 80 compacts total and were exposed to lower temperatures, between 400°C and 1050°C. Therefore, only Capsule 1 contributed to the two highest temperature ranges (T5:1250–1350°C and T4:1050–1250°C) and contributed most of the middle range (T3:900–1050°C), while the other three capsules only contributed to the three low temperature ranges (T1:<600, T2:600–900°C, and T3:900–1050°C), as shown in Figure 27. Capsule 1 temperatures were high for most of the irradiation, except during the two low-power PALM cycles (Cycles 163A and 167A) when temperatures in all capsules were significantly lower and during the last cycle (Cycle 168A), when the capsule was purged prior to the cycle with pure helium. During these three cycles, no fuel in Capsule 1 contributed to the two highest temperature ranges, T4 and T5, as shown in Figure 27, if we assumed that the capsule remained on pure helium throughout the cycle.

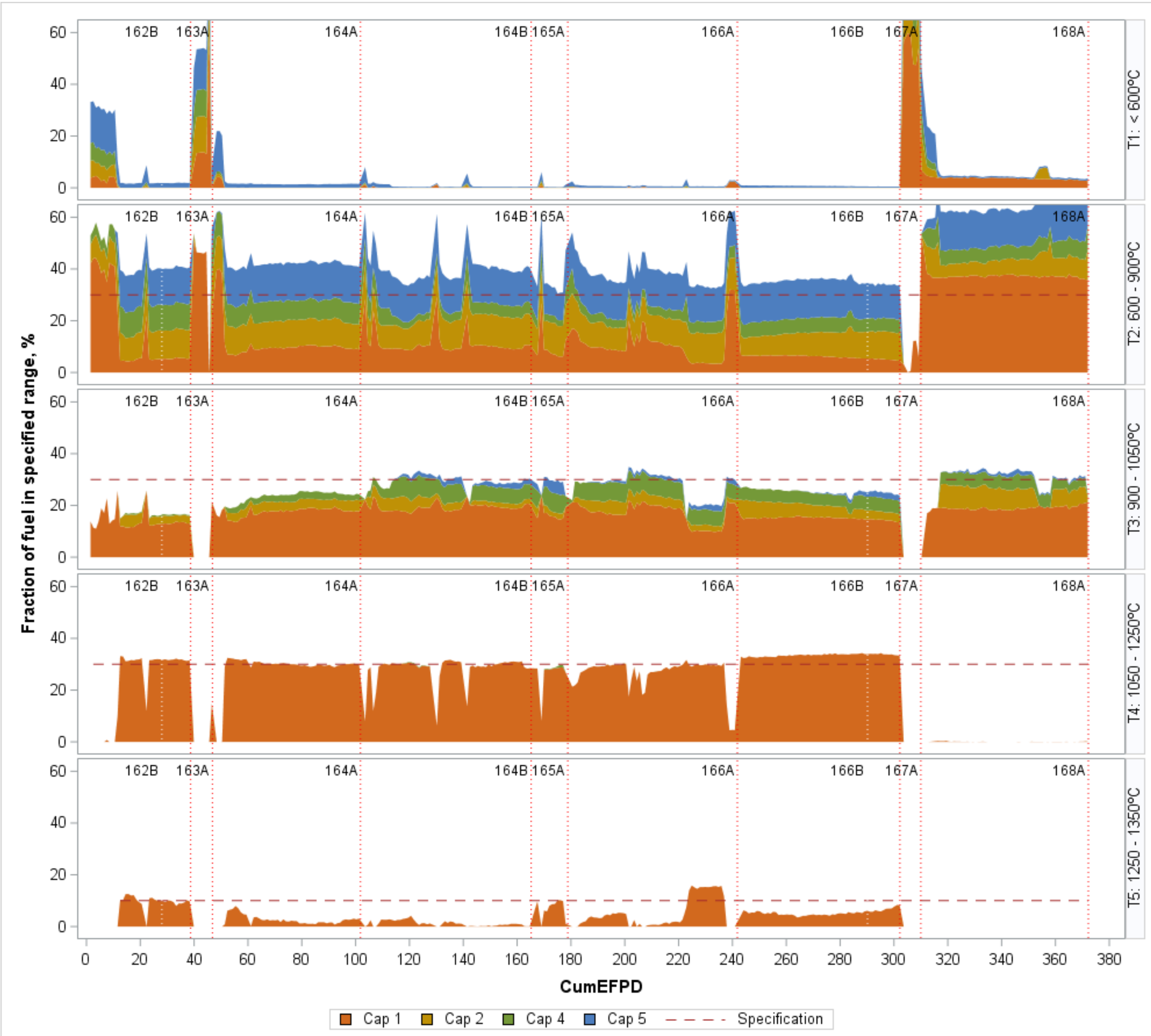

Figure 27. AGR-5/6 daily fuel fraction by instantaneous temperature range and capsule.

Requirements for AGR-7 Capsule 3 temperatures were only associated with peak temperatures. However, the fuel proportion by temperature range plot was also calculated for Capsule 3 (Figure 28). During the two low-power PALM cycles, Cycles 163A and 167A, Capsule 3 temperatures were mostly lower than 900°C; whereas, in other cycles Capsule 3 peak fuel temperatures could be more than 1500°C.

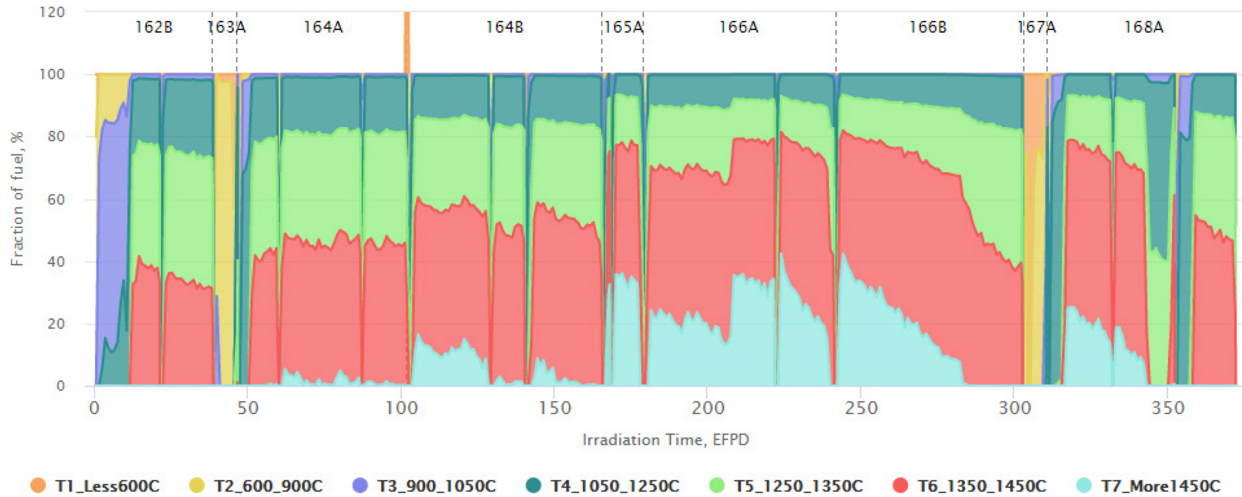

Figure 28. AGR-7 Fuel fraction by instantaneous temperature range as function of irradiation time.

Time-average fuel temperature distributions

To determine the time-average fuel temperature distribution, the time-average temperatures of each finite volume over the entire irradiation were calculated then the fuel volumes were binned into the specified temperature ranges for each day.

The data during the two low-power PALM cycles, Cycles 163A and 167A, were excluded from the time averaging calculation of fuel distribution due to negligible fuel burnup during these cycles. AGR-5/6 fuel fractions by time-average temperature range and capsule are presented in Figure 29 and AGR-7 Capsule 3 fuel fractions are presented in Figure 30. AGR-5/6/7 proportions of fuel particle within a temperature range are shown in Table 10 for two options: exclude Cycles 163A and 167A and include nine cycles (in parenthesis). Also, we assumed zero neon fraction for Capsule 1 during Cycle 168A.

Table 10. Time-averaged fuel temperatures distribution at the end of irradiation for AGR-5/6 capsules.

Temperature Range	Contributing Capsule(s)	Actual Data	Specification
AGR-5/6 Experiment – Capsules 1, 2, 4, and 5			
< 600 °C	1, 2, 4, 5	1.0% (1.3%)	-
≥ 600 °C and < 900 °C	1, 2, 4, 5	47.5% (51.5%)	30%
≥ 900 °C and < 1050 °C	1, 2, 4	27.3% (25.9%)	30%
≥ 1050 °C and < 1250 °C	1	24.2% (21.3%)	30%
≥ 1250 °C and < 1400 °C	1	0.0% (0.0%)	10%

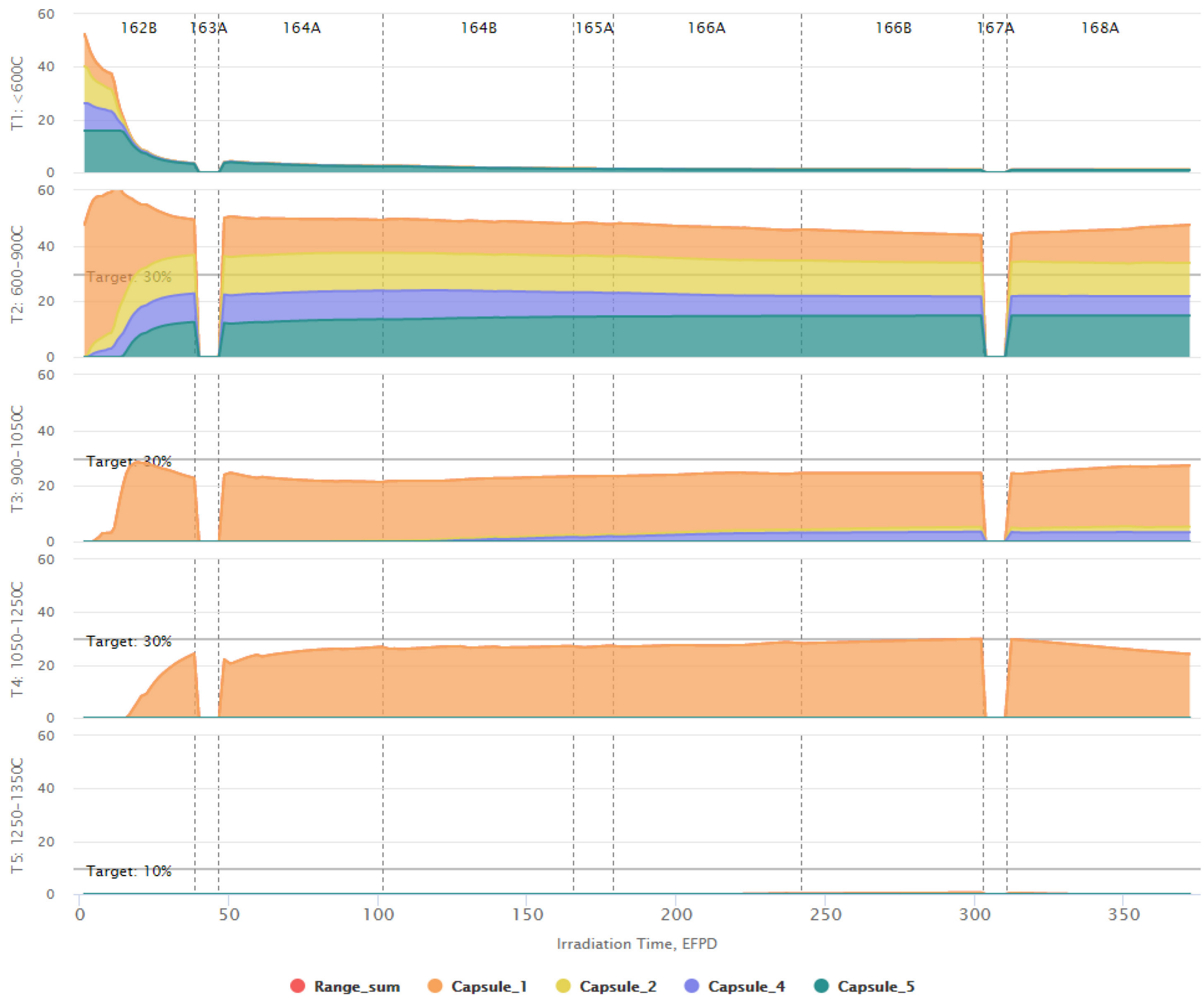

Figure 29. AGR-5/6 fuel fractions by time-average temperature range and capsule (excluded Cycles 163A and 167A).

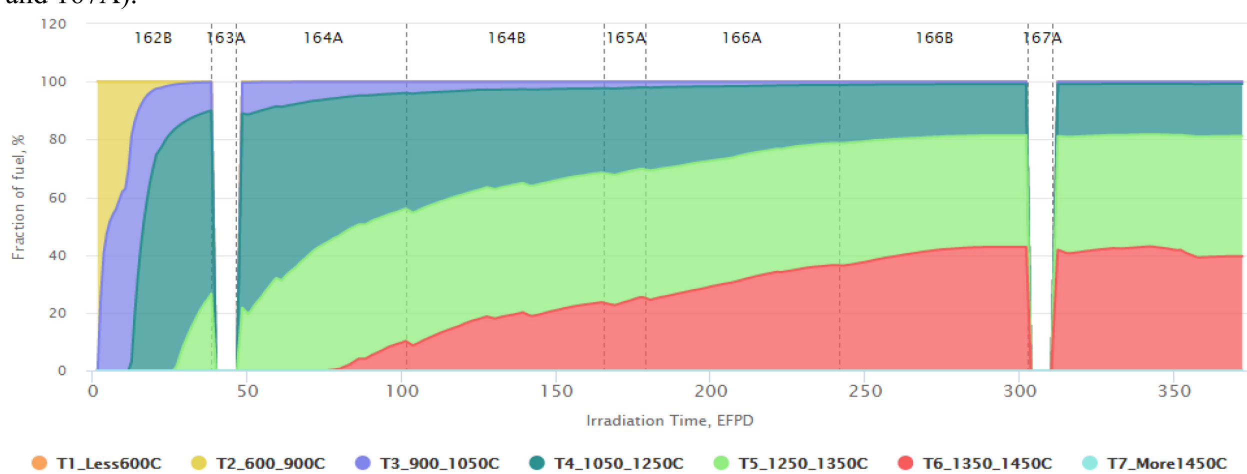

Figure 30. AGR-7 fuel fractions by time-average temperature range (excluded Cycles 163A and 167A).

3.4 As-Run Temperatures Versus Requirements

A range of irradiation fuel temperatures were specified for each AGR-5/6 capsule to achieve the desired fuel-compact temperature distribution in the test train per SPC-1749. This goal led to time-averaged target irradiation temperatures from under 900°C to over 1250°C, which conservatively spans the range expected in a prismatic reactor. The primary goal of AGR-7 was to demonstrate the available performance margin with respect to temperature for UCO fuel; thus, its fuel was tested with a higher time-averaged peak temperature target of 1500°C.

The requirements for fuel compact irradiation temperatures as enumerated in the AGR-5/6/7 Irradiation Test Specification SPC-1749 are listed below with comments on the performance of the experiment with respect to each:

AGR-5/6 Requirements

- *The instantaneous peak temperature for each capsule shall be ≤1800°C* – met requirement. The instantaneous peak temperature reached the highest temperature of 1386°C for fuel compacts in Capsule 1 (Table 9) during Cycle 166A.
- *The time average, peak temperature goal should be 1350 ± 50°C* – lower than requirement. Time-average peak temperature was 1231 °C (in Capsule 1), when the two low-power PALM cycles, Cycles 163A and 167A were excluded and a zero-neon fraction was used for Capsule 1 during Cycle 168A.
- *The time average, minimum temperature goal should be ≤700°C* – met requirement. Time average, minimum temperature is 467 °C (in Capsule 5), when the two low-power PALM cycles, Cycles 163A and 167A, were excluded.
- *The time average temperature distribution goals* – the portion of fuel in the lowest temperature range was higher than anticipated, and no fuel reached the highest temperature range:
  - *≥600°C and <900°C for about 30% of the fuel – 47.5%* actual
  - *≥900°C and <1050°C for about 30% of the fuel – 27.3%* actual
  - *≥1050°C and <1250°C for about 30% of the fuel – 24.2%* actual
  - *≥1250°C and <1400°C for about 10% of the fuel – 0.0%* actual.

AGR-7 Requirements

- *The instantaneous peak temperature for each capsule shall be ≤1800°C* – met requirement. The instantaneous peak temperature reached the highest temperature of 1536°C for fuel compacts in Capsule 3 (Table 9) during the high-power PALM Cycle 165A.
- *The time average, peak temperature goal should be 1500 ± 50°C for at least one capsule* – slightly lower than the requirement. The time-average peak temperature was 1432 °C (in Capsule 3), when the two low-power PALM cycles, Cycles 163A and 167A were excluded (Table 9).

4. FISSION GAS RELEASE ANALYSIS

The performance of a nuclear fuel test is typically evaluated using the R/B ratio, which is the ratio of the released activity of an isotope from the fuel to the predicted creation rate of the isotope during irradiation (or birthrate). For all AGR experiments, the following 12 isotopes were monitored: Kr-85m, Kr-87, Kr-88, Kr-89, Kr-90, Xe-131m, Xe-133, Xe-135, Xe-135m, Xe-137, Xe-138, and Xe-139. These nuclides were selected because they are chemically inert fission-product gases with relatively short half-lives, allowing each isotope to reach equilibrium concentration in the fuel during each cycle. The as-run FG release analysis results for AGR-5/6/7 experiment are documented in ECAR-5352 (Scates, 2021). This ECAR is used as a basis for the qualification of the FG release data.

4.1 Fission Gas Release Analysis Methodology

The FPMS described in Section 1.2.5 was used to measure isotope activities, which were crucial input to quantify release rates for each capsule. These release rates and calculated birthrates were used to calculate the capsule R/B ratios for the radionuclides of interest.

4.1.1 Birth Rate Calculation

Birthrate is the rate of production for a specific isotope. Birthrate is different than isotopic inventory in that the production of an atom is a birth, even if it is immediately lost to transmutation or decay. The birth rates of the noble gas fission products of interest were calculated using ORIGEN2 Version 2.2 (Croff, 1983). These calculations used compact flux and reactions rates from MCNP (LANL, 2004). The ORIGEN2 libraries were modified to remove the isotope depletion procedures (transmutation and decay) for the isotopes of interest to calculate their birth rates. The increase in the concentration of the isotope during the irradiation time interval divided by the irradiation time interval was determined to be the isotope birth rate of the isotope during the time interval.

After the end of each ATR cycle, daily depletion calculations were performed to provide the FPMS team with the daily birthrates of the 12 selected isotopes for each capsule. The as-run JMOCUP physics depletion methodology and calculated results for the AGR-5/6/7 irradiation experiment are documented in ECAR-5321 (Sterbentz, 2020).

4.1.2 Release Rate Calculation

Spectrometer detector systems measured the activities of the 12 selected krypton and xenon isotopes in the sweep gas released from each capsule. Normally, 8-hour counting intervals were used to measure isotope concentrations. To correct for the radionuclides' decay in transit from the capsule to the counters, the actual transport time for each capsule was calculated from outlet-gas flow rates and the capsule-specific volumes through which samples flowed to reach the respective monitoring detector. At equilibrium, given a measured activity, A_a (Bq) or A (mCi) —the radionuclide activity in the sample volume a, R_c (atoms/s) or R (mCi) —release rate of a particular nuclide can be calculated as (Scates, 2021):

$$R_c = \frac{A_a e^{\frac{\lambda \cdot V_t}{f}}}{1-e^{\frac{-\lambda \cdot V_S}{f}}} \quad \text{or} \quad R = 3.17\,x\,10^4 \frac{A \cdot e^{\frac{\lambda \cdot V_t}{f}}}{1-e^{\frac{-\lambda \cdot V_S}{f}}}$$

where V_S is the sample volume (mL), λ is the nuclide-decay constant (s^{-1}), f is the capsule volumetric flow rate (mL/s), and V_T is the transport volume from the capsule to the sample volume (mL). The first exponential involving the transport volume (V_T) accounts for decay before reaching the sample volume, while the remaining factor (V_S) accounts for the decay while passing through the sample volume. Transport volumes for the five AGR-5/6/7 capsules were determined based on data from the leadout flow experiment performed at the beginning of irradiation (Scates, 2021).

The estimated uncertainty in R_c can be determined from standard error propagation techniques as:

$$\sigma_{R_c}^2 = \left[\left(\frac{R_c}{A_a}\right)^2 \cdot \sigma_{A_a}^2\right] + \left[\left(\frac{R_c \cdot \lambda}{f}\right)^2 \cdot \sigma_{V_t}^2\right] + \left[\left(\frac{R_C \cdot \lambda \cdot e^{\frac{-\lambda \cdot V_S}{f}}}{f \cdot \left(1 - e^{\frac{-\lambda \cdot V_S}{f}}\right)}\right)^2 \cdot \sigma_{V_s}^2\right],$$

where $\sigma_{A_a}^2$, $\sigma_{V_t}^2$, and $\sigma_{V_s}^2$ are the uncertainties in terms of variance for the radionuclide activity, transport volume, and sample volume, respectively.

The conversion formula for the capsule release rate is valid only if the FG species remains entrained in the effluent gas, traveling through the gas lines and sample volume at the constant flow rate. Therefore, alongside the measurement uncertainties for FG activity, transport and sample volumes, the uncertainty of the calculated release rate for AGR-5/6/7 capsules was also influenced by the following factors:

- Any species trapped prior to exiting the sample volume.
- Large variations in the flow rate during acquisition: outlet flow rates varied the most for Capsule 1 between approximately 2 sccm and 58 sccm (excluding zero flow during the gas line isolation) and for the other four capsules, between 40 and 70 sccm. The flow rate used in the conversion formula was the average over time of the spectrum acquisition.
- Differences in capsule design can influence the time that FG isotopes lingered inside each capsule.
- Pressure variations for the five capsules and leadout also contribute to uncertainty of the outlet flow.

4.1.3 Gross Gamma Data for Particle Failure Detection

For each capsule, the sweep gas carries released fission-product gases from the capsule to the corresponding detector system, which uses a thallium-doped sodium iodide (NaI[Tl]) detector to measure GG count rates. The GG counts were recorded every 3.5 seconds, which resulted in a large amount of GG data. The temporal GG count profile can help detect each fuel-particle failure up to the first 250 failures. A particle failure would cause a rapid rise and drop (or spike) in the temporal profile of the measured GG-count rate and raise the baseline gamma count afterwards. The spike is the result of a sudden release of stored fission-product inventory inside a just-failed particle, which can be visually detected from data plots. However, accurate particle failure detections can be difficult when multiple failures occur at once and in the presence of possible FG leakage into the capsules. Therefore, the GG count data should be used in combination with other supporting evidence to determine particle failures, such as associated spikes in isotope activities.

4.1.4 Issues in Gas Flow System

Capsule 1 gas line problems started from Cycle 164B and had a significant impact on the interpretation of the FG release data; therefore, they are discussed in this section.

Sweep-gas parameters are mass-flow rates for each constituent gas and moisture content. Moisture content measurements (measured on the outlet side of the capsule and compared to the gas-supply verification measurement) provide indicators of capsule integrity. The mass-flow rates for each constituent gas, measured at the inlet line for each capsule and the leadout, are referred to as inlet flow rates; the total mass-flow rates, measured at each capsule outlet line, are referred to as outlet flow rates. An additional mass-flow rate is measured at the FPMS. In general, inlet gas flow rates for the five AGR-5/6/7 capsules and leadout (Figure 31and Figure 32) are much higher than the previous AGR experiments (up to 60 sccm versus 30 sccm for the other AGRs). However, Capsule 1 gas flow rates from Cycle 164B were significantly lower and were largely at zero during two cycles, Cycles166B and 168A (Figure 31), due to its gas line problems. In addition, the outlet and FPM flow rates for the leadout were zero for the first six cycles 162B–166A, when its outlet isolation valve was closed as intended, but they became high flow rates during the last three cycles 166B–168A, when the leadout outlet isolation valve was opened (Figure 32).

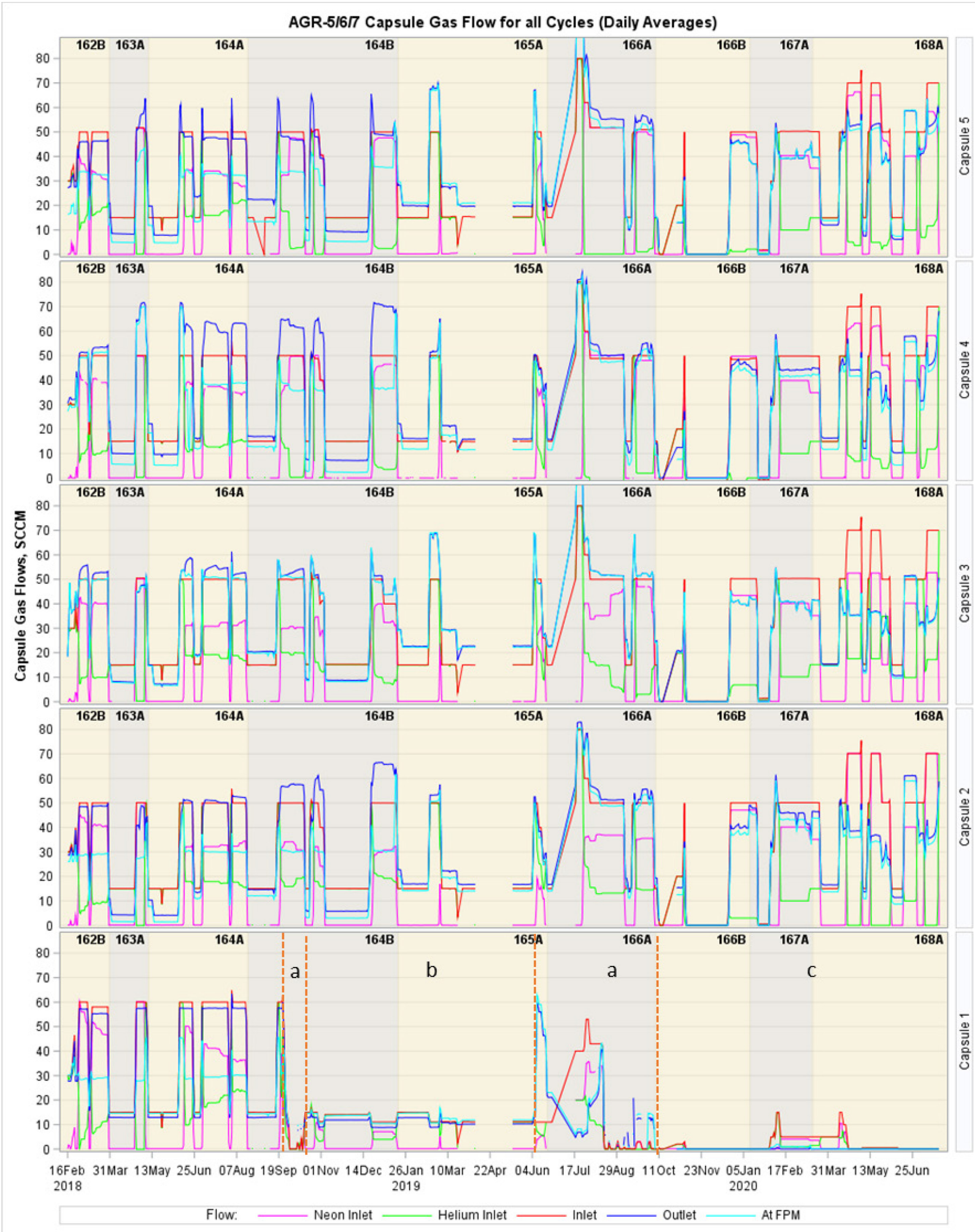

Figure 31. Capsule sweep gas flow rates with Capsule 1 flow history: a) intermittent flow, b) stabilized low flow rate, and c) mostly isolated gas line with an unsuccessful attempt to reestablish flow during Cycles 167A and 168A.

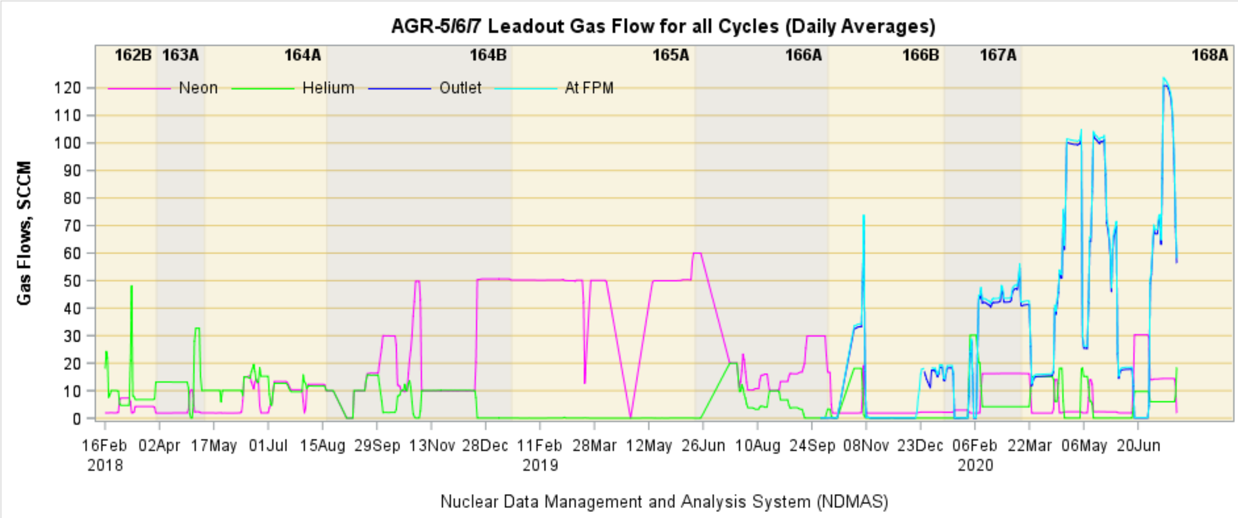

Figure 32. Lead-out sweep-gas flow rates: outlet isolation valve was opened from Cycle 166B.

By design, a nominal helium/neon mixture flow at a higher pressure than the capsule pressure was provided via a mass-flow controller into the lead-out cavity, which then flowed into the common plenums between capsules. The intent of this design was to prevent capsule-to-capsule cross gas leakage ensuring FG signatures remain separated by capsule. However, about half-way through irradiation a clog and then a crack formed in the Capsule 1 outlet line (Figure 33) that prevented its FGs from sweeping out to the detector as intended. Instead, some of the Capsule 1 FGs diffused out, contaminated gas in the leadout, and then entered other capsules. To mitigate this issue, the leadout pressure was reduced to below the capsule pressures and the leadout outlet isolation valve was opened, allowing the leadout contaminated gas to flow to spare Detector 6. This arrangement allowed some gas flow from Capsules 2–5 to the leadout, limiting FG leakage into Capsules 2–5 from the leadout. Consequently, capsule inlet flows are higher than outlet flows (red lines are higher than blue lines in Figure 31 for Capsules 2–5 from Cycle 166B), and the leadout outlet and FPM flow rates are not zero as before Cycle 166B, as shown by the blue and cyan lines in Figure 32. Details of the Capsule 1 gas line problem were documented in ECAR-5114 (Nelson, 2020). The summary of gas line events is presented in Table 11.

Table 11. Summary of gas flow in AGR-5/6/7 capsules after problem in Capsule 1 gas line.

ATR Cycle	Capsule Gas Flow History
164B	A clog developed in the Capsule 1 outlet line, leading the program to periodically shut off the gas flow through this capsule from September 23 to October 16, 2018. For part of Cycle 164B, Capsule 1 was operated in a batch mode, where the capsule was isolated and updated gas blends were sent periodically. From October 16, 2018, gas flow in Capsule 1 was successfully re-established at 11 sccm.
165A (PALM)	A crack or break in the outlet line at a point downstream of the clog caused a sudden increase in the Capsule 1 outlet flow. With a large amount of dilution gas entering the Capsule 1 exhaust line from the leadout through the crack, it was difficult to interpret the FP measurements from Capsule 1 during this time. Gas flows to the other capsules were increased and the leadout flow was increased to 50 sccm (and then to 60 sccm) to ensure that the leadout gas flow was entering Capsules 2–5 to prevent FP crosstalk between capsules.
166A	During the outage, the inlet- and outlet-gas lines for Capsule 1 were swapped to prevent FG leakage to other capsules. At this point, the Capsule 1 inlet line had a crack, so the neon/helium mixture for the leadout and Capsule 1 was kept the same, allowing the Capsule 1 neon fraction to be accurately defined. August 1–16, 2019: the clog appeared to be clearing, as indicated by an increase in outlet flow. The crack was also closing because more flow was being forced through Capsule 1. From August 16, 2019: a new clog developed in the new Capsule 1 outlet gas line causing an increase in pressure; an intermittent flow was implemented to avoid exceeding pressure limits.
166B	Flow to Capsule 1 was isolated during the entire power cycle November 9–December 21, 2019: flows to Capsules 2–5 were also suspended. Beyond December 21, 2019: flows to Capsules 2–5 were resumed, and the leadout outlet line was opened with a lower pressure, so some gas from capsules could flow out to the leadout.
167A (PALM)	Flow to Capsule 1 was isolated and the leadout outlet line was opened with lower pressure than all capsules.
168A	The flow to Capsule 1 was mostly isolated with several unsuccessful attempts to flow a small amount of gas for FG release measurement; the leadout outlet line was opened with a lower pressure than the pressure in Capsules 2–5.

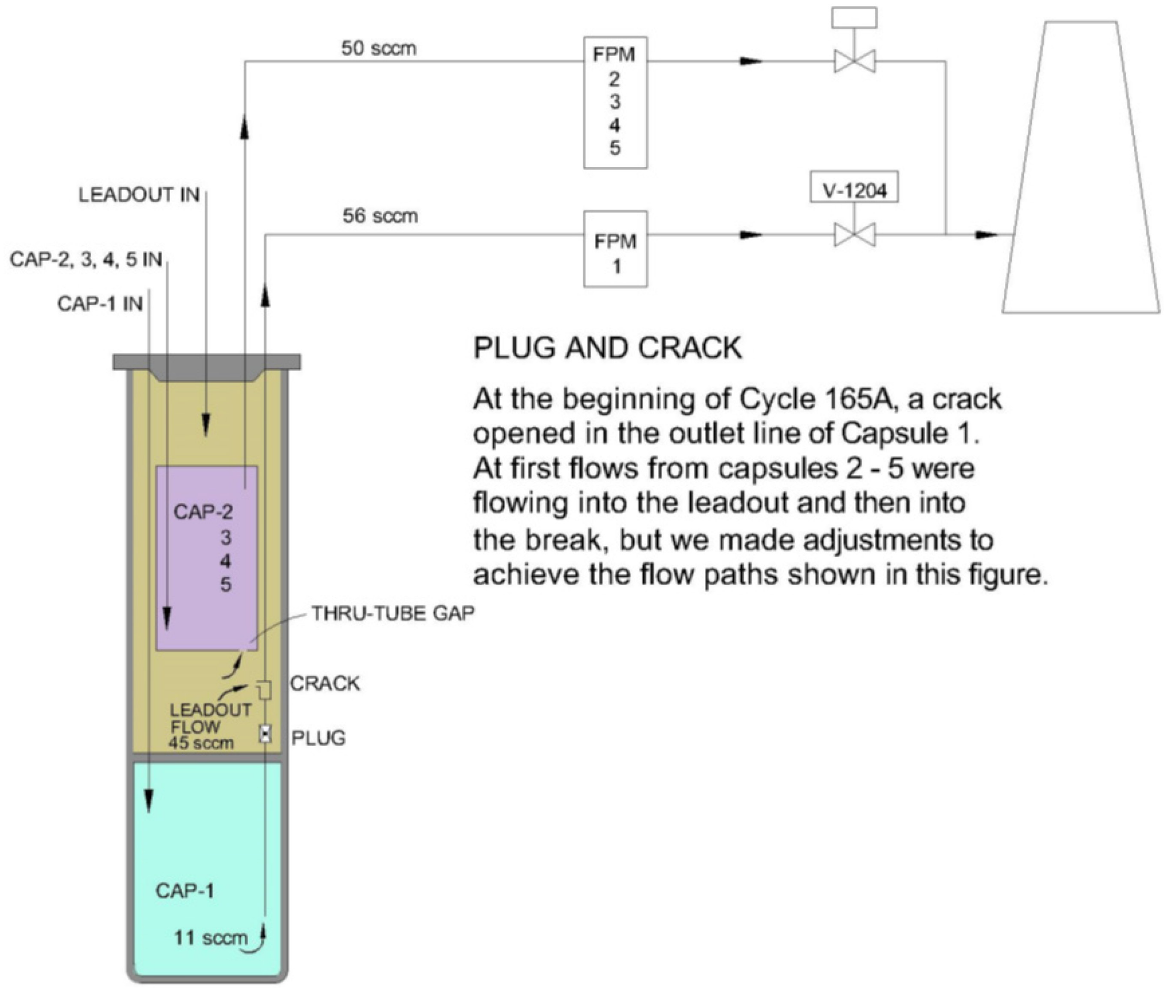

Figure 33. Simplified schematic showing the location of the initial Capsule 1 plug and crack.

4.2 As-Run Fission-Gas Release Results

ECAR-5352 (Scates 2021) detailed the calculation method used to determine release rates and R/B values from the five AGR-5/6/7 capsules for the 12 monitored FG isotopes. Release activities were reported as an average for the 8-hour counting interval during normal irradiation conditions to reduce measurement uncertainty. However, during the initial test of the leadout flow system, release rates were recorded at a much higher frequency, which led to a slightly higher uncertainty. To preclude the use of data with high measurement uncertainty in the analysis of FG release, values where uncertainties are greater than 50% are omitted. Negative values are also excluded. These filters remove data from the short leadout flow runs or incomplete measurements while leaving other runs unaffected. The daily averages of the measured capsule R/B in each of the five AGR-5/6/7 capsules for the 12 measured isotopes are presented as a function of irradiation days in Figure 34 for krypton and Figure 35 for xenon.

The gas line issues in Capsule 1 occurred from the fourth cycle (Cycle 164B) as a clog was formed somewhere downstream of the capsule outlet. This issue was managed to minimize crosstalk between capsule gas lines until the end of the fifth cycle (Cycle 165A), as indicated by the stable R/B in all capsules during Cycles 164A and 165A relative to the three earlier cycles (Figure 34 and Figure 35). Since no in-pile particle failures were detected based on the GG counts during the first five cycles, FG releases during these cycles (162B–165A) were releases from as-manufactured exposed kernel (EK) and dispersed uranium (DU) contamination. During this time, R/B ratios were stable in the 10^{-8}–10^{-6} range, on average for most isotopes (Table 12). The exception is Xe-131m with significantly higher R/Bs, 10^{-3} on average, and associated with high measurement uncertainty of 42%, on average. A higher EK fraction (EKF) and high fuel temperatures in Capsule 1 led to the maximum R/B value of around 2×10^{-6} for Kr-85m.

For the sixth cycle, Cycle 166A, FG releases, especially releases of longer half-life isotopes (i.e., Kr-85m, Kr-88, Xe-133, and Xe-135) from four capsules (Capsules 2–5) increased considerably without any indication of particle failure. Consequently, these FG increases were attributed to an increase in FP leakage from Capsule 1 as the gas line problem was worsening. By the end of Cycle 166A, a significant number of in-pile failures occurred in Capsule 1, causing a substantial increase in FG activities and saturation of the FPMS HPGe detector and increased activity in the 1A primary cubicle that housed the FPMS that was picked up by the GG NaI(Tl) detectors (Demkowicz and Pham, 2019). As a result, gas flow was suspended for Capsule 1, which led to no measured FG release data during the last three cycles (Cycles 166B, 167A, and 168A), except for a short attempt to flow gas through Capsule 1 during the short PALM Cycle 167A.

The Capsule 1 gas line issues caused FG leakage into Capsules 2–5 at various degrees over time starting from Cycle 166A. As a result, R/Bs for all capsules from Cycle 166A are considered uncertain because of undefined contamination from Capsule 1 (Scates 2021). However, they can still be used when the leaking amount from Capsule 1 can be roughly estimated or deemed negligible. For example, FG leakage from Capsule 1 for short-lived isotopes (i.e., Kr-89 and Xe-137 with a 3.2 and 3.8-min half-life, respectively) can be considerably lower due to decay before reaching Capsule 5 on top of the test train.

Table 12. AGR-5/6/7 measured R/B and uncertainty statistics for krypton and xenon isotopes for the first five cycles (162B-165A).

Isotope	Half-Life (min)	Measured R/B			Uncertainty [a] (%)		
		Average	Minimum	Maximum	Average	Minimum	Maximum
Kr-85m	268.7	3.53E-07	2.15E-10	1.95E-06	6.8	5.8	49.5
Kr-88	170.4	2.35E-07	1.16E-09	8.26E-07	6.4	5.8	24.5
Kr-87	76.0	2.88E-07	7.35E-11	1.11E-06	6.9	5.8	42.3
Kr-89	3.2	6.36E-08	5.74E-10	5.11E-07	9.7	5.8	36.2
Kr-90	0.5	1.40E-06	3.02E-09	3.44E-05	33.6	13.9	49.6
Xe-131m	17,162.0	2.60E-03	3.74E-05	3.03E-02	42.0	27.5	50.0
Xe-133	7,558.9	6.10E-07	4.28E-09	7.87E-05	17.8	6.0	50.0
Xe-135	545.8	1.47E-07	1.12E-09	9.09E-07	6.8	5.8	48.5
Xe-135m	15.3	9.89E-08	6.10E-10	6.07E-07	6.5	5.8	27.6
Xe-138	14.1	3.24E-08	5.34E-10	3.16E-07	8.8	5.8	33.8
Xe-137	3.8	5.31E-08	6.51E-11	2.71E-07	6.2	5.8	37.0
Xe-139	0.7	1.89E-08	3.72E-10	1.18E-06	33.0	9.5	50.0

[a] Only R/B values with an uncertainty under 50% and a standard 8-hour interval are used.
Green rows are for the shortest isotopes with uncertainty under 10% on average.
Red rows are for either too short or too long isotopes high uncertainty (more than 30% on average).

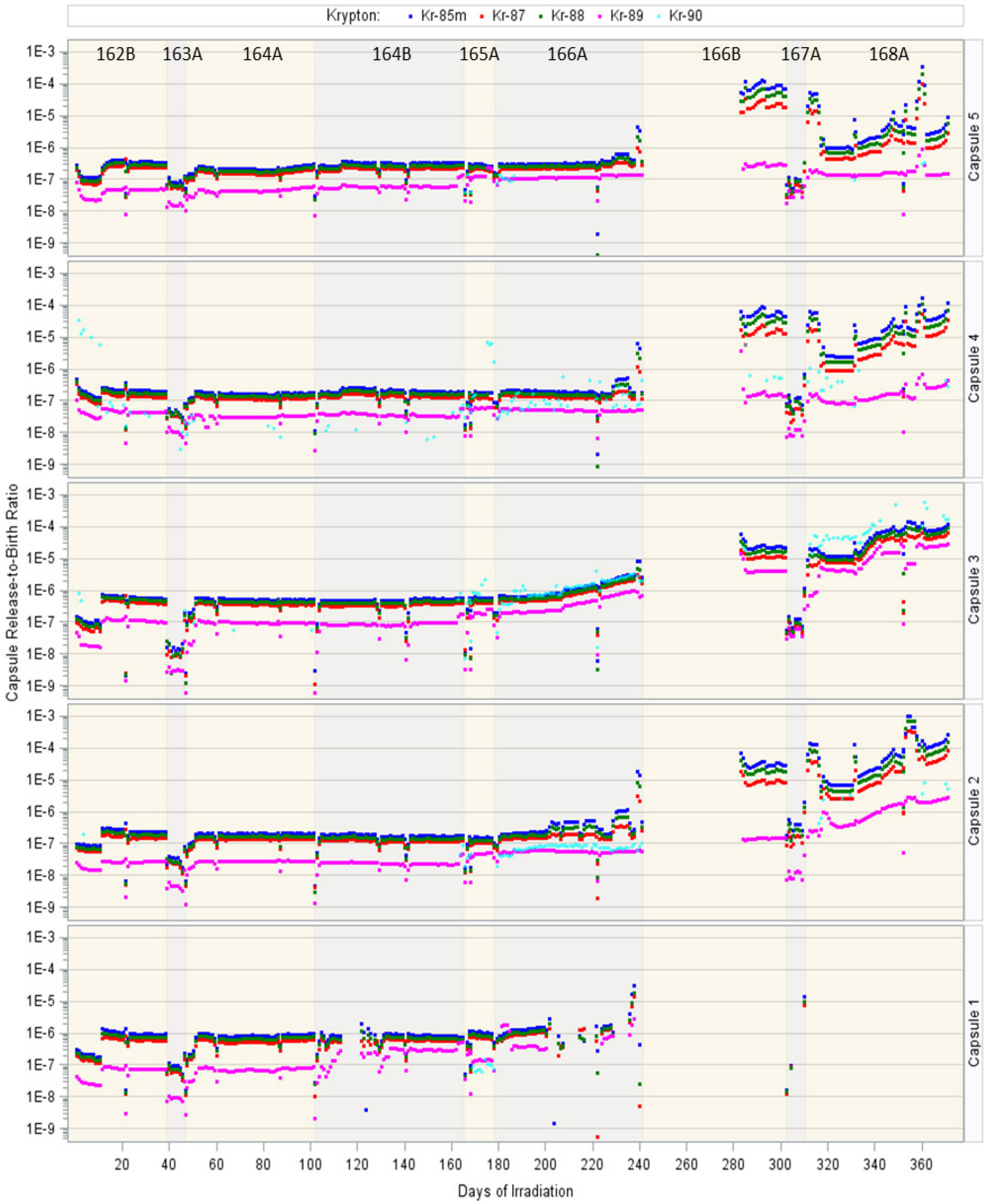

Figure 34. Measured R/B in AGR-5/6/7 capsules for krypton isotopes.

Figure 35. Measured R/B in AGR-5/6/7 capsules for xenon isotopes.

4.3 Particle Failure Estimation

Particle failure during irradiation is an important metric of fuel performance and information on failures is provided in the combined evidence from the GG detectors, gamma-ray spectrometers, and PIE. As PIE has not yet been performed, a preliminary estimate of the number of failed particles is provided here, based on the FPMS data.

4.3.1 Evidence from Gross Gamma Counts

GG counts were recorded every 3.5 seconds. Daily peak and average GG counts in five capsules and two spare detectors were plotted (Figure 36) and used to spot possible in-pile failures manifesting in substantially higher daily peaks and a subsequent increase in daily averages that cannot otherwise be explained. Areas of interest are then examined in further detail using 5-min peaks and average GG data to spot typical peak values caused by particle failure, as shown in Figure 37–Figure 40. Based on the GG record, the following inferences are made:

- For the first five cycles (Cycles 162B−165A), GG averages and peaks were low and stable in all capsules, suggesting that in-pile particle failures did not occur (Figure 36).
- For PALM Cycle 167A, the ATR reactor was at full power for less than a day, and fuel temperatures were significantly lower in all capsules, which resulted in low GG counts, except for the last data point at the end of the cycle. No evidence of failure is apparent.
- For the three remaining regular cycles (Cycles 166A, 166B, and 168A), the GG count averages increased in all capsules relative to previous cycles, and numerous significant peaks were evident in several capsules. Therefore, a more detailed look at the 5-minute GG plots is presented in Figure 37–Figure 40. Apparent evidence of failure is as follows:
    - For Cycle 166A, Figure 37 shows a period when GG counts in all capsules started to increase as issues with the gas flow through Capsule 1 worsened, apparently causing leakage to other capsules. Many particle failures appeared to occur in Capsule 1 between September 30 and October 4, 2019 (near the end of Cycle 166A), as indicated by numerous GG spikes accompanied by a consistent increase in GG averages and FG releases. For the other four capsules, minor spikes were synchronized across capsules, which can be attributed to the response of the other capsule GG detectors, which picked up the increased activities in the 1A primary cubicle caused by the substantial increase in FG activities in the Capsule 1 gas line. In addition, FG leakage from Capsule 1 into the leadout gas, and subsequently, into Capsules 2–5, the leadout slip joints, could also have resulted in increased GG counts for these capsules.
    - For Cycle 166B, flow to all capsules was suspended for most of this cycle, except for the period between December 22, 2019 and January 11, 2020, when gas flows were resumed for Capsules 2–5 (Figure 38). No spikes indicative of particle failures were evident in Capsules 2–5 during this time. The leadout flow, which contained significant amount of FG that originated in Capsule 1, was routed through the spare FPMS Station 6 (Spare 1) located near FPMS Stations 4 and 5, which led to noisy GG counts for these capsules.
    - For Cycle 168A, significant GG spikes occurred during two periods:
        - During the first period (Figure 39), several spikes in Capsule 2 and numerous spikes in Capsule 3 appeared to indicate particle failures. The temporal pattern of these spikes did not appear to indicate a transfer of contamination through the capsule train, as in previous increases in the GG counts in those capsules. In contrast, no clear spikes were apparent in Capsules 4 and 5, so fluctuations in the GG counts in those capsules are inferred to represent FG leakage from Capsule 1.
        - During the second period (Figure 40), synchronized spikes were observable for Capsules 2–4, and that pattern of increase is, again, attributed to FG leakage from Capsule 1.

In conclusion, based on GG data during Cycle 168A, a few failures appear to have occurred in Capsule 2 and numerous failures likely occurred in Capsule 3. There was no strong evidence that particle failures occurred in Capsules 4 and 5. Although it is clear that a large number of failures occurred in Capsule 1 by the end of Cycle 166A, the exact number of failures for the remainder of the experiment was not definable because the FPMS gas flow through that capsule was halted during the last three cycles. An attempt was made by the FPMS staff to estimate the number of in-pile failures in Capsules 2–5 based on manually aligning spikes in GG counts and peaks in hourly isotope activities for long-lived isotopes, such as Xe-133. That study also concluded that particle failures occurred only in Capsules 1, 2, and 3.

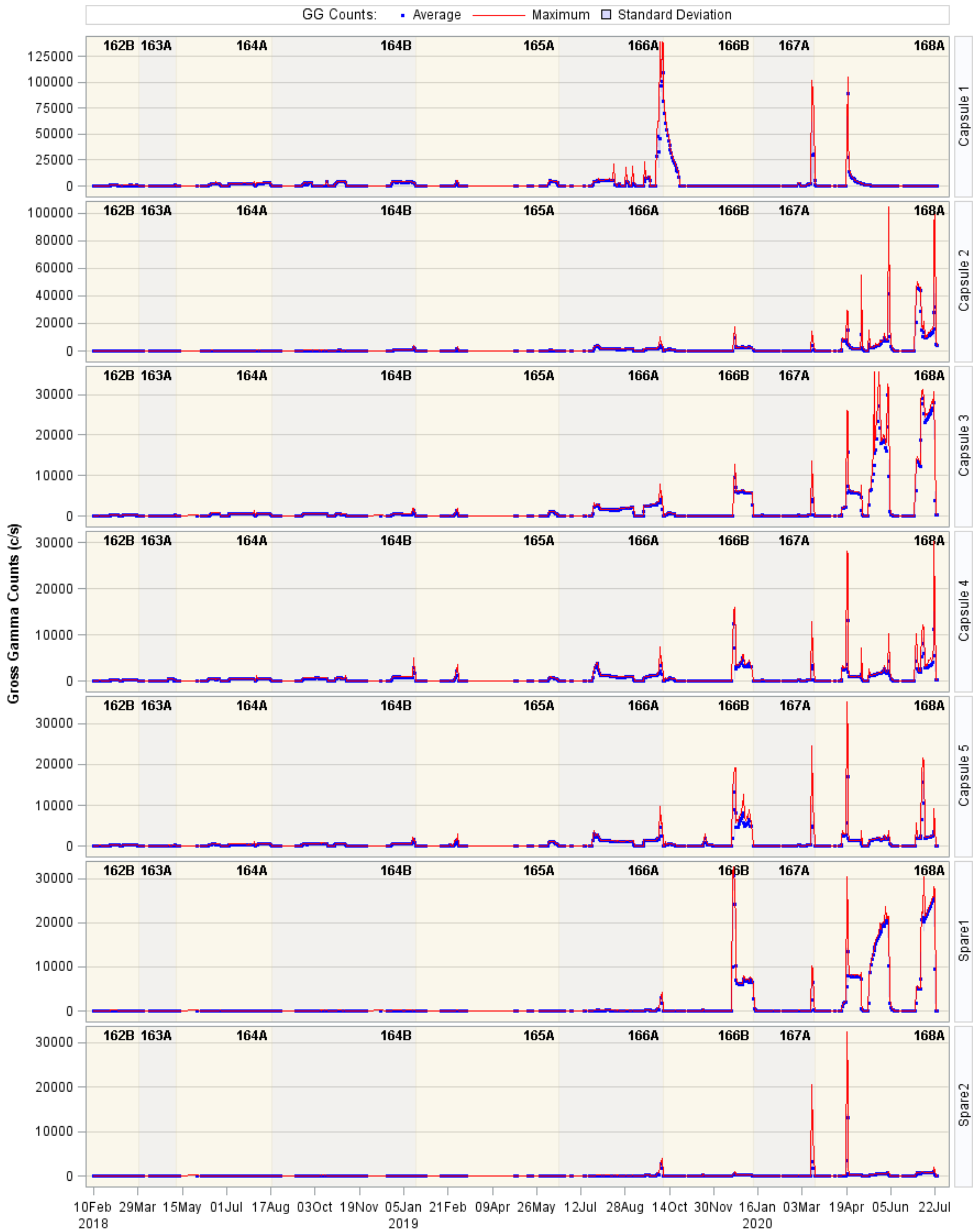

Figure 36. AGR-5/6/7 daily average and maximum GG counts for five capsules and two spare detectors.

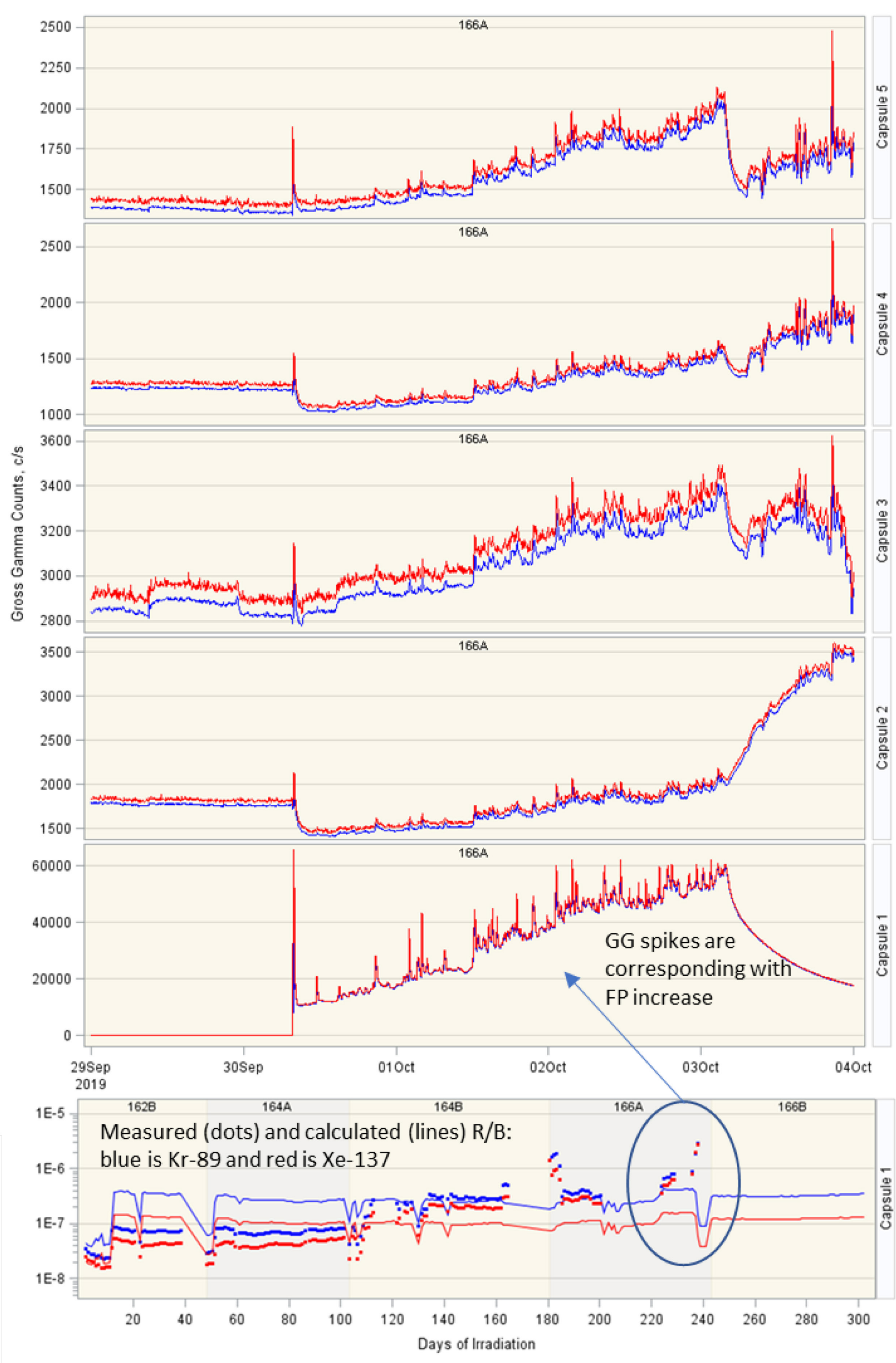

Figure 37. Spikes typically associated with particle failures are observable in Capsule 1 based on 5-minute peak and average GG counts near the end of Cycle 166A.

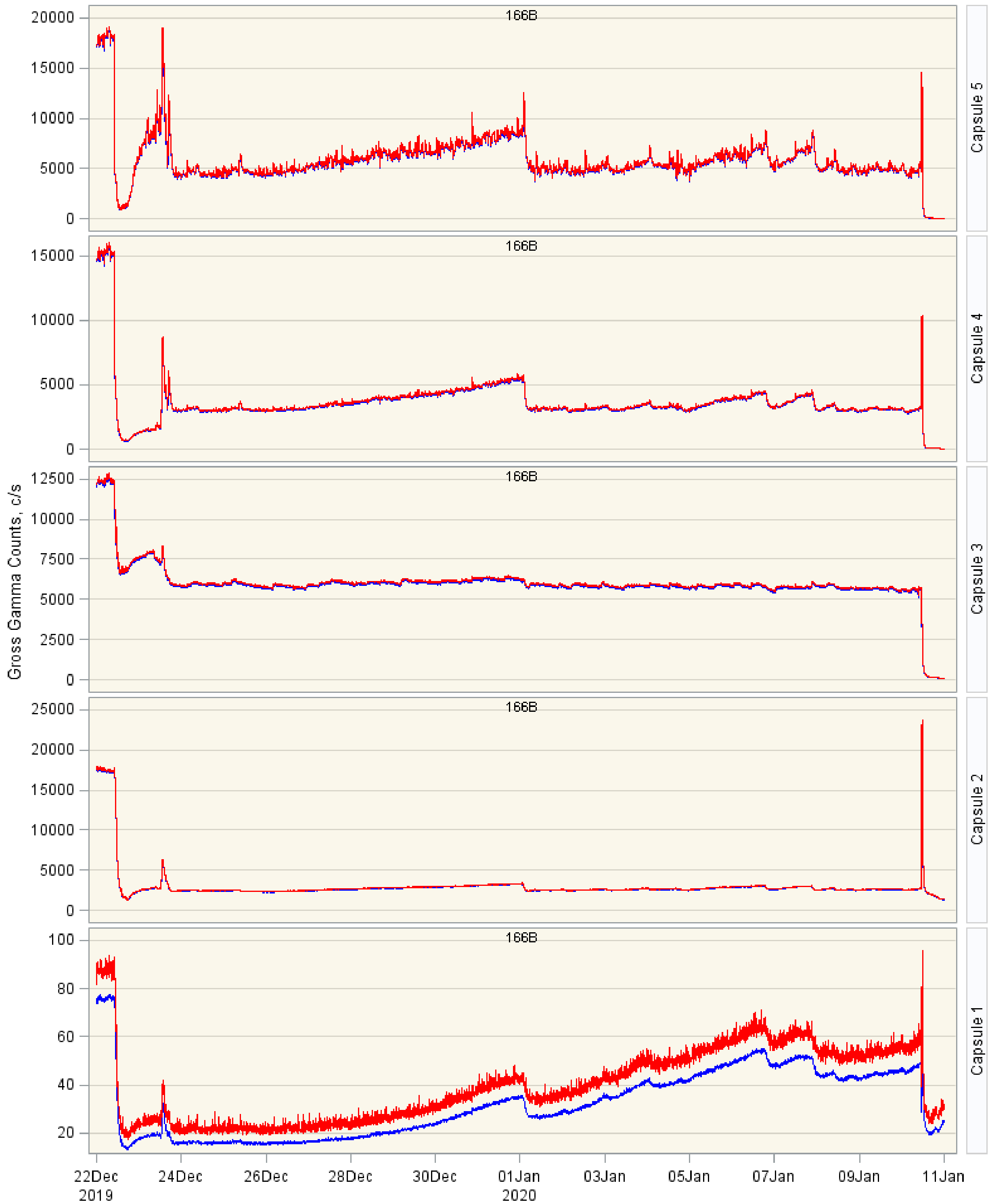

Figure 38. No spikes indicative of particle failures are observable in Capsules 1–5 during Cycle 166B.

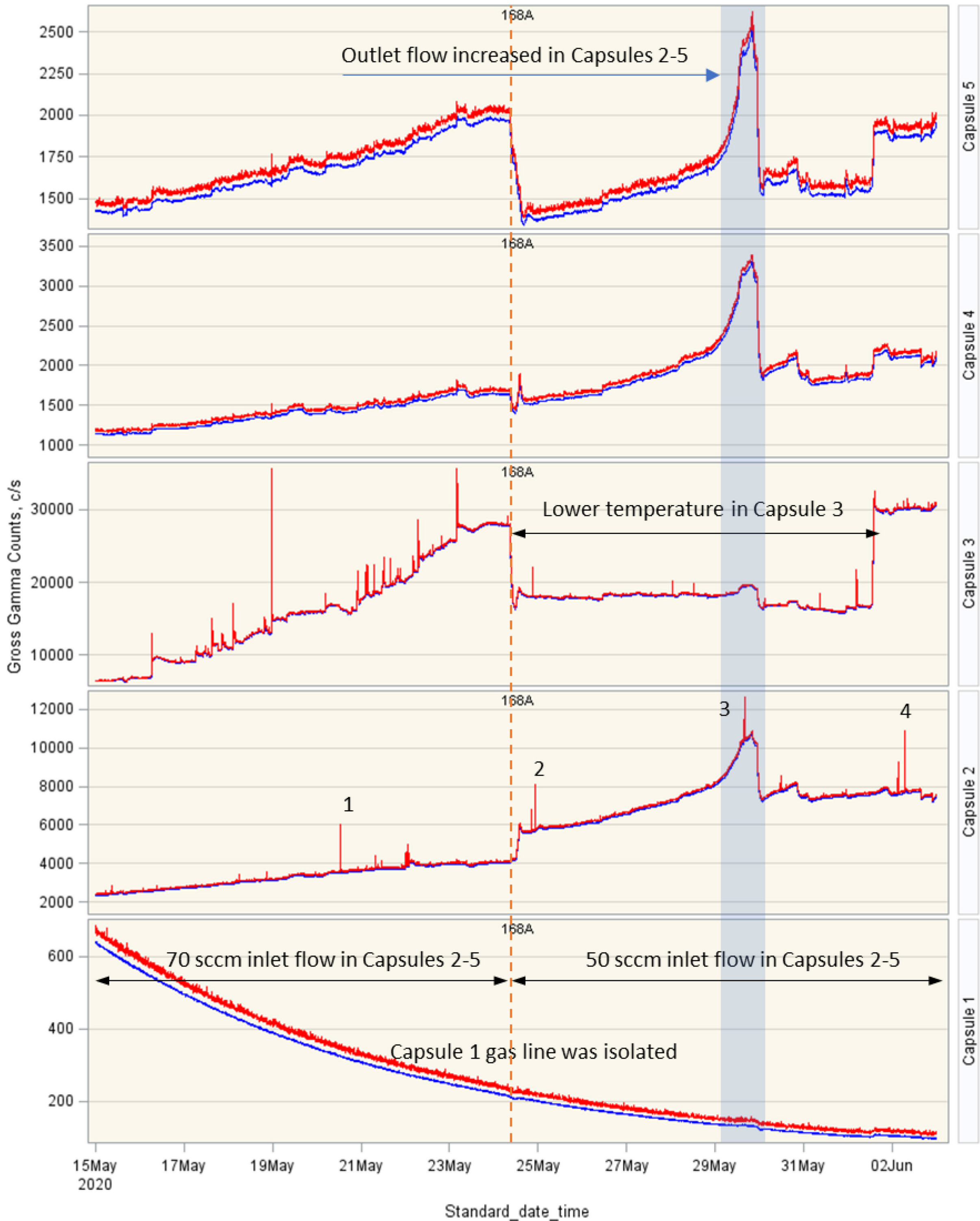

Figure 39. Spikes typically associated with particle failures are observable in Capsules 2 and 3 based on 5-minute peak and average GG counts between May 15 and June 4, 2020 during Cycle 168A.

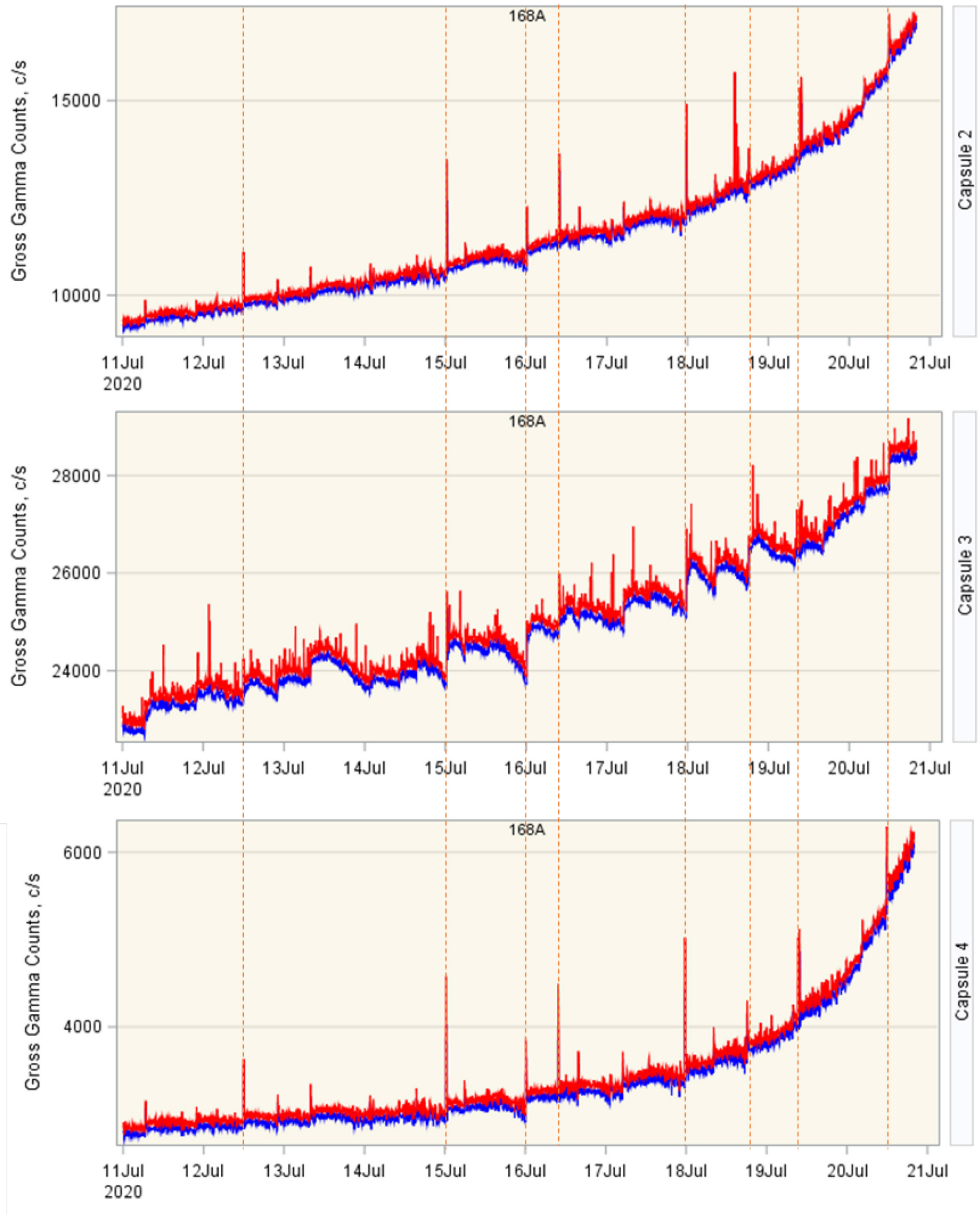

Figure 40. Synchronized pattern of GG spikes in Capsules 2, 3, and 4 seen during the last 10 days of Cycle 168A.

4.3.2 Evidence from Release-to-Birth Ratios

In this section, R/B values for the short-lived isotopes Kr-89 and Xe-137 are used to estimate the number of in-pile particle failures in each capsule. These particular isotopes were selected because the R/B data for isotopes with much shorter half-lives (<3 minutes) are not stable and have a high measurement uncertainty, and the R/B data for much longer lived isotopes were likely impacted to a greater extent by the leakage of FG from Capsule 1, as discussed in Section 4.2.

4.3.2.1 Estimating In-Pile Particle Failures from R/B

At the start of the experiment, FG release rates are a function of the number of EK defects and the amount of DU in the fuel. Increases in FG release rates, relative to those that would be predicted due to continued release from EK defects and DU, may be the result of in-pile particle failures. The calculation of the relative increase thus requires a model that predicts that continued release. The total number of in-pile particle failures ($N_{failures}$) in each capsule can be estimated as:

$$N_{failures} = \frac{R/B_{measured} * N_{particles}}{R/B_{1\_predicted}} - N_{EK\_equivalent}$$

where:
$R/B_{measured}$ is the capsule-measured R/B, the ratio of release rate to birth rate from each capsule; $N_{EK\_equivalent}$ is the initial amount of uranium contributing to FG release in term of EK equivalents, including EK defects and DU, expressed in "equivalent EKs"; and $R/B_{1\_predicted}$ is the predicted R/B per *EK* using following model:

$$\ln(R/B_{1\_predicted}) = n \ln\frac{1}{\lambda} + \frac{B}{T} + C \ ,$$

where *B* is a fuel-particle-specific constant representing diffusion coefficient dependence on temperature (T), *C* is an irradiation-specific constant, λ is the decay constant (s^{-1}), and *n* is introduced in the power of *D*/*λ* to account for the dependence of release on particle coatings (known as recoil effect). The regression analysis is performed to best fit this equation to R/B data obtained from AGR-3/4 irradiation to estimate Parameters *n*, *B*, and *C* (Pham et al, 2019).

The model predicting the release from the initial equivalent EKs has substantial uncertainties associated with the both the initial amount of equivalent EKs and their temperatures. To provide an indication of the magnitude of those uncertainties and to illustrate the sensitivity of the model to these uncertainties, we provide 68% prediction intervals for both parameters.

4.3.2.2 Prediction Interval for Number of Exposed Kernel Release Equivalents

The numbers of EK defects and mass of DU in the AGR-5/6/7 capsules can be estimated based on the average EK and DU fractions measured during particle fabrication (Table 20 and Table 21). However, because each of these variables represents a different statistical distribution with different release rate behavior, they are calculated differently and combined for an effective total number of EK release equivalents.

Neglecting uncertainty in the probability of an EK, 68% prediction intervals for the number of EK defects in each capsule are provided in Table 13, calculated as

$$N_{EK} = binom.inv\left(N_{particle}, EKF, \alpha\right)$$

where
binom.inv is the inverse binomial CDF function;

$N_{particle}$ is the number of particles per capsule;

EKF is the EK defect fraction, measured during fabrication; and

α = *0.84* is the cumulative probability for 68% prediction intervals.

On a mass basis, the release rate from DU is several times greater than the release from an EK. The DU release factor ($F_{DU\_release}$) defines the ratio of release from DU to the release from an EK with the same uranium mass. Based on data from AGR-1, these factors have been estimated as 6.1 for krypton isotopes and 4.0 for xenon isotopes, as reported in INL/EXT-14-32970 (Pham et al, 2019). Different DU release factors used for krypton and xenon lead to different numbers of release equivalent EKs (Table 13). The mean DU, expressed as release equivalent kernels is thus the product of the DU fraction (*DUF*), the number of particles in a capsule, and the DU release factor ($F_{DU\_release}$):

$$N_{DU\_EKequivalents} = N_{particle} * DUF * F_{DU\_release}$$

The DUF is a continuous variable, assumed to have a normal distribution, but fabrication measurements do not provide an estimate of its standard deviation, which is needed for calculation of a DU prediction interval. The standard deviation was thus estimated as one fourth of the range of the 95% CI on that parameter.

The sum of EK defects and DU in release-equivalent kernels is then the number of "equivalent EKs" contributing to FG release at the beginning of the experiment. On average, 25.3 and 22.1 equivalent EKs could be expected in Capsule 1 for krypton and xenon isotopes, respectively. Capsules 3 and 4 have the smallest number of equivalent EKs of ~2 for krypton and ~1 for xenon isotopes, which were solely due to DU because no EK defect was likely to exist in these two capsules based on the average EK fraction.

Table 13. Numbers of equivalent EKs calculated from DU and EK fractions.

Capsule	Total Particles	Kernels of Dispersed Uranium [a]	Exposed Kernel Defects [a]	Equivalent Exposed Kernels for Krypton [a]	Equivalent Exposed Kernels for Xenon [a]
Capsule 1	307625	1.52 [1.41–1.64]	16 [13–21]	25.3 [21.6–31.0]	22.1 [18.6–27.5]
Capsule 2	72480	0.36 [1.41–1.64]	0 [0–1]	2.2 [2.1–3.3]	1.5 [1.4–2.5]
Capsule 3	54360	0.27 [1.41–1.64]	0 [0–1]	1.7 [1.6–2.8]	1.1 [1.0–2.2]
Capsule 4	52728	0.26 [1.41–1.64]	0 [0–1]	1.6 [1.5–2.7]	1.1 [1.0–2.1]
Capsule 5	81432	0.40 [1.41–1.64]	4 [2–6]	6.5 [4.3–8.6]	5.6 [3.5–7.7]

[a] Estimated mean and 68% prediction interval for number of equivalent EKs due to EK defects and DU.

4.3.2.3 Prediction Interval for Release Temperature

Prediction intervals for capsule temperature are based on the distribution of temperatures seen in each capsule during the experiment, as calculated via heat transport simulation. As the locations of EK defects in the capsule are unknown, we estimate the prediction interval as the mean temperature ± one standard deviation (Table 14). As temperature distributions were asymmetric around the mean (Figure 25), lower standard deviations are larger than upper standard deviations. The impacts of uncertainties (in number of equivalent EKs and in temperature) in predicting Kr-89 R/Bs are shown in Figure 41 for the first three regular cycles.

Table 14. Average and standard deviations of fuel temperature during Cycles 162B, 164A, and 164B.

Capsule	Average Fuel Temperature, °C	Upper Standard Deviation, °C	Lower Standard Deviation, °C
Capsule 1	1030	76	135
Capsule 2	827	37	92
Capsule 3	1290	43	111
Capsule 4	842	36	94
Capsule 5	726	33	87

4.3.2.4 In-Pile Particle Failures Based on Increase in Release-to-Birth Ratios

Cycles 162B–164B: During these first three regular cycles, GG counts did not suggest in-pile failures and gas flow functioned as designed for all capsules. Consequently, releases from capsules would likely have been from EK defects and DU. These cycles therefore demonstrate the performance of the AGR model used to predict capsule R/B values (Figure 41). This finding was previously described in detail (Pham and Scates, 2019). To illustrate model sensitivity to uncertainties in temperature as well as the number of EK defects and amount of DU, Figure 41 shows model output bands corresponding to the application of the prediction intervals described in the preceding sections.

The AGR model predicts best for Capsules 2 and 4, where measured values are within both model uncertainty bands. The model underpredicts R/B for Capsule 5 during the first two cycles when the fuel temperature was relatively low, but the prediction improves during the third cycle, as the temperature increases. The model overpredicts R/B for the high-temperature Capsule 3, where no EK defects are likely. Calculated fuel temperatures in Capsule 1 were stable during the first three cycles, so the predicted R/B is relatively constant. Measured R/Bs, however, increased from less-than-predicted values—for the first two cycles—to above predicted values during the third cycle (Cycle 164B). A possible explanation for this behavior is an underprediction of Capsule 1 fuel temperature, as described in Section 3.1.3. However, the AGR model based on Kr-85m performed well for Capsule 1 during all three first cycles (Figure 42).

Cycles 166A–168A (Figure 42): The Capsule 1 gas line problem starting in Cycle 164B and apparent in-pile failures in that capsule starting in Cycle 166A led to unstable R/Bs in Capsule 1. Some corresponding changes in R/Bs in other capsules may be attributed to FG leakage from Capsule 1 through the leadout system into the other capsule gas lines. Evidence of the leakage effect is seen in the comparison of relative increases in R/B of longer versus shorter-lived isotopes. A substantial increase in R/B of the long-lived Kr-85m occurred in Capsules 2–5 during the last three regular cycles. Increases in the R/B of the two shorter-lived isotopes (Kr-89 and Xe-137), however, were substantially less, especially for the top two capsules (Capsules 4 and 5) located furthest from Capsule 1. This apparent decrease with increasing distance from Capsule 1 suggests decay during transport. Therefore, an in-pile particle failure assessment from Cycle 166A onward will be accomplished by considering both the GG data and an analysis of specific FG isotopes (i.e., Kr-89 and Xe-137) that are expected to be least impacted by contamination from Capsule 1.

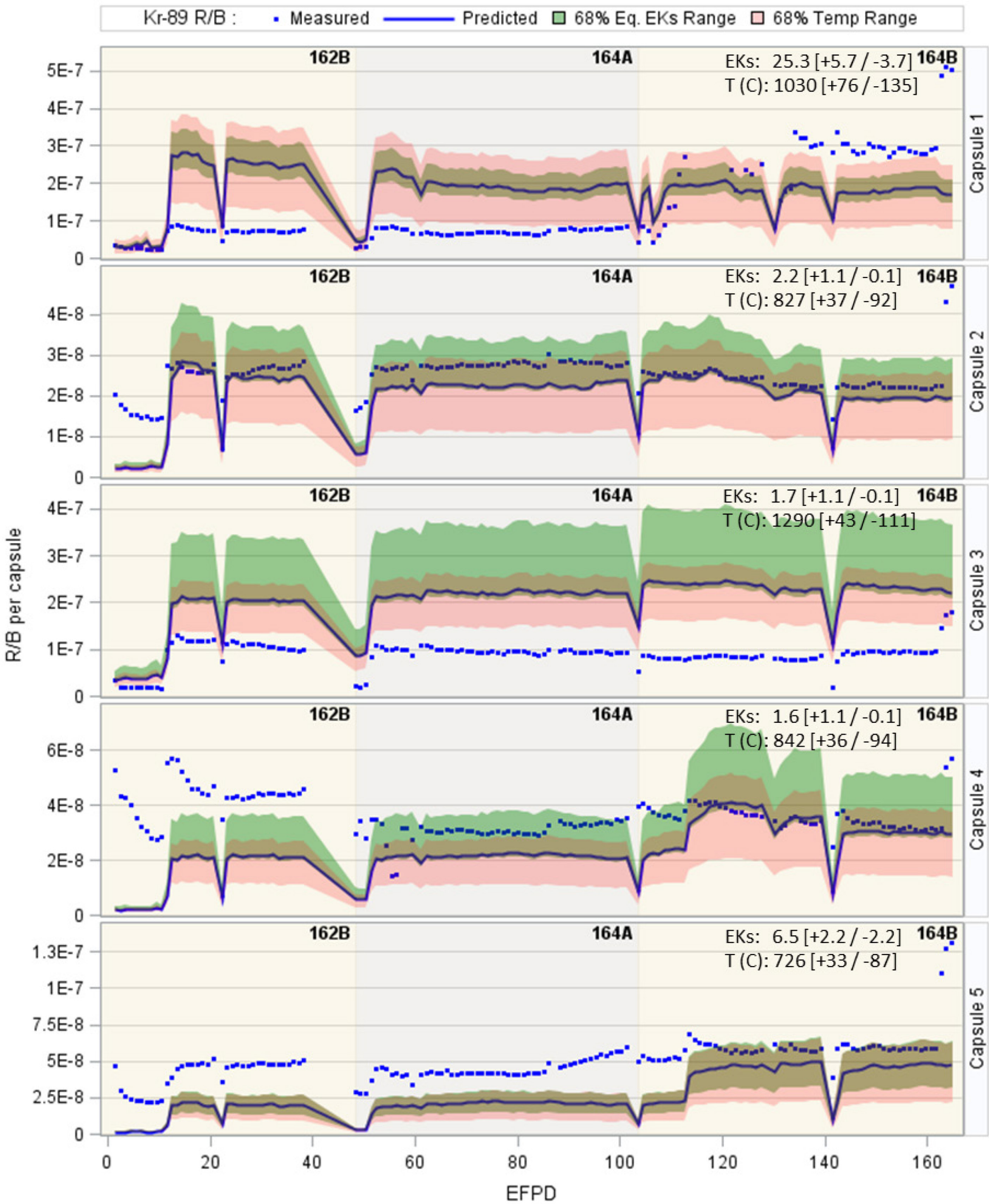

Figure 41. Measured (dots) and predicted (lines) capsule R/B for Kr-89 for three early cycles, to illustrate model sensitivity to uncertainties: Green band: 68% prediction interval for number equivalent EKs due to EK defects and DU; Red band: 68% prediction interval for compact temperature.

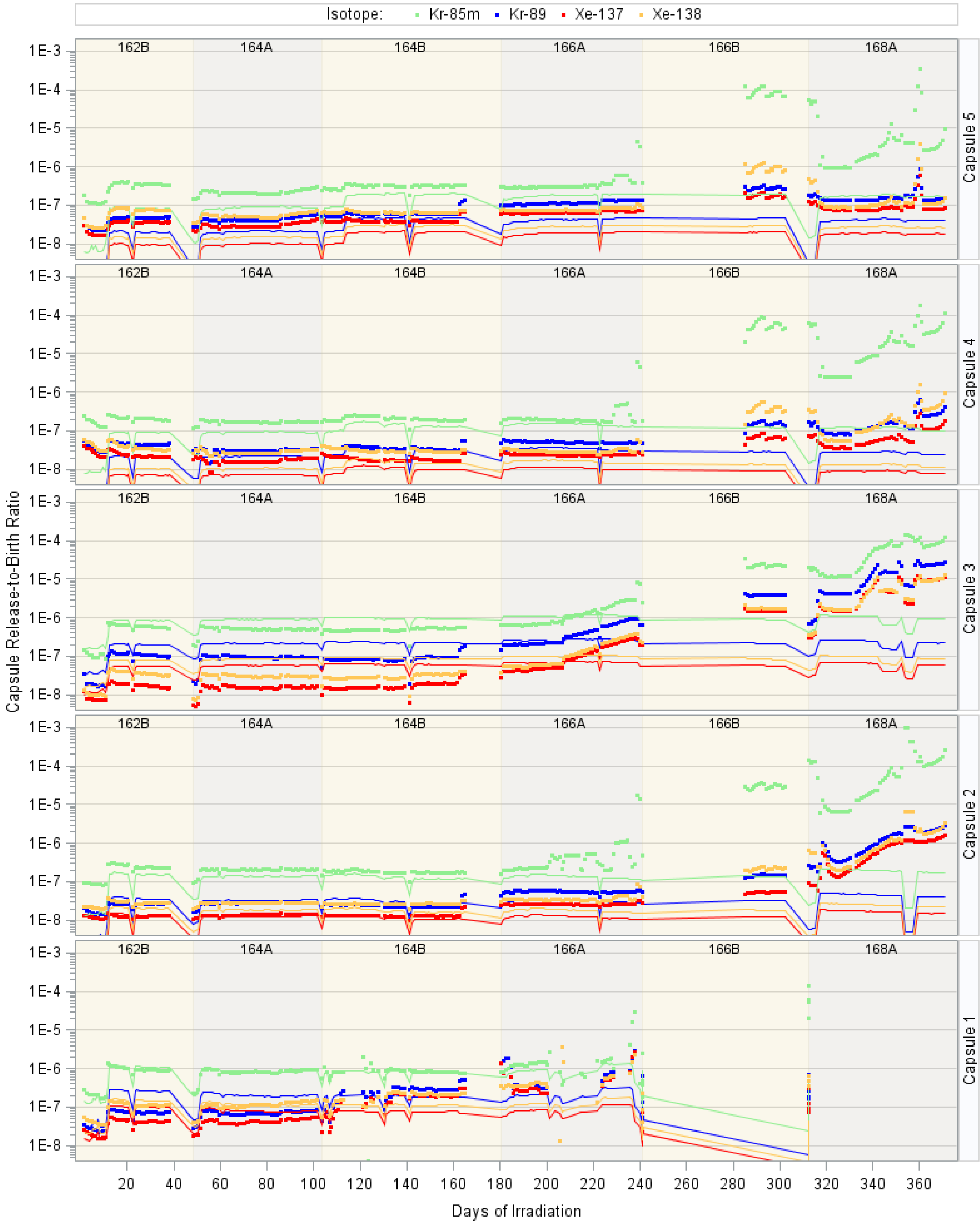

Figure 42. Measured (dots) and predicted (assuming no in-pile failures) capsule R/B for Kr-85m, Kr-89, Xe-137, and Xe-138 isotopes, for all regular cycles.

4.3.3 Estimated Number of Particle Failures

For the calculation of the number of failures, we assumed that all failures occurred at the peak fuel temperature location within a capsule. Model over-prediction will result in negative in-pile failures when no in-pile failure occurred, instead of the expected zero. Even for short-lived isotopes, FG leakage from Capsule 1 can be significant for capsules located closest to it. Evidence used to estimate the number of in-pile particle failures, and those estimates, follow. The estimated number of in-pile failures and as-fabricated release-equivalent EKs are presented in Figure 43.

- The final number of failures in Capsule 1 was indefinable due to lack of FG release and GG data after Cycle 166A. Particle failures in Capsule 1 began near the end of Cycle 166A (Figure 37), however, and R/B data suggests that 180–440 failures (Figure 43) had occurred near the end of that cycle.
- Capsule 2 is estimated to have had approximately four particle failures based on the following observations and analyses:
  - No apparent particle failures occurred up through Cycle 166B. R/B values were low and stable (Figure 43), consistent with the absence of GG spikes during these cycles (Figure 36–Figure 38).
  - During Cycle 168A, the number of apparent failures, based on changes in R/B, increased until it reached 130 by the end of that cycle (Figure 43). However, most of the increase in FG releases could be attributed to FG leakage from neighboring Capsule 1. Ultimately, only four possible failures were identified, based on analysis of the GG data during two distinct periods (before and after scram) when the GG in capsules behaved differently, as shown in Figure 39 and Figure 40.
    - Period "A" (Figure 44): Four GG spikes indicated possible particle failures. However, only the GG spike on May 20, 2020 corresponded to a clear spike in Xe-133 activity, the primary isotope that contributes to the "spike" in the GG system (Scates, 2021). Thus, in this time period, the data indicate one particle failure with good confidence, and potentially three additional failures.
    - Period "B" (Figure 45): GG spikes were not associated with any clear and consistent spikes in measured isotope activities. In addition, all the GG spikes were perfectly synchronized with spikes in Capsules 3 and 4 (Figure 40), so all spikes are attributed to FG leakage from Capsule 1. Thus, no particle failures are inferred to have occurred during this time.
- Capsule 3 is estimated to have had approximately 15 particle failures based on the following observations and analysis:
  - No in-pile failures were apparent through the end of Cycle 166B (Figure 43). R/B-based evidence of failures prior to Cycle 168A are attributed to FG leakage from Capsule 1 because R/B levels dropped back down at the beginning of Cycle 168A. In addition, no GG spikes indicating particle failures were apparent during this time (Figure 36–Figure 38).
  - Roughly 15 failures were inferred from spikes in GG counts and/or isotope activities data during Cycle 168A. Like Capsule 2, most of the increase in FG release through Cycle 168A in Capsule 3 (Figure 43) is attributed to FG leakage from Capsule 1. GG in Capsule 3 behaved differently in two periods in Cycle 168A (before and after scram):
    - Period "A" (Figure 46): 15 particle failures were associated with GG spikes during the period between May 15 and June 2, 2020. These apparent failures were also evidenced by spikes in isotope activities (bottom plots).
    - Period "B" (Figure 47): Multiple GG spikes in Capsule 3 are attributed to the same FG leakage events from Capsule 1 because they did not correspond with clear and consistent spikes in measured activities for all isotopes (bottom plots). As a result, no particle failures were likely to have occurred during this time.

- No in-pile failures were apparent in Capsule 4. The small and unstable increases in R/B, relative to predicted values, during short periods in Cycle 166B and Cycle 168A (Figure 43) are attributed to FG leakage from Capsule 1 because no coincident GG spikes occurred. A few GG spikes during Period "B" of Cycle 168A (Figure 48) are perfectly synchronized with spikes in Capsules 2 and 3 (Figure 40), suggesting, again, leakage from Capsule 1.
- No in-pile failures were apparent in Capsule 5. R/B-based estimates of release rate were roughly constant for all cycles including Cycle 168A (Figure 43). Capsule 5 exhibited the least evidence of FG leakage from Capsule 1, as only a few scattered data points suggested a larger release source during Cycle 166B and 168A when FG leakage from Capsule 1 was substantial. GG spikes typical of particle failures were not observed in Capsule 5 during the entire irradiation, even during Cycle 166B (Figure 38) and Cycle 168A (Figure 49), when R/B values suggested a slightly larger source.

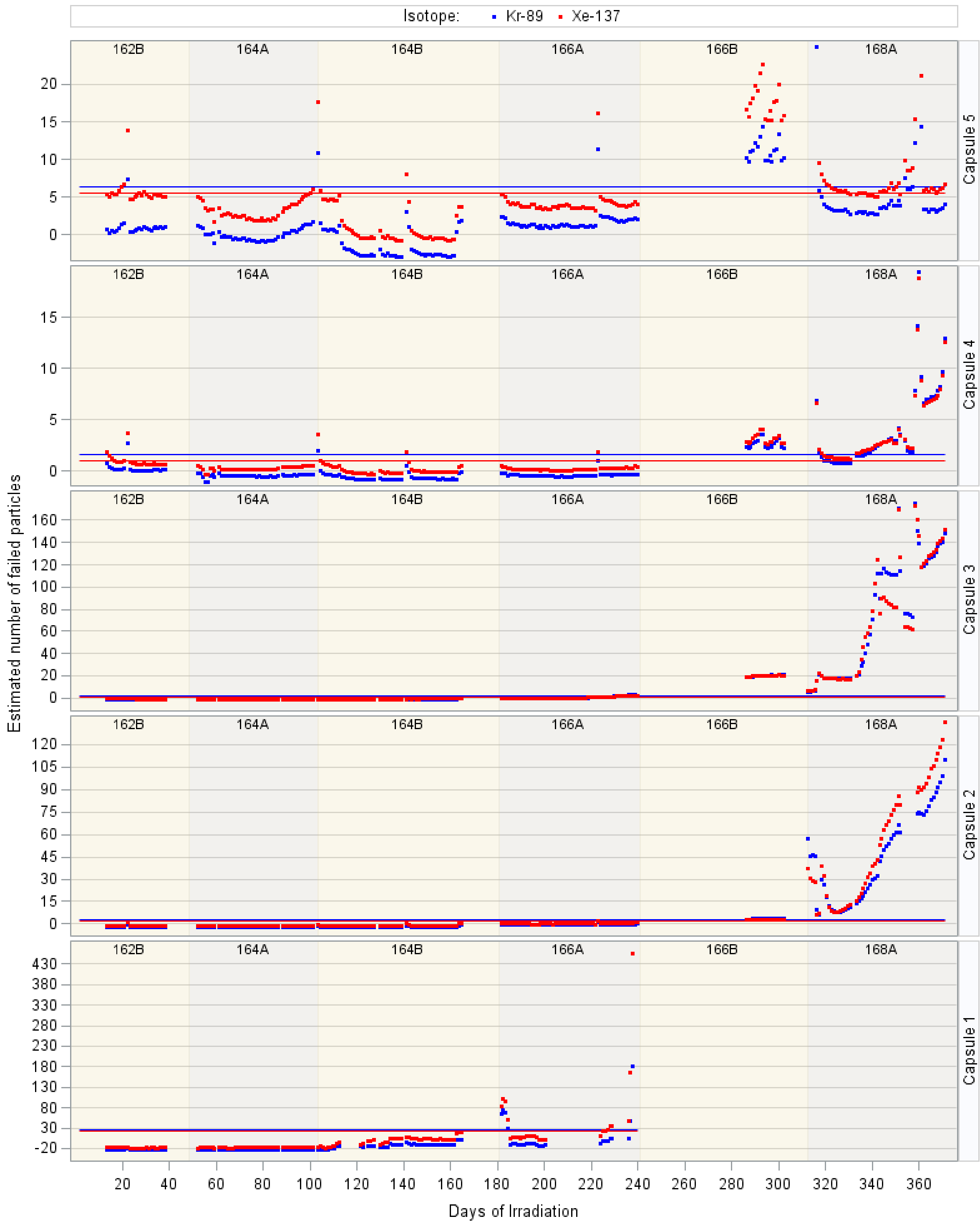

Figure 43. Estimated number of particle failures for AGR-5/6/7 capsules based on Kr-89 (blue color) and Xe-137 (red color): lines are as-fabricated equivalent EKs, and dots are in-pile failures.

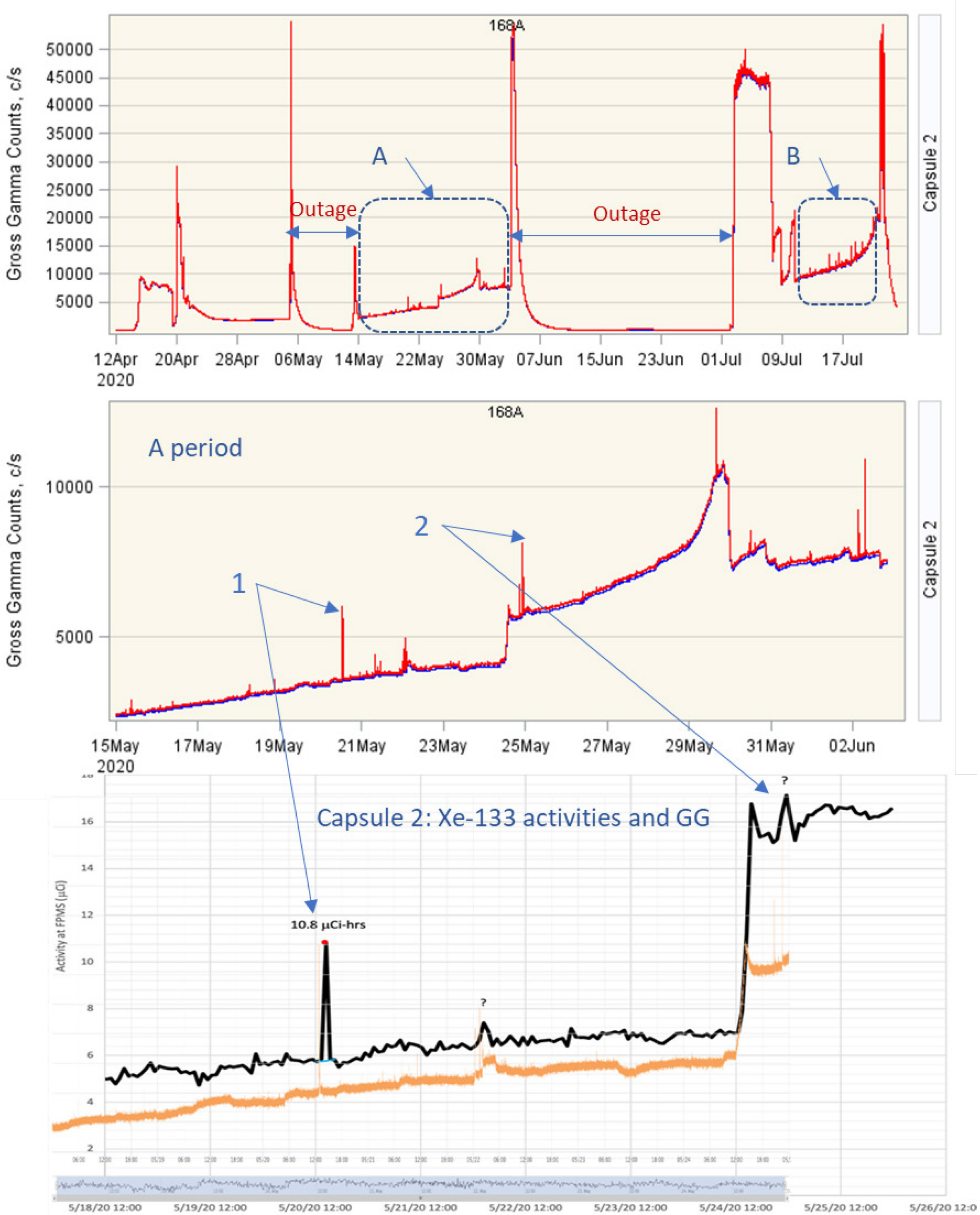

Figure 44. Capsule 2 ATR Cycle 168A – "A" period: 2–4 particle failures were likely. Top – average (blue line) and peak (red line) GG for full cycle, middle – average and peak GG for "A" period, and bottom – for Xe-133 activity (black) overlayed GG data (orange) for "A" period.

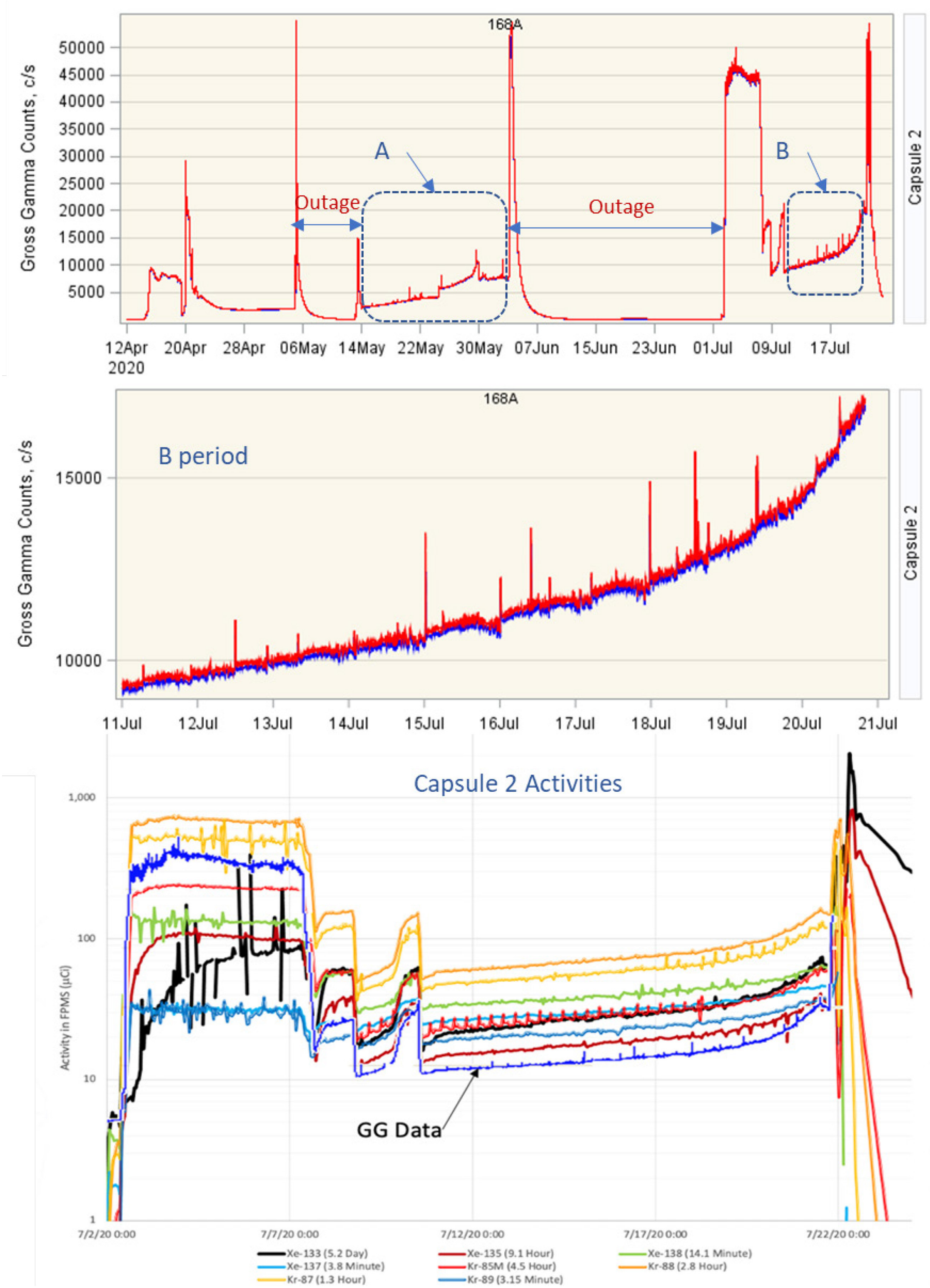

Figure 45. Capsule 2 ATR Cycle 168A – "B" period: No particle failures were likely. Top – full cycle average (blue line) and peak (red line) GG, middle – 'B' period average and peak GG, and bottom – isotopes' activities overlayed with average and peak GG data.

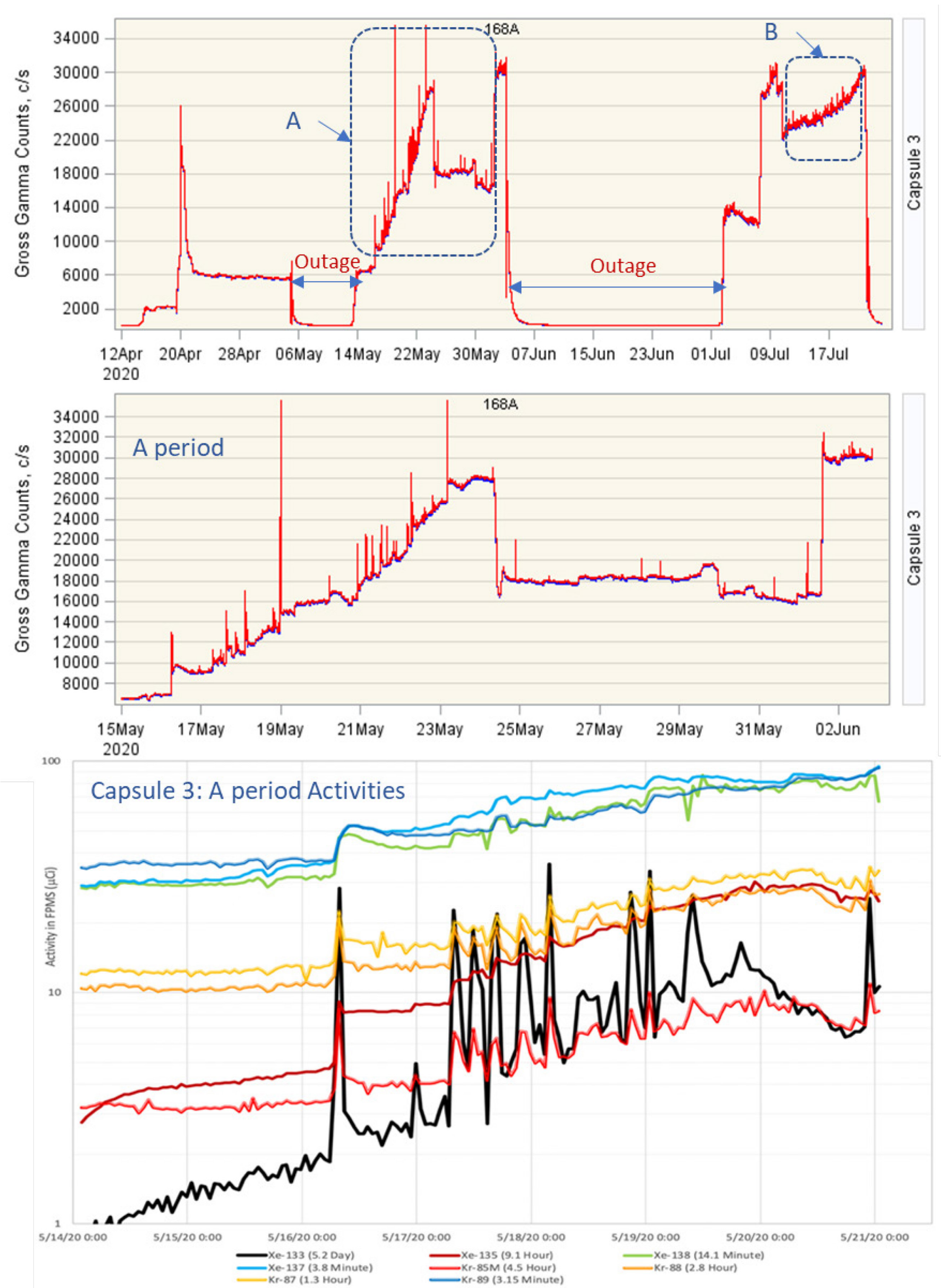

Figure 46. Capsule 3 ATR Cycle 168A – “A” period: up to 15 particle failures were likely due to both GG and isotope activity spikes. Top – average (blue line) and peak (red line) GG for full cycle, middle – GG for “A” period, and bottom – isotopes’ activities for “A” period.

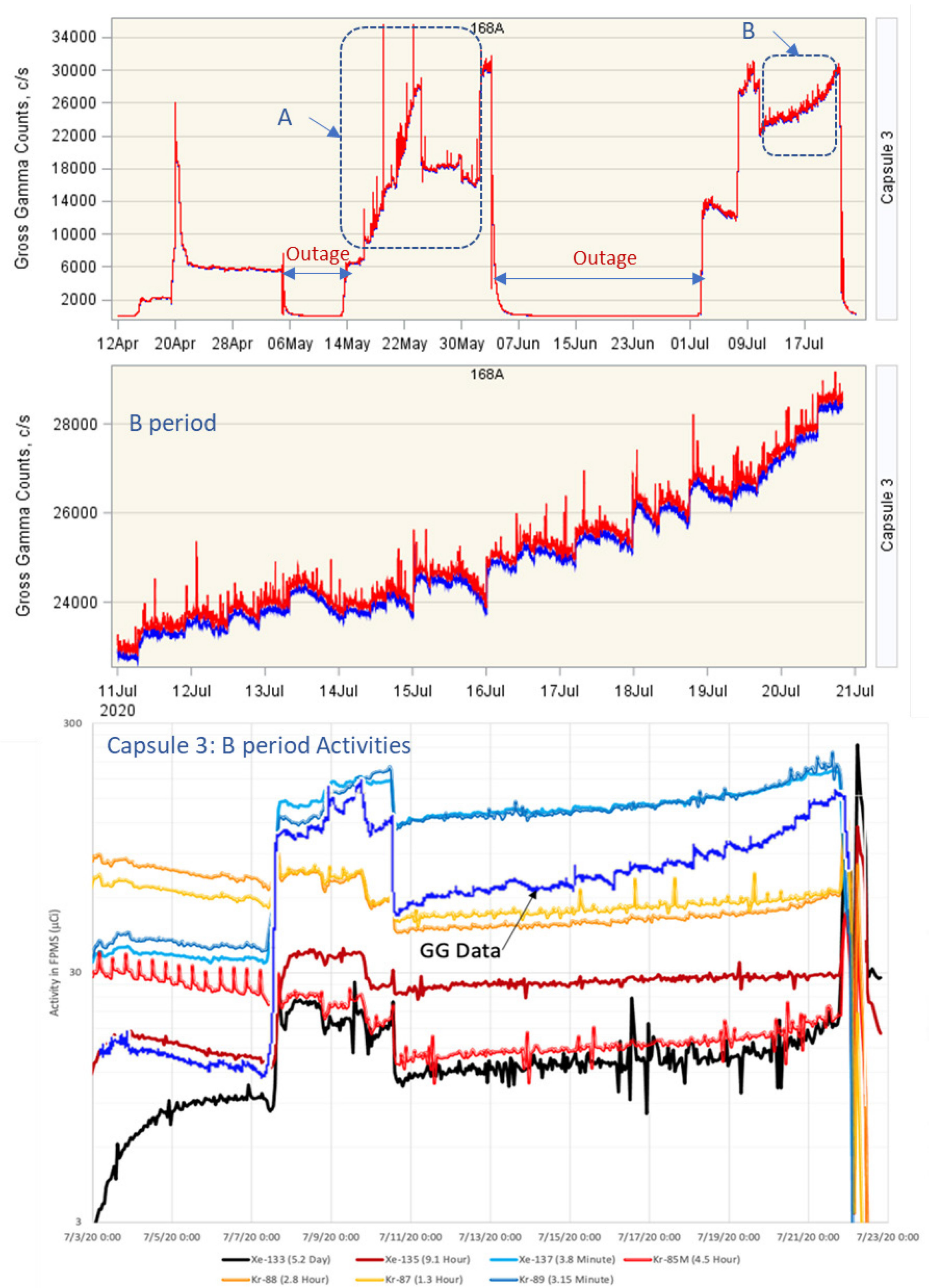

Figure 47. Capsule 3 ATR Cycle 168A – “B” period: No particle failures were likely because GG spikes and isotopes’ spikes are random. Top – full cycle average (blue line) and peak (red line) GG, middle – “B” period GG, and bottom – isotopes’ activities overlayed with GG data.

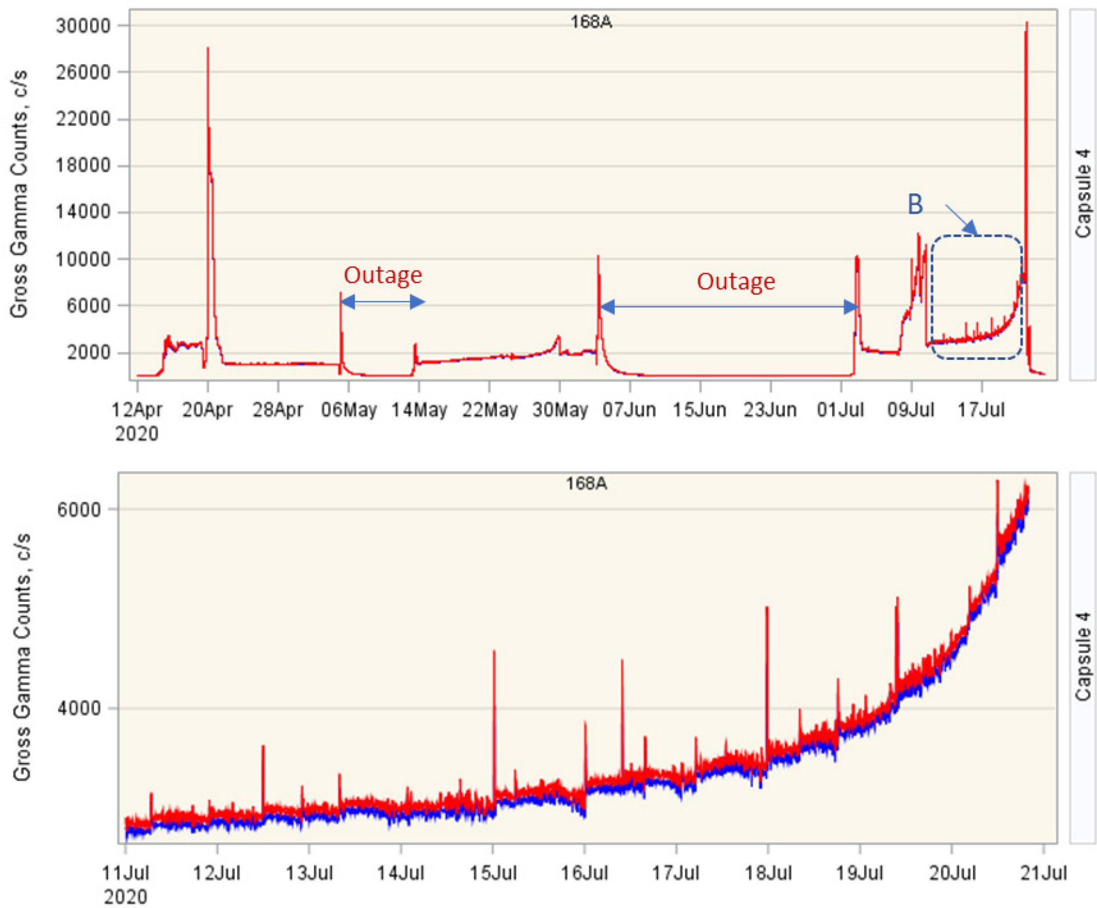

Figure 48. Capsule 4 average (blue line) and peak (red line) GG counts during ATR Cycle 168A: Top – for all cycle and bottom – for "B" period, GG spikes are more likely caused by FG leakage from Capsule 1 because they occurred at the same time of spikes in other capsules, Capsules 2 and 3 (Figure 40).

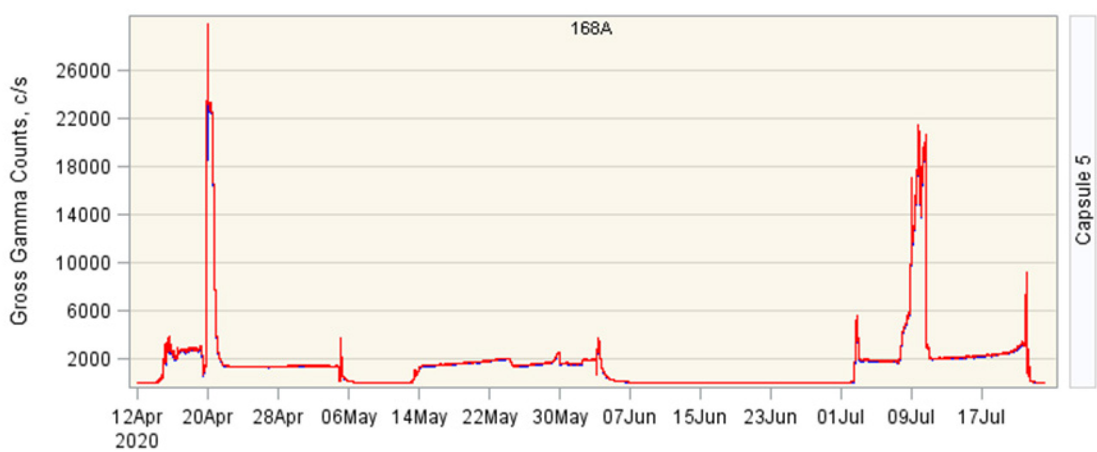

Figure 49. Capsule 5 average (blue line) and peak (red line) GG counts during ATR Cycle 168A: No GG spikes were observable.

4.4 Fission Gas Release Analysis Conclusion

For the AGR-5/6/7 experiment, there are virtually no indications that the FPMS failed to capture data reliably with the exception of the end of Cycle 166A where experimental conditions involving Capsule 1 lead to total detector saturation for FPMS Station 1 (Scates, 2021). During irradiation and at the end of each cycle, each FPM is put through an "On the Fly" energy calibration and a standard energy calibration test, and all data were reliably verified per test plans.

During the first five cycles (162B–165A), FG isotope R/B ratios were stable in the 10^{-8}–10^{-6} range for 11 out of the 12 measured isotopes, (all isotopes except Xe-131m). No in-pile particle failures were observed based on the GG counts during this time. The EK fraction and relatively high fuel particle temperatures in Capsule 1 led to a maximum Kr-85m R/B value of around 2×10^{-6}.

Gas line issues in Capsule 1 occurred from the fourth cycle (Cycle 164B) and were mitigated to minimize crosstalk between capsule gas lines. Capsule 1 fission-product release measurements were not possible during the last three cycles (Cycles 166B, 167A, and 168A) because of the isolation of Capsule 1. Capsule 1 gas line issues also caused FG leakage into Capsules 2–5 to various degrees over time starting from the sixth cycle (i.e., Cycle 166A). Capsule 1 FG leakage to the top capsule (Capsule 5) was lowest because of its position at the top of the test train. As a result, R/B values for all capsules from the mid-cycle of Cycle 166A onward are considered uncertain because of unquantifiable contamination from Capsule 1. However, they can be used when the leaking amount from Capsule 1 can be deemed negligible (i.e., FG activity leakage from Capsule 1 for short-lived isotopes can be lower than for longer lived isotopes due to decay before reaching Capsules 4 and 5).

A summary of the estimated number of in-pile failures in the AGR-5/6/7 capsules is provided in Table 15. By the end of Cycle 166A, a significant number of in-pile failures appear to have occurred in Capsule 1, causing a substantial increase in FG activity and saturation of the FPMS HPGe detector and an increased activity in the 1A primary cubicle that was picked up by the GG NaI(Tl) detectors. However, the final number of particle failures in Capsule 1 is unknown due to the absence of measured activities. Approximately 15 particle failures are estimated to have occurred in Capsule 3 and between one and four failures in Capsule 2 based on spikes of GG counts and measured activities at the FPM detectors during the last cycle, Cycle 168A. In contrast, no in-pile failures in Capsules 4 and 5 were indicated based on the AGR-3/4 R/B models and the lack of distinct increases in isotope activities and GG counts.

Table 15. Estimated number of in-pile failures in the AGR-5/6/7 capsules.

Capsule 1	180–440 prior to the end of 166A; unknown after 166A
Capsule 2	1–4
Capsule 3	~15
Capsule 4	None
Capsule 5	None

5. AGR-5/6/7 OPERATIONAL ASSESSMENT

5.1 Power Increase

It was requested that the ATR power in the NE lobe be increased over the course of the AGR-5/6/7 irradiation. A progressive power increase ensured that the temperature control could be maintained by the helium/neon sweep gas mixture as the fissile fuel content was consumed and the heat generation rate dropped. The NE lobe power was increased from roughly 14 MW during the first AGR-5/6/7 cycle, Cycle 162B, to roughly 20 MW during the last AGR-5/6/7 cycle, Cycle 168B (Table 4).

5.2 Fuel Temperature Control

A range of irradiation fuel temperatures were specified for each AGR-5/6/7 capsule to achieve the desired fuel compact temperature distribution in the test train (per SPC-1749). The goal for AGR-5/6 was to adequately bound the irradiation conditions expected in an HTGR, which led to time-averaged target irradiation temperatures from under 900°C to over 1250°C that will conservatively span the range expected in a prismatic reactor. The primary goal of AGR-7 was to demonstrate the available performance margin with respect to temperature for UCO fuel; thus, it had a higher time-averaged peak fuel temperature target of 1500°C. To shape the temporal and spatial fuel power distribution (subsequently, fuel temperature distribution) in the capsules, two techniques were used to adjust the neutron-flux incident to the AGR 5/6/7 test train. These techniques included placing a neutron filter around the capsules and raising the ATR NE lobe power throughout the irradiation, as discussed in Section 1.2.1.

Before irradiation, preliminary neutronics and thermal analyses were performed for AGR-5/6/7 capsules based on the original 13-cycle schedule, as documented in ECAR-2961 (Sterbentz, 2017) and ECAR-2966 (Murray, 2018), respectively. Besides confirming the AGR-5/6/7 requirements of fast fluence and burnup can be met, the neutronics analysis provides heat rates and fast fluence for input to the thermal models. In turn, the thermal analysis provides confirmation that the chosen gas-gap widths and gas mixtures will allow the test fuel to meet the temperature requirements. The projected fuel compact and TC temperatures were also used to determine setpoint temperatures for the designated control TC for each capsule. In addition to the primary control TC, two TCs were selected as primary and secondary backup TCs for use in the event of primary TC failure. Corresponding setpoint temperatures are also defined to these backup TCs.

During irradiation, temperature control is based on temperature feedback from the designated control TC for each capsule and is performed by varying the sweep gas composition (between 100% helium for high conductivity and 100% neon for low conductivity). A single blend of inert gases from a capsule-specific gas controller is routed by an independent gas line to each capsule to provide temperature control.

As irradiation progressed and ATR lobe power was progressively increased, temperature adjustments were made to keep the capsules in their desired temperature bands. TC set points were redefined based on FG release measurements, TC readings, and thermal calculations. The control TC setpoints were periodically adjusted in response to changing events in the capsules, including TC drift, irradiation-induced changes in gas-gap widths and material thermal conductivities, and replacement of the designated control TC due to failure. These TC setpoint adjustments were based on fuel temperatures, as calculated by the as-run thermal analysis. After the completion of each cycle, the as-run thermal analysis was performed based on the fast fluence, heat rate (predicted by the as-run neutronics analysis using actual ATR operating conditions) and actual neon/helium gas mixtures in AGR-5/6/7 capsules. Calculated fuel temperature distributions were compared against requirements, as shown by plots in Figure 29 for AGR-5/6 and Figure 30 for AGR-7. The fraction of fuel from each capsule in each temperature range was color-coded and displayed in these interactive plots. Based on these plots, control TC setpoints were adjusted accordingly to improve the match with fuel-temperature requirements.

5.3 Thermocouple Set Point Adjustments

For the AGR-5/6 capsules (1, 2, 4, and 5), the low portion of fuel in the middle range of temperatures (i.e., 900–1050°C) at the end of Cycle 164A (see Figure 29) prompted the first TC setpoint adjustment on September 30, 2018 (Cycle 164B), when the control TC setpoints for Capsules 4 and 5 were raised by 90°C to increase fuel temperatures (Table 16). As a result, the portion of AGR-5/6 fuel in the 900–1050°C range increased from 20 to 25.7%, which was closer to the 30% requirement. In addition, the TC setpoint in Capsule 2 was increased by 40°C for Cycle 166A (Table 16). On the other hand, the decreasing fraction of fuel for the highest range (i.e., 1250–1350°C) was caused by a decrease in Capsule 1 fuel temperatures over time. To meet the requirement for this temperature range, the TC setpoint for Capsule 1 was increased by 70°C for Cycle 166A. However, the last TC in Capsule 1 failed during Cycle 166A, and flow issues were worsening, causing fuel temperatures to drop back significantly during the last cycle (Cycle 168A) as the Capsule 1 gas line was isolated with pure helium flowing just before the ATR powering up.

For AGR-7 Capsule 3, by the end of the fourth cycle (Cycle 164B), the time-averaged fuel temperature was about 120°C less than specification. Therefore, the TC setpoint for Capsule 3 was increased by 50°C during Cycle 166A (Table 16). As a result, the calculated time-averaged peak fuel temperature by the end of Cycle 167A was only ~60°C lower than the specification if Cycles 163A and 167A were excluded from time averaging (1432°C calculated versus the 1500°C required as shown in Table 10).

Table 16. TC set points adjustments.

Capsule / Control TC	Original, °C	New Set Point (Change), °C – Change Date (Cycle)
1 / TC14	1315	1385 (+70) – 7/28/2019 (166A)
2 / TC3	860	900 (+40) – 7/28/2019 (166A)
3 / TC13	1180	1230 (+50) – 8/22/2019 (166A)
4 / TC1	855	945 (+90) – 9/30/2018 (164B)
5 / TC2	725	815 (+90) – 9/30/2018 (164B)

5.4 Thermocouple Performance

Of fifty-four installed TCs, 48 had failed by the end of Cycle 168A (Table 17). The six surviving TCs are in the top Capsules 4 and 5, so they were used to maintain fuel temperature in these capsules over the entire irradiation. The three bottom capsules had no operational TCs left (Capsule 1 from Cycle 166B, Capsule 2 from Cycle 167A, and Capsule 3 from 168A). When all TCs failed in a capsule, the appropriate neon fraction was determined based on the thermal models so that fuel temperatures could be maintained as close to specified levels as possible. The exception was Capsule 1 during the last cycle 168A, when its gas line was totally isolated. Thus, the Capsule 1 neon fraction was not well-defined and had to be bounded between zero and neon fraction in the leadout, including portions of outflow gas from Capsules 2–5.

Among the failed TC in the AGR-5/6/7 experiment, 10 TCs in the three upper capsules (Capsules 3, 4, and 5) were broken before irradiation, during handling and assembly of the test train. The other 38 TCs failed throughout the irradiation campaign. Figure 50 shows the daily average temperatures of all functioning TCs as a function of EFPDs; the plots are discontinued at the time of TC failures.

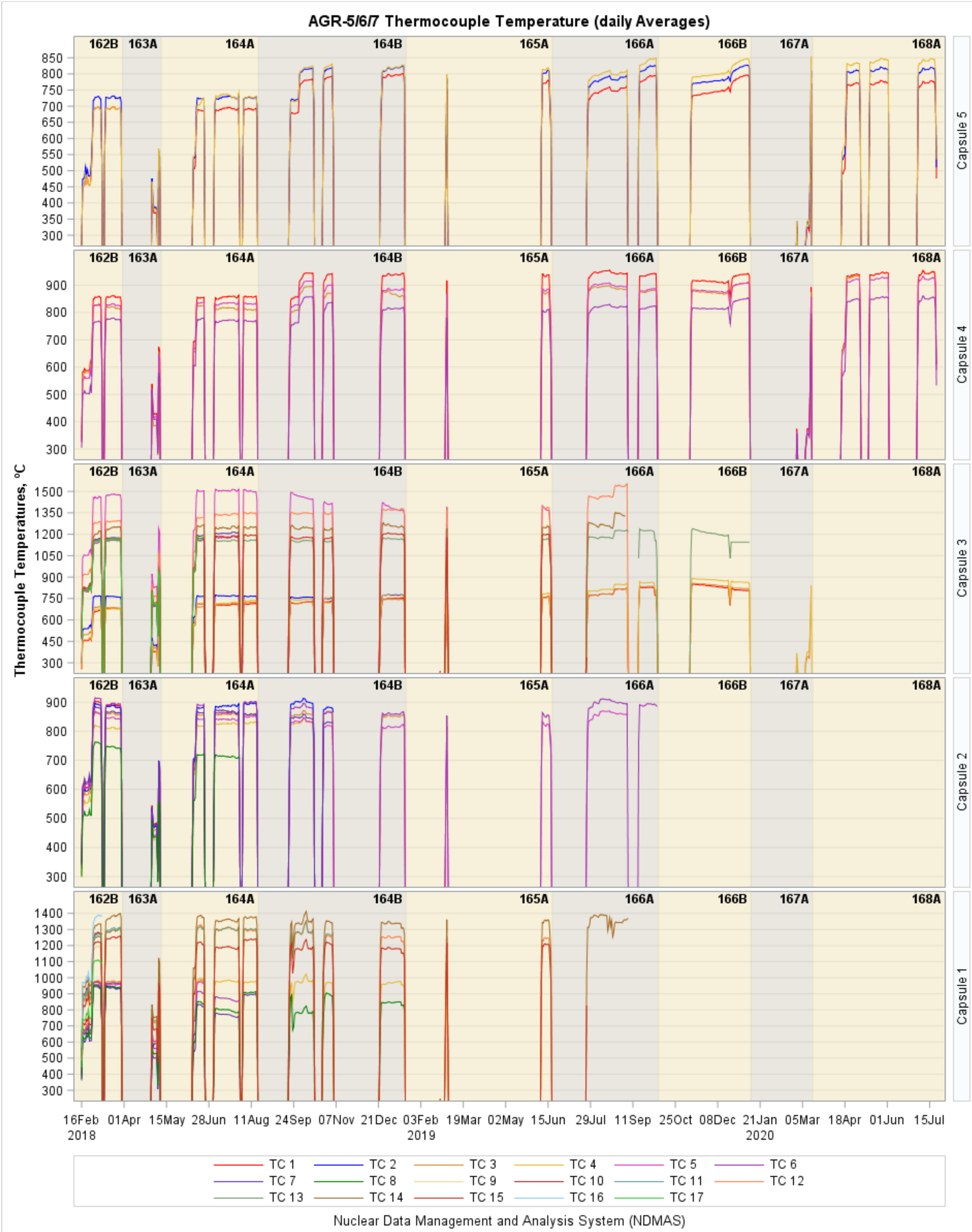

Figure 50. AGR-5/6/7 measured TC temperatures.

Most TC failures occurred at scrams, when temperatures dropped rapidly to room temperature after ATR power dropped from full to zero within approximately 5 minutes. Powering up also causes TC failures, but to a lesser extent, because powering up is usually much more gradual than powering down. Failures were identified when TC readings stopped or became stuck at the same level for extended period when neighboring TC readings were fluctuating. These events are detailed in the AGR-5/6/7 irradiation data qualification report (Pham 2021). TC failures by capsule (Table 17) are summarized below.

- Capsule 1: all 17 installed TCs failed, which led to no operational TCs remaining in this capsule after Cycle 166A (Cycle 6). This is consistent with TC failures in previous AGR experiments because wires of TCs in the bottom capsule had to pass through all other capsules, including the high temperature Capsule 3. Multiple TC failures occurred during the first cycle, Cycle 162B. Interestingly, the longest surviving TC was exposed to the highest temperature range in this capsule, up to 1400°C.
- Capsule 2: all eight installed TCs failed by the end of Cycle 166B. These Type N TCs were exposed to lower temperatures (up to 900°C) and started to fail from the third cycle, Cycle 164A. Capsule 2 TC wires also had to pass through the highest temperature capsule (Capsule 3).
- Capsule 3: five of the 17 TCs were broken during assembly and the remaining 12 TCs failed during irradiation; no operational TC remained in this capsule after Cycle 167A. Capsule 3 TC-12 was exposed to temperatures as high as 1550°C but still survived for almost six cycles.
- Capsules 4 and 5: only one TC failed in Capsule 4 during operation, and this failure occurred during the last cycle of irradiation. This could be because TC wires in these capsules do not have to pass through the hottest capsule (Capsule 3). Other TC failures (two in Capsule 4 and three in Capsule 5) occurred before irradiation, during handling and assembly.

According to the AGR-5/6/7 final data qualification report (Pham 2021), a total of 57,746,693 TC temperature readings were captured from all TCs. Among them, 10,034,676 TC temperature records (only 17.4%) were *Qualified* and 47,701,371 TC temperatures (or 82.6%) are *Failed* due to 48 TC failures (63.5%) and due to missing values (19.1%). Figure 50 shows the readings of all functioning TCs as a function of EFPDs; the plots are discontinued at the time of TC failures. Plots for all TCs are mostly parallel to each other, which indicates similar behavior among the TCs. An exception is TC-5, located in the center of Capsule 3, with gradually decreasing readings during Cycle 164B until its failure on July 26, 2019 (Cycle 166A).

The temperature difference between TCs in the same capsule should generally remain constant over time. Any other trend or discontinuity in the data could suggest that one of the TCs is drifting. Thus, control charts for a pair of the primary and secondary-control TCs are used for monitoring consistency of the control TCs. Measured TCs are also compared with the calculated values from capsule thermal models to demonstrate that the control TCs are behaving as physically expected. These TC temperature trends are used to assess the performance of the operational TCs. Analyses on control charts of TC temperature differences revealed trending in TC readings for TC2, 4, 5, and 13 in Capsule 3, but there is no conclusive indication of TC drift failure that caused those trends (Pham 2021). Therefore, TC control charts are not used to disqualify TC data, but only for users' consideration. A summary of TC performance in the AGR-5/6/7 experiment offered in the conference paper (Palmer et al., 2021) also indicated little evidence of TC drift in all capsules.

Table 17. 48 TC failures in AGR-5/6/7 experiment.

Capsule (No. TCs)	Failed TCs	Failure Date and Time	ATR Cycle	Associated Event
1 (17)	1, 9, 10, 16, 17	3/9/2018 17:00	162B	Scram
	11	3/29/2018 07:00	162B	Scram
	2	5/7/2018 07:30	163A	High power
	3	6/24/2018 06:00	164A	Scram
	5	7/3/2018 12:30	164A	Ramp up
	6	7/30/2018 12:00	164A	Scram
	7	9/20/2018 12:30	164B	Ramp up
	13	11/4/2018 18:00	164B	Scram
	8	1/17/2019 14:30	164B	Scram
	4	6/8/2019 09:00	165A	Restart
	12	6/18/2019 14:00	165A	Scram
	15	7/25/2019 20:00	166A	Ramp up
	14	9/06/2019 07:00	166A	Scram
2 (8)	1	6/14/2018 18:00	164A	Ramp up
	8	7/30/2018 12:00	164A	Scram
	4	10/24/2018 22:00	164B	Ramp up
	2, 7	11/4/2018 19:00	164B	Scram
	3	3/1/2019 12:00	165A	Scram
	5	9/06/2019 08:00	166B	Scram
	6	10/06/2019 01:00	166B	Power-down
3 (17)	8, 9, 10, 11, 16	Assembly	—	Assembly
	17	6/24/2018 06:00	164A	Scram
	6, 7	8/2/2018 13:00	164A	Restart
	2	1/17/2019 15:00	164B	Scram
	5, 15	7/25/2019 09:00	166A	Ramp up
	14	9/03/2019 14:00	166A	Scram
	12	9/10/2019 13:00	166A	Ramp up
	13	12/21/2019 18:00	166B	Full power
	1, 13	1/10/2020 11:30	166B	Power-down
	3, 4	3/14/2020 12:00	167A	Power-down
4 (6)	2, 4	Assembly	—	Assembly
	3	5/13/2020 1:00	168A	Ramp up
5 (6)	3, 5, 6	Assembly	—	Assembly

6. CONCLUSION

The AGR 5/6/7 fuel test has been irradiated for nine complete cycles (four short of the originally planned 13-cycle schedule), resulting in approximately 360 EFPDs. At the end of Cycle 167A, burnup, fast fluence, and temperature histories may be summarized as follows:

- Compact-average burnups ranged from 5.66% FIMA (Compact 1-1-2 in Capsule 1) to 15.26% FIMA (Compact 2-8-4 in Capsule 2)
- Compact-average fast fluences ranged from 1.62×10^{25} n/m^2 (Compacts 1-1-1 and 1-1-2 in Capsule 1) to 5.55×10^{25} n/m^2 (Compact 1-1-1 in Capsule 3)
- For AGR-5/6 capsules (Capsules 1, 2, 4, and 5), the time-averaged, volume-averaged fuel temperatures, on a compact basis, ranged from 458°C to 1244°C at the end of irradiation, where temperatures during the two low-power PALM cycles were excluded and the neon faction was assumed to be zero in Capsule 1 during the last cycle, Cycle 168A. The actual fuel proportions are close to the 30% specification for the middle ranges (between 900°C and 1050°C); lower for the higher ranges (between 1050°C and 1250°C); and higher for the lowest range (<900°C). The proportion of fuel in highest temperature range (≥1250°C) was 0% (a specification of 10%).
- For AGR-7 Capsule 3, the time-averaged peak fuel temperature is 1432°C (close to the specification of 1500 ± 50°C) when data from the two low-power PALM cycles were excluded from time averaging.

Of the fifty-four installed TCs, 48 failed by the end of Cycle 168A. The six surviving TCs were in the top Capsules 4 and 5. The three bottom capsules had no operational TCs left (i.e., Capsules 1 from Cycle 166A, Capsule 2 from Cycle 167A, and Capsule 3 from 168A). When all TCs failed in a capsule, the appropriate neon fraction was determined based on thermal models so that the fuel temperatures could be maintained within the specified range. The exception was Capsule 1 during Cycle 168A, when its gas line was totally isolated. Thus, the Capsule 1 neon fraction was bounded between zero (neon fraction at the start of the irradiation) and the neon fraction in the leadout.

During the first five cycles (Cycles 162B–165A), FG isotope R/Bs were stable in the 10^{-8}–10^{-6} range and no in-pile particle failures were observed based on the GG counts. The higher EK fraction and high fuel temperatures in Capsule 1 led to the maximum R/B value of around 2×10^{-6} for Kr-85m.

Gas line issues in Capsule 1 occurred from the fourth cycle (Cycle 164B) and were mitigated to minimize crosstalk between capsule gas lines. Capsule 1 FG release measurements were not possible during the last three cycles (Cycles 166B, 167A, and 168A) because of the gas flow isolation. Capsule 1 gas line issues also caused noticeable FG leakage into Capsules 2–5 to various degrees over time starting from the sixth cycle, Cycle 166A. Therefore, R/Bs for all capsules from Cycle 166A onward are considered uncertain because of undefined contamination from Capsule 1. However, they can be used when the leaking amount from Capsule 1 can be roughly estimated or deemed negligible.

By the end of Cycle 166A, a significant number of in-pile failures occurred in Capsule 1, but the final number of in-pile failures is unknown due to the absence of measured FG release activities during the last three cycles. Fifteen particle failures in Capsule 3 and four failures in Capsule 2 were estimated based on GG count spikes and measured isotope activities at the FPM detectors during the last cycle, Cycle 168A. In contrast, no in-pile failures for Capsules 4 and 5 were estimated based on the AGR-3/4 R/B model and an absence of distinct increases in isotope activities and GG counts.

The results of this test will provide irradiation-performance data for the reference fuel manufactured at a pilot scale for a typical HTGR temperature range (AGR-5/6) as well as at temperatures beyond the normal range (AGR-7). Together with previous AGR data, the AGR-5/6/7 data will form a link between fabrication processes, fuel-product properties, and irradiation performance.

7. REFERENCES

Abaqus, 2014. Abaqus Version 6.14-2 documentation. Dassault Systèmes.

ASTM, 2014. Standard practice for testing graphite and boronated graphite materials for high-temperature gas-cooled nuclear reactor components. C781-08, ASTM International, West Conshohocken, Pennsylvania. https://doi.org/10.1520/C0781-08R14

B&W Nuclear Operations Group, 2013. J52L, Industrial Fuel Fabrication and Development – Lot J52L-16-69316, Book 1, Lynchburg, VA: B&W Nuclear Operations Group.

BWXT, 2017. "Industrial Fuel Fabrication and Development LEU Compact Certification Package." Data Certification Package, August 2017.

Collin B.P., 2018. "AGR-5/6/7 Irradiation Experiment Test Plan." INL/MIS-17-43095, Rev. 1, Idaho National Laboratory. https://www.osti.gov/biblio/1511042-agr-irradiation-experiment-test-plan.

Croff, A.G., 1983. "ORIGEN2: A Versatile Computer Code for Calculating the Nuclide Compositions and Characteristics of Nuclear Materials." Nuclear Technology 62(3): 335–352. https://doi.org/10.13182/NT83-1.

Demkowicz P. and B.T. Pham, 2019. "ECAR-4802 Fission Gas Activity Criteria for Operation of the AGR-5/6/7 Experiment in the Advanced Test Reactor," INL/MIS-19-56800, Rev. 0, Idaho National Laboratory. https://doi.org/10.2172/1599404.

Folsom, C., C. Xing, C. Jensen, H. Ban, and D.W. Marshall, 2015. "Experimental measurement and numerical modeling of the effective thermal conductivity of TRISO fuel compacts." Journal of Nuclear Materials 458: 198–205. https://doi.org/10.1016/j.jnucmat.2014.12.042.

Gontard, R. and H. Nabielek, 1990. Performance Evaluation of Modern HTR TRISO Fuels. Report HTA IB-05/90, Forschungszentrum Jülich GmbH (FZJ).Gonzo, E.E., 2002. "Estimating Correlations for the Effective Thermal Conductivity of Granular Materials," *Chemical Engineering Journal*, 90, 299–302.

Gonzo, E.E., 2002. "Estimating correlations for the effective thermal conductivity of granular materials." Chemical Engineering Journal 90(3): 299–302. https://doi.org/10.1016/S1385-8947(02)00121-3.

Hawkes, G.L., 2021. "AGR-5/6/7 Daily As-Run Thermal Analyses." ECAR-5633, Rev. 0, August 2021.

Hawkes, G.L., 2020. "Cylindricity Sensitivity Thermal Model of the AGR-5/6/7 Experiment in the Advanced Test Reactor." IMECE2020-23329, International Mechanical Engineering Congress and Exposition, Portland, OR, USA, November 16-19, 2020. https://doi.org/10.1115/IMECE2020-23329.

Hawkes, G.L., J. W. Sterbentz, and M. Plummer, 2019. "Thermal Model Details and Description of the AGR-5/6/7 Experiment." ICAPP 2019 – International Congress on Advances in Nuclear Power Plants, France, Juan-les-pins, May 12-15, 2019.

Kestin, J., K. Knierim, E.A. Mason, B. Najafi, S.T. Ro, and M. Waldman, 1984. "Equilibrium and Transport Properties of the Noble Gases and Their Mixtures at Low Density." Journal of Physical and Chemical Reference Data 13: 229–303. https://doi.org/10.1063/1.555703.

LANL, X 5 Monte Carlo Team. 2004. MCNP—A General Monte Carlo N Particle Transport Code, Version 5, Volume I, LA UR 03 1987, Los Alamos National Laboratory, April 24, 2003 (Revised 6/30/2004), and Volume II, LA CP 0245, Los Alamos National Laboratory, April 24, 2003 (Revised 6/30/2004). https://mcnp.lanl.gov/pdf_files/la-ur-03-1987.pdf.

Lybeck, N.J., 2016. "Nuclear Data Management and Analysis System Plan." PLN 2709, Rev. 5, Idaho National Laboratory.

Maki, J.T., 2015. “AGR-5/6/7 Irradiation Test Specification.” SPC-1749, Rev. 0, Idaho National Laboratory.

Marshall D.W., 2017. “AGR-5/6/7 Fuel Specification.” INL/MIS-11-21423, Rev. 8, Idaho National Laboratory. https://www.osti.gov/biblio/1529089-agr-fuel-specification.

Marshall D.W., 2019. “AGR-5/6/7 Fuel Fabrication Report.” INL/EXT-19-53720, Rev. 1, Idaho National Laboratory. https://doi.org/10.2172/1512795.

Mitchell, T. R., 2020. “Technical Program Plan for INL Advanced Reactor Technologies Advanced Gas Reactor Fuel Development and Qualification Program.” PLN-3636, Rev. 9, Idaho National Laboratory. https://www.osti.gov/biblio/1776792-technical-program-plan-inl-advanced-reactor-technologies-advanced-gas-reactor-fuel-development-qualification-program.

Murray P.E., 2018. “Thermal Analysis of the AGR-5-6-7 Experiment” ECAR-2966, Rev.5, Idaho National Laboratory.

Nelson M.M., 2020. “AGR-5/6/7 Gas System – Analysis of Various Anomalies Encountered During Irradiation.” ECAR-5114, Rev. 0, Idaho National Laboratory.

Palmer A. J., R.S. Skifton, M. Scervini, G. L. Hawkes, B. T. Pham, and T. L. Checketts, 2021. “Summary of Thermocouple Performance in the Advanced Gas Reactor Experiment AGR-5/6/7 During Irradiation in the Advanced Test Reactor.” Conference Proceeding of ANIMMA 2021, Paper 04-196, Prague, Czech Republic, June 21–25, 2021.

Petti, D.A., J.T. Maki, J. Buongiorno, R.R. Hobbins, and G.K. Miller, 2002. “Key Differences in the Fabrication, Irradiation and Safety Testing of U.S. and German TRISO-coated Particle Fuel and Their Implications on Fuel Performance.” INEEL/EXT-02-00300, Idaho National Engineering and Environmental Laboratory. https://doi.org/10.2172/910651.

Pham B.T. and D.M. Scates., 2019. “AGR-5/6/7 Release-to-Birth Ratio Data Analysis for Cycles 162B, 163A, 164A, and 164B.” INL/EXT-19-54457, Rev. 0, Idaho National Laboratory. https://www.osti.gov/biblio/1542583-agr-release-birth-ratio-data-analysis-cycles.

Pham, B.T., J.J. Einerson, D.M. Scates, J.T. Maki, and D.A. Petti., 2019. “AGR-1, AGR-2 and AGR-3/4 Release-to-Birth Ratio Data Analysis.” INL/EXT-14-32970, Rev. 2, Idaho National Laboratory. https://doi.org/10.2172/1599785.

Pham, B.T., 2021. “AGR-5/6/7 Data Qualification Report for ATR Cycles 162B through 168A.” INL/EXT-21-62180, Rev. 0, Idaho National Laboratory. https://www.osti.gov/biblio/1777247-agr-data-qualification-report-atr-cycles-through.

Scates, D.M., J. Walter, M. Drigert, E. Reber, and J. Harp., 2010. “Fission Product Monitoring and Release Data for the Advanced Gas Reactor 1 Experiment.” Proceedings HTR 2010, Paper 52, Prague, Czech Republic, October 18–20, 2010. https://www.osti.gov/biblio/1009169-gHSEgl/.

Scates, D.M., 2021. “Release-to-Birth Ratios for AGR-5/6/7 Operating Cycles 162B through 168A.” ECAR-5352, Rev. 0, Idaho National Laboratory.

Sharp, M., 2020. “Idaho National Laboratory Advanced Reactor Technologies Quality Assurance Program Plan.” PLN-2690, Rev. 19, Idaho National Laboratory. https://www.osti.gov/biblio/1615631-idaho-national-laboratory-advanced-reactor-technologies-quality-assurance-program-plan.

Shibata T., M. Eto, E. Kunimoto, S. Shiozawa, K. Sawa, T. Oku, and T. Maruyama., 2010. *Draft of Standard for Graphite Core Components in High Temperature Gas-cooled Reactors,* Japan Atomic Energy Agency Research 2009-042.

Sterbentz, J.W., 2020. "JMOCUP Physics Depletion Calculation for the As-Run AGR-5/6/7 TRISO Particle Experiment in ATR Northeast Flux Trap," ECAR-5321, Rev. 0, Idaho National Laboratory. https://www.osti.gov/biblio/1774808-jmocup-physics-depletion-calculations-run-agr-triso-particle-experiment-atr-northeast-flux-trap.

Sterbentz, J.W., 2017. "JMOCUP Physics Depletion Calculation for the Design of the AGR-5/6/7 TRISO Particle Experiment in ATR Northeast Flux Trap," ECAR-2961, Rev. 1, Idaho National Laboratory.

Sterbentz, J.W., 2015. "JMOCUP As-Run Daily Physics Depletion Calculation for the AGR-3/4 TRISO Particle Experiment in ATR Northeast Flux Trap," ECAR-2753, Idaho National Laboratory.

Swank D., J. Lord, D. Rohrbaugh, and W. Windes., 2012. "AGC-2 Graphite Preirradiation Data Package." INL/EXT-10-19588, Rev 1, Idaho National Laboratory. https://doi.org/10.2172/1070123.

Windes, W.E., D. T. Rohrbaugh, and D. W. Swank., 2017. "AGC-2 Irradiated Material Properties Analysis," INL/EXT-17-41165, Idaho National Laboratory. https://doi.org/10.2172/1369362.

Windes, W.E., W. D. Swank, D. Rohrbaugh, and J. Lord., 2013. "AGC-2 Graphite Preirradiation Data Analysis Report." INL/EXT-13-28612, Rev 1, Idaho National Laboratory. https://doi.org/10.2172/1097190.

Windes, W.E., 2012. "Data Report on Post-Irradiation Dimensional Change of AGC-1 Samples." INL/EXT-12-26255, Idaho National Laboratory. https://doi.org/10.2172/1056006.

APPENDIX A

As-Manufactured Fuel Characterization Data

Appendix A

As-Manufactured Fuel Characterization Data

Kernels for AGR-5/6/7 consist of LE UCO fuel. The kernels were fabricated by BWX Technologies Nuclear Operations Group (B&W Nuclear Operations Group, 2013) in accordance with the AGR-5/6/7 Fuel Product Specification (Marshall, 2017). Selected as-fabricated properties of the AGR-5/6/7 fuel presented below are extracted from the fuel fabrication report, INL/EXT-19-53720 (Marshall, 2019). Characterization properties for the kernel lots, fuel specifications, and measured property data are given in Table 18. All properties were compliant with the fuel specification at the specified confidence levels, except for the impurities in Lot J52R-16-69318. Some of the impurities failed to show compliance at the 95% confidence level because the sample set was too small. All the results were reported as being below the statistical detection limit for the respective elements, so the upper limit at 95% confidence would be similar to that of Lot J52R-16-69317 if the same number of replicate analyses had been performed.

The composited TRISO particle lot (J52R-16-98005) met all fuel specifications on the mean and for dispersion except for the OPyC thickness (shown in red in Table 19). The OPyC thickness was deficient in mean and the lower limit of the mean but not in the lower dispersion limit. Measurements taken for the composited lot used a significantly larger sample size, which decreased the uncertainty in the statistical calculation and yielded an estimate of the true defect fraction that passed the specification at 95% confidence. Preburn and postburn leaches were performed to get an indication of the DUF and EKF to ensure that only TRISO products with low defect fractions were used in subsequent fuel fabrication processes. These analyses were not required by the fuel specification at the particle level but are specified for compact batches. From these preliminary results, it was understood that the compacts may fail the DU specification but were expected to pass the EK and defective silicon carbide specifications.

Characterization data for the compacts are reported in Table 20 for a 45% packing fraction and Table 21 for a 25% packing fraction. Data include those tables reported by BWX Technology for most properties and from Oak Ridge National Laboratory for the DUF, EKF, and silicon carbide defect fraction values. The chemical impurities analyses are shown in Table 22.

AGR-5/6/7 compacts are nominally 25.0 mm in length and 12.3 mm in diameter. The AGR-5/6/7 fuel compacts were fabricated with two different nominal particle loadings (packing fractions of 25 and 40%). A summary of selected properties is listed in Table 23 along with mean value specifications, where applicable, for comparison purposes (Collin, 2018). Data for compact mass, diameter, and length are based on averages of the 432 compacts sent to INL (batches J52R-16-14154A and J52R-16-14155A for a 40% packing fraction and batches J52R-16-14156A and J52R-16-14157A for a 25% packing fraction). Most of the fabrication data were based on actual characterization data (BWXT, 2017), except for the destructive chemical analyses results. Specifically, the DUF, EKF, and silicon carbide defect fraction values were based on the destructive chemical analyses from Oak Ridge National Laboratory and taken from Table 20 and Table 21.

Table 18. AGR-5/6/7 certified UCO-kernel lot characterization data.

Kernel Lot Properties	Specification	J52R-16-69317 [a]	J52R-16-69318 [a, b] (backup lot)
Diameter (µm)	425 ± 10 ≤ 1% < 375 ≤ 1% > 475	425.78 ± 10.42 1% < 397.81 1% > 453.74	422.69 ± 5.52 1% < 407.88 1% > 437.50
Envelope density (g/cm^3)	≥ 10.4	11.048 ± 0.044 LL ≥ 11.018	11.075 ± 0.035 LL ≥ 10.917
Uranium fraction (g U/g UCO)	≥ 0.885	0.8968 ± 0.0004 LL ≥ 0.8965	0.8965 ± 0.00014 LL ≥ 0.8958
^{235}U enrichment (g ^{235}U/g U)	0.155 ± 0.001	0.15477 ± 0.00013 LL ≥ 0.1546 UL ≤ 0.1549	0.15433 ± 0.00099 LL ≥ 0.1534 UL ≤ 0.1552
C:U (atomic ratio)	0.40 ± 0.10	0.370 ± 0.000	0.330 ± 0.000
O:U (atomic ratio)	1.50 ± 0.20	1.441 ± 0.0035 LL ≥ 1.438 UL ≤ 1.444	1.470 ± 0.014 LL ≥ 1.343 UL ≤ 1.597
(C+O)/U (atomic ratio)	≤2.0	1.811 ± 0.0035 UL ≤ 1.814	1.795 ± 0.007 UL ≤ 1.827
Individual impurities (ppmw):			
Cl, Ca, & Fe Al, Co, Cr, Cu, Mn, Na, Ni, & Zn Li & V	≤100 each	< 25; UL < 30.9 ≤ 10.3; UL ≤ 13.7 < 5; UL < 6.2	< 25; UL < 124 [c] < 10; UL < 49.6 < 5; UL < 24.8
Process impurities (ppmw):			
P S	≤1,500 each	< 25; UL < 30.9 246.6; UL < 255.9	< 25; UL < 124 241.5; UL < 301.5
Aspect ratio	≤10% ≥1.05	10% ≥ 1.020	10% ≥1.023
Countable fissure fractions [d]	—	0.59% LL ≥ 0.36% UL ≤ 0.93%	1.02% LL ≥ 0.70% UL ≤ 1.43%

a. All variable property upper limits (UL), lower limits (LL), and dispersion tests (e.g., 1% < …) are at 95% confidence levels.
b. Failures to conform to the fuel specifications at the designated confidence level (generally 95%) are denoted in red.
c. The averages of all impurities were below detection levels (25 ppmw or less). Few replicate analyses resulted in a large estimated standard deviation and a large upper-limit estimate for Ca, Cl, and Fe. All others were UL <50 ppmw at 95% confidence.
d. Countable fissure is one that terminates within the oxidic rind at two or more positions along the kernel perimeter, which is thought to be more prone to fracturing and becoming a source of misshapen particles and resulting in DU contamination within the coating layers.

Table 19. TRISO-coated particle J52R-16-98005 lot characteristics.

TRISO Particle Property	Specification	J52R-16-98005 [a, b, d]
Buffer thickness (μm)	100 ± 15 ≤1% ≤ 58	100.4 ± 5.6 (range 99.6 - 101.1) 1% <88.4
IPyC thickness (μm)	40 ± 4 ≤1% ≤30 ≤1% ≥52	39.24 ± 1.26 (range 39.06 - 39.41) 1% <36.53 1% >41.94
SiC thickness (μm)	35 ± 3 ≤1% 28	36.15 ± 0.65 (range 36.06 - 36.24) 1% <34.75
OPyC thickness (μm)	40 ± 4 ≤1% ≤20	35.03 ± 1.99 (range 34.75 - 35.31) 1% <30.76
Buffer density (g/cm^3)	1.05 ± 0.10	1.031 ± 0.022 (range 0.996 - 1.065)
IPyC density (g/cm^3)	1.90 ± 0.05 ≤1% ≤1.80 ≤1% ≥2.00	1.897 ± 0.099 (range 1.896 - 1.898) 1% <1.876 1% >1.918
SiC density (g/cm^3)	≥3.19 ≤1% ≤3.17	3.195 ± 0.002 (range ≥ 3.1945) 1% <3.1913
OPyC density (g/cm^3)	1.90 ± 0.05 ≤1% ≤1.80 ≤1% ≥2.00	1.897 ± 0.004 (range 1.897 - 1.898) 1% <1.876 1% >1.918
IPyC diattenuation [c]	≤ 0.0170 ≤1% ≥0.0242	0.0153 ± 0.0010 (range ≤0.016) 1% >0.019
OPyC diattenuation [c]	≤ 0.0122 ≤1% ≥0.0242	0.0102 ± 0.0006 (range ≤0.010) 1% >0.012
SiC aspect ratio (faceting)	— ≤1% ≥1.14	1.053 ± 0.009 1% >1.0735
Defective IPyC coating fraction [c]	≤1.0E-4	<0.75E-4
Defective OPyC defect fraction	≤3.0E-4	<0.86E-4
Preburn, mean	—	1.11E-5
Postburn, mean	—	2.19E-5

a. Failures to conform to the fuel specifications at the designated confidence level are shown in red.
b. All variable property UL, LL, and dispersion tests (e.g., 1% < …) are at 95% confidence levels.
c. Data are from ORNL/TM-2017/036-R1 and ORNL/TM-2017/037 – Rev. 0.
d. 95% confidence limits are shown in parentheses for these variable properties: (LL – UL), (≥ LL), or (≤ UL).

Table 20. Characterization data for nominally 40% PF compacts after heat treatment.

Property	Specification	J52R-16-14154	J52R-16-14155
Variable Properties			
Mean uranium loading (gU/compact) Nominally 40% packing fraction	1.36 ± 0.10	1.370 ± 0.005 LL = 1.370 UL = 1.370	1.347 ± 0.006 LL = 1.348 UL = 1.347
Diameter (mm)	— 0 ≤12.20 0 ≥12.44	12.29 ± 0.01 0 ≤ 12.25 0 ≥ 12.35	12.29 ±0.02 0 ≤ 12.25 0 ≥ 12.34
Length (mm) [a]	— 0 ≤24.40 0 ≥25.30	25.03 ± 0.08 0 ≤ 24.80 0 ≥ 25.24	24.69 ± 0.10 0 ≤24.46 3 ≥ 25.30
Mass (g)	—	6.71 ±0.02	6.61 ± 0.03
Compact density (g/cm^3)	—	2.26 ±0.01	2.26 ± 0.01
Matrix density (g/cm^3)	≥1.65	1.75 ±0.01 0 ≤1.73	1.75 ± 0.01 0 ≤1.72
Dispersed uranium fraction (DUF) ($g{\cdot}U_{leached}/g{\cdot}U_{sample}$)	≤1.0E-5	4.95E-6 average and ≤5.7E-6 [b]	
Attribute Properties			
Defective OPyC coating fraction	≤0.01	Not measured	0/4200 ≤7.13E-4
Exposed kernel fraction (EKF) (kernel equiv./particle count)	≤5.0E-5	5.39E-5 average and ≤8.3E-5 [b]	
Defective SiC coating fraction (kernel equiv./particle count)	≤1.0E-4	≤7.5E-5 [b]	

a. No compacts were used in the AGR-5/6/7 test train that failed to meet dimensional specifications for the test capsule.
b. Pooled data for 40% PF compacts are at 95% confidence and analyzed at ORNL.

Table 21. Characterization data for nominally 25% PF compacts after heat treatment.

Property	Specification	J52R-16-14156	J52R-16-14157
Variable Properties			
Mean uranium loading (gU/compact) Nominally 25% packing fraction	0.90 ± 0.08	0.901 ± 0.004 LL = 0.900 UL = 0.901	0.870 ± 0.005 LL = 0.869 UL = 0.870
Diameter (mm)	— 0 ≤12.20 0 ≥12.44	12.24 ± 0.01 0 ≤ 12.20 0 ≥ 12.29	12.27 ± 0.01 0 ≤12.23 0 ≥12.31
Length (mm)[a]	— 0 ≤24.40 0 ≥25.30	25.10 ± 0.10 0 ≤24.76 12 ≥25.30	24.78 ± 0.13 0 ≤24.55 2 ≥25.30
Mass (g)	—	6.20 ± 0.03	6.09 ± 0.04
Compact density (g/cm^3)	—	2.10 ± 0.01	2.08 ± 0.01
Matrix density (g/cm^3)	≥1.65	1.76 ± 0.01 0 ≤1.73	1.75 ± 0.01 0 ≤1.73
Dispersed uranium fraction (DUF) (g·Uleached/g·Usample)	≤1.0E-5	5.02E-6 average and ≤ 5.6E-6[b]	
Attribute Properties			
Defective OPyC coating fraction	≤0.01	0/4200 ≤7.13E-4	Not measured
Exposed kernel fraction (EKF) (kernel equiv./particle count)	≤5.0E-5	7.27E-6 average and ≤3.5E-5[b]	
Defective SiC coating fraction (kernel equiv./particle count)	≤1.0E-4	≤5.7E-5[b]	

a. No compacts were used in the AGR-5/6/7 test train that failed to meet dimensional specifications for the test capsule.
b. Pooled data for 25% PF compacts are at 95% confidence and analyzed at ORNL.

Table 22. Chemical impurities analyses for AGR-5/6/7 compacts.

Impurity[a]	BWXT Pooled Data[b]	ORNL (40% PF) 14154C	ORNL (25% PF) 14156C, D	Fuel Specification
Compact Count	24 (6 ea.)	20	20	—
Iron (µg)[c]	5 ± 1.28 UL = 5.5 ≤1% ≥ 9.1	77.62 ± 4.75 UL = 79.5 ≤1% ≥ 94	48.16 ± 5.11 UL = 50.1 ≤1% ≥ 65	≤25 ≤1% ≥100
Transition metals (µg)[c]				
Cr	25 ± .42	0.39 ± 0.06	0.65 ± 0.22	≤50 each
Mn	10 ± 2.57	0.561 ± 0.029	0.345 ± 0.013	
Co	10 ± 2.57	0.043 ± 0.005	0.021 ± 0.004	
Ni	10 ± 2.57	1.24 ± 0.26	1.64 ± 0.46	
Σ(Cr, Mn, Co, Ni)	55 ± 7.81	2.24 ± 0.27	2.65 ± 0.51	
Σ UL	≤1% Σ ≥ 80	≤1% Σ ≥ 3.2	≤1% Σ ≥ 4.4	≤1% Σ ≥200
Calcium[c,d] (µg)	25.5 ± 7.76 UL = 28.3	135.21 ± 5.83 UL = 137.5	114.27 ±8.38 UL = 117.5	≤50
Aluminum[c,d] (µg)	27.7 ±16.0 UL = 33.3	166.80 ±4.16 UL = 168.4	133.95 ±4.33 UL = 135.6	≤50
Ti + V (µg)				
Ti	10 ± 2.57	12.11 ± 2.85	9.66 ± 0.41	
V	10 ± 2.57	5.46 ± 0.08	5.54 ± 0.08	
Σ(Ti, V)[c]	20 ± 3.63	17.57 ± 2.85	15.20 ± 0.42	
Σ UL	≤ 21.3	≤ 18.7	≤ 15.4	Σ ≤ 240

a. Impurity units are µg per compact outside of the SiC layer.
b. BWXT data was pooled from six compacts from each of the four-compact series. Averages from all sets were below the analytical detection limits for the analytes, except for a few individual compacts. Integer values for the means reflect the detection limits. BWXT data are the data used to certify the compacts for inclusion in the AGR-5/6/7 experiment.
c. Reported UL is the 95% upper confidence limit.
d. ORNL has a known cross-contamination issue with Al and Ca. Reported values may not be accurate.

Table 23. Selected properties for AGR-5/6/7 compacts.

Property	Specified Range for Mean Value	Actual Mean Value ± Population Standard Deviation
Compact mass (g)		
Capsule 1	Not specified	6.676 ± 0.065
Capsule 2		6.182 ± 0.026
Capsule 3		6.187 ± 0.021
Capsule 4		6.100 ± 0.034
Capsule 5		6.603 ± 0.021
Mean uranium loading (g U/compact)		
Capsule 1	1.36 ± 0.10	1.362 ± 0.014
Capsule 2	0.90 ± 0.08	0.898 ± 0.004
Capsule 3	0.90 ± 0.08	0.898 ± 0.003
Capsule 4	0.90 ± 0.08	0.871 ± 0.005
Capsule 5	1.36 ± 0.10	1.346 ± 0.004
Diameter [a] (mm)		
Capsule 1	12.20–12.44	12.293 ± 0.007
Capsule 2		12.241 ± 0.007
Capsule 3		12.245 ± 0.006
Capsule 4		12.248 ± 0.006
Capsule 5		12.296 ± 0.006
Length [a] (mm)		
Capsule 1	24.40–25.30	24.947 ± 0.219
Capsule 2		24.991 ± 0.098
Capsule 3		25.000 ± 0.078
Capsule 4		24.770 ± 0.119
Capsule 5		24.675 ± 0.059
Estimated mean number of particles per compact [b]		
Capsule 1	Not specified	3434
Capsule 2		2264
Capsule 3		2265
Capsule 4		2197
Capsule 5		3393
Particle volume packing fraction (%)		
Capsule 1	40	38.4
Capsule 2	25	25.5
Capsule 3	25	25.5
Capsule 4	25	24.9
Capsule 5	40	38.4
Effective overall compact density [b] (g/cm^3)		
Capsule 1	Not specified	2.26
Capsule 2		2.10
Capsule 3		2.10
Capsule 4		2.09
Capsule 5		2.25
Compact matrix density (g/cm^3)	≥1.65	1.748 ± 0.007
Capsule 1		1.772 ± 0.005
Capsule 2		1.771 ± 0.005
Capsule 3		1.766 ± 0.006

Property	Specified Range for Mean Value	Actual Mean Value ± Population Standard Deviation
Capsule 4 Capsule 5		1.747 ± 0.007
Compact weight% U [b] Capsule 1 Capsule 2 Capsule 3 Capsule 4 Capsule 5	Not specified	 20.40 14.52 14.52 14.28 20.38
Compact weight% O [b] Capsule 1 Capsule 2 Capsule 3 Capsule 4 Capsule 5	Not specified	 1.98 1.41 1.41 1.39 1.98
Compact weight% Si [b] Capsule 1 Capsule 2 Capsule 3 Capsule 4 Capsule 5	Not specified	 7.18 5.11 5.11 5.03 7.18
Compact weight% C [b] Capsule 1 Capsule 2 Capsule 3 Capsule 4 Capsule 5	Not specified	 70.44 78.96 78.96 79.31 70.47
Iron content (μg Fe outside of SiC/compact)	≤25	<5
Chromium content (μg Cr outside of SiC/compact)	≤50	<25
Manganese content (μg Mn outside of SiC/compact)	≤50	<10
Cobalt content (μg Co outside of SiC/compact)	≤50	<10
Nickel content (μg Ni outside of SiC/compact)	≤50	<10
Calcium content (μg Ca outside of SiC/compact)	≤50	<25
Aluminum content (μg Al outside of SiC/compact)	≤50	<25

Property	Specified Range for Mean Value	Actual Mean Value ± Population Standard Deviation
Titanium content (μg Ti outside of SiC/compact)	Note (c)	<10
Vanadium content (μg V outside of SiC/compact)	Note (c)	<10
Dispersed uranium fraction [(d)] (g leached U/g U in compact)		
Nominal 25% packing fraction	$\leq 1.0 \times 10^{-5}$	$\leq 5.6 \times 10^{-6}$ [(e)]
Nominal 40% packing fraction	$\leq 1.0 \times 10^{-5}$	$\leq 5.7 \times 10^{-6}$ [(e)]
Exposed kernel fraction [(d)] (kernel equivalent/particle count)		
Nominal 25% packing fraction	$\leq 5.0 \times 10^{-5}$	$\leq 3.5 \times 10^{-5}$ [(e)]
Nominal 40% packing fraction	$\leq 5.0 \times 10^{-5}$	$\leq 8.3 \times 10^{-5}$ [(e)]
Defective SiC coating fraction [(d)]		
Nominal 25% packing fraction	$\leq 1.0 \times 10^{-4}$	$\leq 5.7 \times 10^{-5}$ [(e)]
Nominal 40% packing fraction	$\leq 1.0 \times 10^{-4}$	$\leq 7.5 \times 10^{-5}$ [(e)]
Defective IPyC coating fraction [(d)]	$\leq 1.0 \times 10^{-4}$	$\leq 7.6 \times 10^{-5}$
Defective OPyC coating fraction [(d)]	$\leq 1.0 \times 10^{-2}$	$\leq 7.1 \times 10^{-4}$ [(e)]

(a) Allowable range corresponding to upper and lower critical limits specified with no compacts exceeding the limits, which require 100% inspection of all compacts.
(b) Calculated value derived from other characterized properties.
(c) Mean value specification of ≤240 μg Ti+V outside of SiC per compact.
(d) 95% confidence fraction.
(e) The 95% confidence fraction exceeds the specification; it was taken from INL/EXT-19-53720 (Marshall, 2019).

APPENDIX B

Compact Time-Averaged Temperature, Burnup, and Fast Neutron Fluence at the End of Irradiation

Appendix B

Compact Time-Averaged Temperature, Burnup, and Fast Neutron Fluence at the End of Irradiation

The low fission powers during the two low-power PALM cycles (Cycle 163A and 167A) led to significantly lower fuel temperatures in all capsules. Therefore, the time-average temperature calculations were performed for two scenarios: the first one included all days of irradiation and the second one excluded two low-power PALM cycles. The time-average fuel temperatures in Table 24 for both scenarios, and Capsule 1 neon fractions during Cycle 168A were zero.

Table 24. Compact time-averaged temperature, burnup, and fast neutron fluence at the end of irradiation.

Capsule	Compact	Time-Averaged Minimum Temperature (°C)	Time-Averaged Volume-Averaged Temperature (°C)	Time-Averaged Peak Temperature (°C)	Burnup (% FIMA)	Fast Neutron Fluence (10^{25} n/m^2, E >0.18MeV)
Capsule 5	5-1-1	489 / 499	696 / 711	805 / 822	9.16	3.27
Capsule 5	5-1-2	489 / 499	695 / 710	804 / 821	9.17	3.25
Capsule 5	5-1-3	495 / 505	706 / 721	818 / 835	9.38	3.39
Capsule 5	5-1-4	496 / 506	706 / 721	817 / 834	9.40	3.4
Capsule 5	5-2-1	686 / 700	774 / 790	829 / 846	8.84	3.01
Capsule 5	5-2-2	685 / 699	774 / 789	828 / 845	8.82	2.99
Capsule 5	5-2-3	696 / 710	786 / 802	842 / 859	8.98	3.12
Capsule 5	5-2-4	695 / 709	785 / 801	842 / 859	8.99	3.13
Capsule 5	5-3-1	707 / 721	785 / 800	832 / 849	8.43	2.71
Capsule 5	5-3-2	706 / 720	784 / 800	832 / 849	8.43	2.7
Capsule 5	5-3-3	716 / 730	796 / 812	846 / 863	8.59	2.81
Capsule 5	5-3-4	716 / 730	796 / 812	846 / 863	8.60	2.82
Capsule 5	5-4-1	724 / 738	791 / 807	834 / 850	7.98	2.4
Capsule 5	5-4-2	723 / 738	791 / 807	834 / 851	7.96	2.39
Capsule 5	5-4-3	734 / 748	803 / 819	847 / 864	8.16	2.48
Capsule 5	5-4-4	734 / 748	803 / 819	847 / 864	8.17	2.49
Capsule 5	5-5-1	663 / 677	747 / 762	813 / 830	7.43	2.06
Capsule 5	5-5-2	662 / 676	747 / 762	813 / 830	7.44	2.05
Capsule 5	5-5-3	672 / 685	757 / 773	826 / 842	7.64	2.13
Capsule 5	5-5-4	672 / 686	758 / 774	826 / 843	7.67	2.14
Capsule 5	5-6-1	459 / 468	622 / 635	727 / 742	6.75	1.68
Capsule 5	5-6-2	458 / 467	621 / 634	726 / 741	6.75	1.67
Capsule 5	5-6-3	464 / 473	630 / 643	737 / 752	7.03	1.74
Capsule 5	5-6-4	464 / 473	631 / 644	738 / 753	7.05	1.74
Capsule 5 compacts		**458 / 467**	**741 / 756**	**847 / 864**	**8.20**	**2.57**

Capsule	Compact	Time-Averaged Minimum Temperature (°C)	Time-Averaged Volume-Averaged Temperature (°C)	Time-Averaged Peak Temperature (°C)	Burnup (% FIMA)	Fast Neutron Fluence (10^{25} n/m^2, E >0.18MeV)
Capsule 4	4-1-1	547 / 559	758 / 775	868 / 887	13.77	4.8
Capsule 4	4-1-2	546 / 558	757 / 774	867 / 886	13.72	4.78
Capsule 4	4-1-3	553 / 565	769 / 786	882 / 902	14.06	5.01
Capsule 4	4-1-4	553 / 565	769 / 786	882 / 901	14.09	5.03
Capsule 4	4-2-1	750 / 766	850 / 868	913 / 933	13.72	4.7
Capsule 4	4-2-2	750 / 765	849 / 867	912 / 932	13.70	4.68
Capsule 4	4-2-3	761 / 777	863 / 882	928 / 948	14.02	4.9
Capsule 4	4-2-4	761 / 777	863 / 881	928 / 947	14.07	4.93
Capsule 4	4-3-1	785 / 801	875 / 893	930 / 950	13.55	4.57
Capsule 4	4-3-2	784 / 800	875 / 893	930 / 950	13.53	4.55
Capsule 4	4-3-3	796 / 812	889 / 907	945 / 965	13.83	4.77
Capsule 4	4-3-4	796 / 812	888 / 907	945 / 965	13.87	4.79
Capsule 4	4-4-1	806 / 822	888 / 907	935 / 955	13.24	4.42
Capsule 4	4-4-2	805 / 822	888 / 906	935 / 954	13.21	4.4
Capsule 4	4-4-3	816 / 833	901 / 919	948 / 968	13.52	4.61
Capsule 4	4-4-4	817 / 833	902 / 920	950 / 970	13.56	4.62
Capsule 4	4-5-1	771 / 787	865 / 884	927 / 947	12.84	4.24
Capsule 4	4-5-2	770 / 786	864 / 882	927 / 946	12.83	4.23
Capsule 4	4-5-3	780 / 796	876 / 894	940 / 960	13.11	4.42
Capsule 4	4-5-4	781 / 797	877 / 896	942 / 962	13.15	4.44
Capsule 4	4-6-1	566 / 578	765 / 782	872 / 891	12.37	4.01
Capsule 4	4-6-2	565 / 577	763 / 779	870 / 889	12.35	4
Capsule 4	4-6-3	571 / 583	773 / 790	883 / 902	12.62	4.18
Capsule 4	4-6-4	572 / 584	774 / 791	884 / 903	12.65	4.2
Capsule 4 compacts		**546 / 558**	**839 / 857**	**950 / 970**	**13.39**	**4.55**
Capsule 2	2-1-1	536 / 546	736 / 752	844 / 861	13.51	4.56
Capsule 2	2-1-2	536 / 546	736 / 752	844 / 861	13.52	4.56
Capsule 2	2-1-3	542 / 552	748 / 763	858 / 875	13.82	4.77
Capsule 2	2-1-4	541 / 552	746 / 761	855 / 873	13.81	4.77
Capsule 2	2-2-1	728 / 743	828 / 845	896 / 914	14.03	4.72
Capsule 2	2-2-2	728 / 743	828 / 845	896 / 914	14.02	4.72
Capsule 2	2-2-3	739 / 753	842 / 859	911 / 929	14.33	4.94
Capsule 2	2-2-4	737 / 752	840 / 856	909 / 927	14.33	4.94
Capsule 2	2-3-1	768 / 782	857 / 874	912 / 931	14.38	4.85
Capsule 2	2-3-2	768 / 782	857 / 874	913 / 931	14.36	4.85
Capsule 2	2-3-3	779 / 794	872 / 889	929 / 947	14.67	5.07

Capsule	Compact	Time-Averaged Minimum Temperature (°C)	Time-Averaged Volume-Averaged Temperature (°C)	Time-Averaged Peak Temperature (°C)	Burnup (% FIMA)	Fast Neutron Fluence (10^{25} n/m^2, E >0.18MeV)
Capsule 2	2-3-4	778 / 792	870 / 886	926 / 945	14.69	5.07
Capsule 2	2-4-1	763 / 777	858 / 875	913 / 931	14.60	4.96
Capsule 2	2-4-2	763 / 777	859 / 875	913 / 931	14.61	4.95
Capsule 2	2-4-3	775 / 789	874 / 890	929 / 948	14.91	5.18
Capsule 2	2-4-4	773 / 788	871 / 888	927 / 945	14.92	5.19
Capsule 2	2-5-1	733 / 747	835 / 851	900 / 917	14.78	5.05
Capsule 2	2-5-2	734 / 747	836 / 852	901 / 918	14.78	5.04
Capsule 2	2-5-3	745 / 759	850 / 867	917 / 935	15.09	5.28
Capsule 2	2-5-4	744 / 757	848 / 864	914 / 933	15.09	5.29
Capsule 2	2-6-1	726 / 739	821 / 838	880 / 898	14.89	5.13
Capsule 2	2-6-2	726 / 739	822 / 838	881 / 899	14.88	5.12
Capsule 2	2-6-3	736 / 750	835 / 852	897 / 915	15.21	5.36
Capsule 2	2-6-4	735 / 749	834 / 850	895 / 913	15.21	5.36
Capsule 2	2-7-1	706 / 720	808 / 824	871 / 889	14.92	5.18
Capsule 2	2-7-2	705 / 719	808 / 824	872 / 889	14.92	5.17
Capsule 2	2-7-3	716 / 729	820 / 836	886 / 903	15.25	5.42
Capsule 2	2-7-4	715 / 729	819 / 836	885 / 903	15.26	5.42
Capsule 2	2-8-1	544 / 554	743 / 758	844 / 861	14.93	5.21
Capsule 2	2-8-2	542 / 553	742 / 757	843 / 861	14.93	5.2
Capsule 2	2-8-3	549 / 560	753 / 769	857 / 874	15.25	5.44
Capsule 2	2-8-4	549 / 560	753 / 768	856 / 874	15.26	5.44
Capsule 2 compacts		**536 / 546**	**817 / 833**	**929 / 948**	**14.66**	**5.07**
Capsule 1	1-1-1	579 / 588	750 / 762	867 / 882	5.78	1.62
Capsule 1	1-1-2	579 / 588	749 / 761	866 / 881	5.66	1.62
Capsule 1	1-1-3	583 / 592	752 / 765	870 / 885	5.86	1.64
Capsule 1	1-1-4	585 / 594	759 / 772	878 / 893	6.13	1.69
Capsule 1	1-1-5	592 / 602	767 / 779	887 / 903	6.47	1.73
Capsule 1	1-1-6	594 / 603	772 / 785	895 / 910	6.63	1.75
Capsule 1	1-1-7	595 / 604	773 / 786	896 / 911	6.67	1.75
Capsule 1	1-1-8	593 / 603	768 / 781	890 / 906	6.42	1.73
Capsule 1	1-1-9	586 / 595	761 / 774	883 / 898	6.16	1.69
Capsule 1	1-1-10	584 / 593	754 / 767	874 / 889	5.89	1.65
Capsule 1	1-2-1	725 / 737	869 / 884	976 / 993	7.34	2.07
Capsule 1	1-2-2	725 / 736	868 / 883	975 / 991	7.35	2.07
Capsule 1	1-2-3	728 / 739	872 / 887	979 / 996	7.42	2.11
Capsule 1	1-2-4	733 / 745	880 / 894	987 / 1004	7.56	2.16

Capsule	Compact	Time-Averaged Minimum Temperature (°C)	Time-Averaged Volume-Averaged Temperature (°C)	Time-Averaged Peak Temperature (°C)	Burnup (% FIMA)	Fast Neutron Fluence (10^{25} n/m^2, E >0.18MeV)
Capsule 1	1-2-5	740 / 752	888 / 903	997 / 1014	7.71	2.21
Capsule 1	1-2-6	746 / 757	896 / 911	1006 / 1023	7.84	2.23
Capsule 1	1-2-7	746 / 758	897 / 912	1007 / 1024	7.85	2.23
Capsule 1	1-2-8	742 / 754	892 / 907	1002 / 1019	7.73	2.2
Capsule 1	1-2-9	736 / 747	885 / 900	994 / 1011	7.58	2.16
Capsule 1	1-2-10	729 / 741	876 / 890	984 / 1001	7.42	2.11
Capsule 1	1-3-1	798 / 810	951 / 967	1057 / 1075	8.11	2.48
Capsule 1	1-3-2	798 / 810	950 / 966	1055 / 1073	8.11	2.48
Capsule 1	1-3-3	800 / 812	954 / 969	1059 / 1077	8.15	2.52
Capsule 1	1-3-4	806 / 818	961 / 977	1068 / 1086	8.26	2.58
Capsule 1	1-3-5	814 / 826	971 / 987	1078 / 1096	8.40	2.63
Capsule 1	1-3-6	819 / 831	979 / 995	1087 / 1105	8.50	2.65
Capsule 1	1-3-7	820 / 833	980 / 997	1090 / 1108	8.50	2.66
Capsule 1	1-3-8	817 / 829	976 / 992	1085 / 1103	8.40	2.63
Capsule 1	1-3-9	810 / 822	968 / 984	1076 / 1095	8.29	2.58
Capsule 1	1-3-10	803 / 815	958 / 974	1065 / 1084	8.17	2.52
Capsule 1	1-4-1	850 / 863	1011 / 1027	1112 / 1131	8.68	2.85
Capsule 1	1-4-2	850 / 862	1009 / 1026	1110 / 1129	8.69	2.84
Capsule 1	1-4-3	852 / 865	1012 / 1029	1113 / 1132	8.73	2.89
Capsule 1	1-4-4	858 / 871	1020 / 1036	1121 / 1140	8.80	2.96
Capsule 1	1-4-5	866 / 878	1029 / 1046	1130 / 1150	8.95	3.02
Capsule 1	1-4-6	871 / 884	1037 / 1054	1140 / 1159	9.05	3.04
Capsule 1	1-4-7	873 / 886	1040 / 1057	1143 / 1162	9.03	3.04
Capsule 1	1-4-8	869 / 882	1036 / 1053	1138 / 1158	8.95	3.02
Capsule 1	1-4-9	862 / 875	1028 / 1045	1130 / 1150	8.82	2.96
Capsule 1	1-4-10	855 / 868	1018 / 1035	1120 / 1139	8.74	2.89
Capsule 1	1-5-1	866 / 878	1036 / 1053	1132 / 1152	9.17	3.19
Capsule 1	1-5-2	865 / 878	1035 / 1052	1130 / 1149	9.19	3.18
Capsule 1	1-5-3	867 / 880	1038 / 1055	1133 / 1153	9.21	3.23
Capsule 1	1-5-4	872 / 884	1044 / 1061	1141 / 1160	9.27	3.3
Capsule 1	1-5-5	878 / 891	1053 / 1070	1151 / 1170	9.36	3.37
Capsule 1	1-5-6	883 / 896	1061 / 1078	1158 / 1178	9.46	3.39
Capsule 1	1-5-7	885 / 898	1064 / 1081	1160 / 1180	9.46	3.39
Capsule 1	1-5-8	882 / 895	1060 / 1077	1157 / 1177	9.38	3.36
Capsule 1	1-5-9	876 / 889	1053 / 1070	1149 / 1169	9.29	3.3
Capsule 1	1-5-10	870 / 883	1043 / 1060	1140 / 1160	9.23	3.24

Capsule	Compact	Time-Averaged Minimum Temperature (°C)	Time-Averaged Volume-Averaged Temperature (°C)	Time-Averaged Peak Temperature (°C)	Burnup (% FIMA)	Fast Neutron Fluence (10^{25} n/m^2, E >0.18MeV)
Capsule 1	1-6-1	866 / 878	1048 / 1065	1159 / 1179	9.61	3.49
Capsule 1	1-6-2	865 / 877	1047 / 1064	1157 / 1177	9.61	3.49
Capsule 1	1-6-3	867 / 879	1050 / 1067	1161 / 1181	9.63	3.54
Capsule 1	1-6-4	872 / 884	1056 / 1073	1168 / 1188	9.68	3.62
Capsule 1	1-6-5	878 / 891	1066 / 1083	1178 / 1198	9.79	3.68
Capsule 1	1-6-6	883 / 896	1072 / 1090	1184 / 1204	9.88	3.7
Capsule 1	1-6-7	885 / 897	1073 / 1091	1185 / 1205	9.86	3.7
Capsule 1	1-6-8	882 / 895	1071 / 1088	1182 / 1203	9.78	3.68
Capsule 1	1-6-9	876 / 889	1064 / 1082	1176 / 1196	9.70	3.62
Capsule 1	1-6-10	870 / 883	1055 / 1072	1167 / 1187	9.64	3.55
Capsule 1	1-7-1	879 / 893	1073 / 1091	1184 / 1205	10.00	3.76
Capsule 1	1-7-2	879 / 892	1072 / 1090	1185 / 1206	10.01	3.76
Capsule 1	1-7-3	881 / 894	1076 / 1094	1189 / 1210	10.02	3.82
Capsule 1	1-7-4	886 / 899	1082 / 1100	1196 / 1217	10.12	3.9
Capsule 1	1-7-5	892 / 905	1091 / 1109	1204 / 1225	10.19	3.97
Capsule 1	1-7-6	897 / 911	1096 / 1115	1208 / 1229	10.36	3.99
Capsule 1	1-7-7	898 / 912	1097 / 1115	1209 / 1230	10.34	3.99
Capsule 1	1-7-8	895 / 908	1094 / 1113	1206 / 1227	10.22	3.97
Capsule 1	1-7-9	890 / 903	1088 / 1106	1199 / 1221	10.13	3.9
Capsule 1	1-7-10	884 / 897	1079 / 1097	1190 / 1211	10.04	3.82
Capsule 1	1-8-1	872 / 886	1075 / 1094	1186 / 1207	10.43	4
Capsule 1	1-8-2	872 / 886	1077 / 1096	1187 / 1208	10.44	4
Capsule 1	1-8-3	875 / 889	1081 / 1100	1191 / 1213	10.49	4.06
Capsule 1	1-8-4	879 / 893	1087 / 1106	1198 / 1219	10.59	4.14
Capsule 1	1-8-5	884 / 898	1093 / 1112	1205 / 1227	10.75	4.21
Capsule 1	1-8-6	888 / 902	1097 / 1116	1209 / 1231	10.89	4.23
Capsule 1	1-8-7	888 / 903	1097 / 1116	1210 / 1231	10.91	4.23
Capsule 1	1-8-8	885 / 899	1094 / 1114	1207 / 1229	10.76	4.21
Capsule 1	1-8-9	880 / 894	1088 / 1107	1200 / 1222	10.62	4.14
Capsule 1	1-8-10	875 / 889	1079 / 1098	1191 / 1212	10.49	4.06
Capsule 1	1-9-1	601 / 611	934 / 951	1141 / 1163	11.09	4.17
Capsule 1	1-9-2	602 / 612	936 / 953	1143 / 1165	11.12	4.16
Capsule 1	1-9-3	603 / 613	939 / 956	1148 / 1169	11.22	4.22
Capsule 1	1-9-4	607 / 617	944 / 961	1154 / 1175	11.33	4.31
Capsule 1	1-9-5	608 / 618	949 / 966	1160 / 1182	11.53	4.38
Capsule 1	1-9-6	612 / 622	952 / 969	1163 / 1185	11.68	4.4

Capsule	Compact	Time-Averaged Minimum Temperature (°C)	Time-Averaged Volume-Averaged Temperature (°C)	Time-Averaged Peak Temperature (°C)	Burnup (% FIMA)	Fast Neutron Fluence (10^{25} n/m^2, E >0.18MeV)
Capsule 1	1-9-7	611 / 621	952 / 969	1164 / 1185	11.67	4.4
Capsule 1	1-9-8	609 / 620	950 / 967	1161 / 1183	11.57	4.38
Capsule 1	1-9-9	606 / 616	944 / 962	1154 / 1176	11.40	4.31
Capsule 1	1-9-10	604 / 614	937 / 955	1146 / 1168	11.24	4.22
Capsule 1 compacts		**579 / 588**	**984 / 1001**	**1210 / 1231**	**9.12**	**3.18**
All AGR-5/6 compacts		**458 / 467**	**898 / 914**	**1210 / 1231**	**10.64**	**3.64**
Capsule 3	3-1-1	970 / 990	1167 / 1191	1301 / 1328	13.58	5.37
Capsule 3	3-1-2	969 / 990	1169 / 1193	1302 / 1329	13.76	5.48
Capsule 3	3-1-3	970 / 991	1169 / 1193	1303 / 1329	13.77	5.49
Capsule 3	3-2-1	1177 / 1200	1293 / 1318	1374 / 1400	14.43	5.42
Capsule 3	3-2-2	1180 / 1203	1295 / 1320	1375 / 1401	14.61	5.54
Capsule 3	3-2-3	1180 / 1203	1295 / 1320	1374 / 1401	14.62	5.54
Capsule 3	3-3-1	1235 / 1258	1329 / 1354	1391 / 1417	14.67	5.42
Capsule 3	3-3-2	1238 / 1261	1330 / 1355	1392 / 1418	14.84	5.55
Capsule 3	3-3-3	1238 / 1262	1330 / 1355	1391 / 1418	14.88	5.55
Capsule 3	3-4-1	1246 / 1268	1335 / 1359	1393 / 1419	14.73	5.41
Capsule 3	3-4-2	1249 / 1271	1336 / 1361	1394 / 1420	14.91	5.54
Capsule 3	3-4-3	1249 / 1272	1336 / 1361	1394 / 1420	14.95	5.54
Capsule 3	3-5-1	1241 / 1264	1332 / 1356	1392 / 1418	14.69	5.39
Capsule 3	3-5-2	1245 / 1267	1334 / 1358	1394 / 1420	14.86	5.51
Capsule 3	3-5-3	1245 / 1268	1334 / 1358	1394 / 1420	14.89	5.52
Capsule 3	3-6-1	1236 / 1259	1336 / 1361	1404 / 1430	14.56	5.34
Capsule 3	3-6-2	1239 / 1262	1338 / 1363	1405 / 1431	14.72	5.46
Capsule 3	3-6-3	1241 / 1264	1338 / 1363	1405 / 1432	14.77	5.47
Capsule 3	3-7-1	1190 / 1213	1318 / 1343	1401 / 1428	14.27	5.28
Capsule 3	3-7-2	1191 / 1214	1319 / 1344	1402 / 1429	14.46	5.4
Capsule 3	3-7-3	1193 / 1216	1320 / 1345	1402 / 1429	14.49	5.41
Capsule 3	3-8-1	969 / 989	1192 / 1217	1339 / 1366	13.62	5.18
Capsule 3	3-8-2	971 / 991	1193 / 1217	1340 / 1366	13.80	5.29
Capsule 3	3-8-3	971 / 991	1193 / 1218	1340 / 1367	13.81	5.3
All AGR-7 compacts		**969 / 989**	**1289 / 1313**	**1405 / 1432**	**14.45**	**5.43**